

**INFLUENCE OF THE LEFT ATRIUM DYSFUNCTION ON THE LEFT
VENTRICULAR FUNCTION IN HEART FAILURE WITH PRESERVED
EJECTION FRACTION**

by
Badhan Saha


A thesis submitted in partial fulfillment of the requirements for the degree of
MASTER OF SCIENCE IN MECHANICAL ENGINEERING



Department of Mechanical Engineering
BANGLADESH UNIVERSITY OF ENGINEERING AND TECHNOLOGY
Dhaka, Bangladesh
April 2022

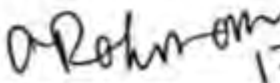
The thesis titled "INFLUENCE OF THE LEFT ATRIUM DYSFUNCTION ON THE LEFT VENTRICULAR FUNCTION IN HEART FAILURE WITH PRESERVED EJECTION FRACTION" submitted by **Badhan Saha**, Roll No.: 0419102128, Session: April, 2019, has been accepted as satisfactory in partial fulfillment of the requirement for the degree of MASTER OF SCIENCE IN MECHANICAL ENGINEERING on April 17, 2022.

BOARD OF EXAMINERS


17/04/2022

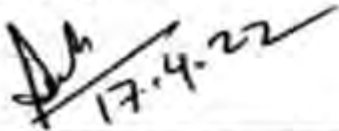
Dr. Sheikh Mohammad Shavik
Assistant Professor
Department of Mechanical Engineering,
BUET, Dhaka- 1000

Chairman (Supervisor)


17.4.22

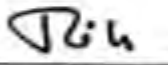
Dr. Muhammad Ashiqur Rahman
Professor and Head
Department of Mechanical Engineering,
BUET, Dhaka- 1000

Member (Ex- officio)


17.4.22

Dr. Mohammad Abdul Motalab
Professor
Department of Mechanical Engineering,
BUET, Dhaka- 1000

Member


17/4/22

Dr. Muhammad Tarik Arafat
Associate Professor
Department of Biomedical Engineering,
BUET, Dhaka- 1000

Member (External)

CANDIDATE'S DECLARATION

It is hereby declared that this thesis or any part of it has not been submitted elsewhere for the award of any degree or diploma.

April 2022



Badhan Saha
Author

CERTIFICATE OF RESEARCH

This is to certify that the work presented in this thesis has been carried out by the author under the supervision of **Dr. Sheikh Mohammad Shavik**, Assistant Professor, Department of Mechanical Engineering, Bangladesh University of Engineering and Technology, Dhaka.



Dr. Sheikh Mohammad Shavik



Badhan Saha

DEDICATION

Dedicated to My Parents, Brother and Spouse

Table of Contents

LIST OF FIGURES	ix
LIST OF TABLES	xiii
ACKNOWLEDGEMENT.....	xiv
ABSTRACT	xv
CHAPTER 1.....	1
INTRODUCTION.....	1
1.1 Human Heart Anatomy in Brief.....	3
1.2 Physiology of Left Ventricle (LV).....	6
1.3 Physiology of Left Atrium (LA).....	11
1.4 Heart Failure and Ejection Fraction.....	13
1.4.1 Heart Failure with Preserved Ejection Fraction (HFpEF)	16
1.4.2 Progression of HFpEF	18
1.5 Finite Element Analysis of Human Heart.....	18
1.6 Background and present state of the problem.....	20
1.7 Objectives of the Study.....	20
CHAPTER 2.....	21
LITERATURE REVIEW.....	21
CHAPTER 3.....	26
MODELING THE LEFT VENTRICLE AND CIRCULATORY SYSTEM	26
3.1 Modeling the Systemic Circulatory System	26
3.2 Formulation of The Left Ventricular Finite Element model.....	31
3.3 The LV's constitutive law	32
3.4 LV Geometry and Mesh	35
3.5 Simulation Cases.....	39

3.6 Calculation of Myocardial Strain.....	40
3.7 Grid Independence Test.....	41
CHAPTER 4.....	43
RESULTS AND DISCUSSION	43
4.1 Comparison of the Models: Normal, and HFpEF-I, and HFpEF-II Cases	43
4.1.1 Comparison of the PV loops, volume waveforms, and pressure waveforms among the Normal, HFpEF-I, and HFpEF-II cases.....	43
4.1.2 Comparison of Strains among the Normal, HFpEF-I and HFpEF-II Cases	49
4.1.3 Summary.....	51
4.2 Effects of the variations of LA contractility (end-systolic elastance parameter (E_{es})) on LV function for Normal, HFpEF-I, and HFpEF-II cases.....	52
4.2.1 Effects of change of LA contractility on LV PV Loops	57
4.2.2 Effects of change of LA contractility on LV Strains.....	58
4.3 Effects of the variations of LA stiffness (Scaling Factor (A_{LA})) on LV function for Normal, HFpEF-I, and HFpEF-II cases	60
4.3.1 Effects of change of LA stiffness on LV PV Loops	65
4.3.2 Effects of change of LA stiffness on LV Strains.....	66
4.4 Combined effects of varying LA contractility and stiffness on LV function for normal, HFpEF-I, and HFpEF-II cases	68
4.4.1 Effects of change of LA time varying elastance parameters on LV PV loop for Normal, HFpEF-I, and HFpEF-II cases	73
4.4.2 Effects of change of LA time varying elastance parameters on LV Strains for Normal, HFpEF-I, and HFpEF-II cases	75
4.5 Summary.....	79
CHAPTER 5.....	82
CONCLUSION	82

5.1 Conclusion	82
5.2 Limitations of the Work.....	83
5.3 Recommendation for Future Works	84
REFERENCES.....	85
NOMENCLATURE.....	93

LIST OF FIGURES

Figure 1. 1: Human heart blood circulation circuits	1
Figure 1. 2: Simplified structure of the human heart, and direction of blood flow through the heart chambers and heart valves.	4
Figure 1. 3: Heart's circulatory relay during systemic and pulmonary circulatory processes [8] .	6
Figure 1. 4: Cardiac Cycle Overview: The cardiac cycle begins with atrial systole and continues through ventricular systole, atrial diastole, and ventricular diastole before starting all over again. Correlations with the electrocardiogram (ECG) are emphasized	8
Figure 1. 5: A typical pressure – volume (PV) loop with identifiable physiological parameters, and ESPVR and EDPVR	9
Figure 1. 6: Wiggers diagram showing aortic, left atrial, left ventricular pressure; left ventricular volume; electrocardiogram; phonocardiogram with respect to heart cycle time [13]	11
Figure 1. 7: Phases of left atrial function. During ventricular systole, the left atrial chamber operates as a reservoir for blood from the pulmonary vein, whereas during ventricular diastasis, the left atrial chamber serves as a conduit for pulmonary vein flow that empties into the ventricle once the mitral valve opens. During ventricular end diastole, the left atrium finally contracts and actively empties, completing ventricular filling. LV, left ventricle; V_p , left atrial volume before atrial contraction; V_{max} , maximum volume (measured at left ventricular end-systolic phase); and V_{min} , left atrial minimum volume (as defined at left ventricular end-diastolic phase) [27]	12
Figure 1. 8: Pressure volume loop of the left atrium (LA)	13
Figure 1. 9: HFpEF, or heart failure with preserved ejection fraction, as well as the risk factors associated with it (comorbid diseases).....	17
Figure 3. 1: Systemic circulatory compartments and their electrical analogs are shown in a schematic representation of the modeling framework [42]	26
Figure 3. 2: Myocardial fiber direction f , sheet direction s and sheet normal direction n [60]..	33
Figure 3. 3: LV geometry defined using a half prolate ellipsoid and discretized with quadratic tetrahedral elements constructed based on the acquired MRI images of (a) normal subject (b) HFpEF-I and (c) HFpEF-II (d) dimensioning of the ellipsoidal LV model of heart geometry	37

Figure 3. 4: Linear transmural variation of helix angle associated with the myofiber direction from endocardium to the epicardium shown in a (a) real heart image and (b) computational model [42].....	38
Figure 3. 5: Variation of the helix angle associated with the myofiber direction from the LV endocardium to the epicardium used in the FE model.....	38
Figure 3. 6: Using the coupled LV FE lumped parameter systemic circulation model, a simulation flow diagram is shown to find the steady state solution.	40
Figure 3. 7: Comparison of steady-state LV (A) PV loop, (B) volume waveforms, (C) pressure waveforms and LA (D) PV loops for normal case for different number of quadratic tetrahedral elements.	42
Figure 4. 1: The Normal: LA1 LV's (a) PV loop (b) pressure waveform (c) volume waveform (d) LA's PV loop matched with the literature [54].....	44
Figure 4. 2: The HFpEF-I: LA1 LV's (a) PV loop (b) pressure waveform (c) volume waveform (d) LA's PV loop matched with the literature [54].....	46
Figure 4. 3: The HFpEF-II: LA1 LV's (a) PV loop (b) pressure waveform (c) volume waveform (d) LA's PV loop matched with the literature [40].....	47
Figure 4. 4: Circumferential strain waveform calculated by the model for Normal: LA1, HFpEFI: LA1, and HFpEFII LA1 cases compared with echo measurements (dashed magenta color [66] and dotted cyan color [67] lines)	50
Figure 4. 5: Longitudinal strain waveform calculated by the model for Normal: LA1, HFpEFI: LA1, and HFpEFII LA1 cases compared with echo measurements (dashed magenta color [66] and dotted cyan color [68] lines)	50
Figure 4. 6: Comparison among Normal LV of (A) PV loops, (B) volume waveforms, (C) pressure waveforms, (D) circumferential strains, (E) longitudinal strains, and (F) radial strains by varying end-systolic elastance (Ees) parameter	53
Figure 4. 7: Comparison among HFpEF-I LV of (A) PV loops, (B) volume waveforms, (C) pressure waveforms, (D) circumferential strains, (E) longitudinal strains, and (F) radial strains by varying end-systolic elastance (Ees) parameter	54

Figure 4. 8: Comparison among HFpEF-II LV of (A) PV loops, (B) volume waveforms, (C) pressure waveforms, (D) circumferential strains, (E) longitudinal strains, and (F) radial strains by varying end-systolic elastance (E_{es}) parameter	55
Figure 4. 9: Comparison among Normal LA of PV loops by varying end-systolic elastance (E_{es}) parameter.....	56
Figure 4. 10: Comparison among HFpEF-I LA of PV loops by varying end-systolic elastance (E_{es}) parameter	56
Figure 4. 11: Comparison among HFpEF-II LA of PV loops by varying end-systolic elastance (E_{es}) parameter	57
Figure 4. 12: Comparison among Normal LV of (A) PV loops, (B) volume waveforms, (C) pressure waveforms, (D) circumferential strains, (E) longitudinal strains, and (F) radial strains by varying scaling factor (A_{LA}) for EDPVR	61
Figure 4. 13: Comparison among HFpEF-I LV of (A) PV loops, (B) volume waveforms, (C) pressure waveforms, (D) circumferential strains, (E) longitudinal strains, and (F) radial strains by varying scaling factor (A_{LA}) for EDPVR	62
Figure 4. 14: Comparison among HFpEF-II LV of (A) PV loops, (B) volume waveforms, (C) pressure waveforms, (D) circumferential strains, (E) longitudinal strains, and (F) radial strains by varying scaling factor (A_{LA}) for EDPVR	63
Figure 4. 15: Comparison among Normal LA of PV loops by varying scaling factor (A_{LA}) for EDPVR	64
Figure 4. 16: Comparison among HFpEF-I LA of PV loops by varying scaling factor (A_{LA}) for EDPVR	64
Figure 4. 17: Comparison among HFpEF-II LA of PV loops by varying scaling factor (A_{LA}) for EDPVR	65
Figure 4. 18: Comparison among Normal LV (A) PV loops, (B) volume waveforms, (C) pressure waveforms, (D) circumferential strains, (E) longitudinal strains, and (F) radial strains by varying LA time varying elastance parameters (E_{es} , A_{LA} , B_{LA} , T_{max} , τ).....	69
Figure 4. 19: Comparison among HFpEF-I LV (A) PV loops, (B) volume waveforms, (C) pressure waveforms, (D) circumferential strains, (E) longitudinal strains, and (F) radial strains by varying LA time varying elastance parameters (E_{es} , A_{LA} , B_{LA} , T_{max} , τ)	70

Figure 4. 20: Comparison among HFpEF-II LV (A) PV loops, (B) volume waveforms, (C) pressure waveforms, (D) circumferential strains, (E) longitudinal strains, and (F) radial strains by varying LA time varying elastance parameters (E_{es} , A_{LA} , B_{LA} , T_{max} , τ)	71
Figure 4. 21: Comparison among Normal LA PV loops by varying LA time varying elastance parameters (E_{es} , A_{LA} , B_{LA} , T_{max} , τ)	72
Figure 4. 22: Comparison among HFpEF-I LA PV loops by varying time varying elastance parameters (E_{es} , A_{LA} , B_{LA} , T_{max} , τ)	72
Figure 4. 23: Comparison among HFpEF-II LA PV loops by varying time varying elastance parameters (E_{es} , A_{LA} , B_{LA} , T_{max} , τ)	73

LIST OF TABLES

Table 3. 1: LA time-varying elastance model parameters for all cases	29
Table 3. 2: LA time-varying elastance model for all cases (combine case)	30
Table 3. 3: Fixed values of the model parameters for all simulation cases	31
Table 3. 4: Fixed parameter values of the LV FE model.....	34
Table 3. 5: Geometrical dimensions and mass.....	35
Table 4. 1: Hemodynamic indices of LV and LA for Normal: LA1 case.	45
Table 4. 2: Hemodynamic indices of LV and LA for HFpEF-I: LA1, and HFpEF-II: LA1 case.....	48
Table 4. 3: Model predicted hemodynamic and functional indices for Normal: LA1, HFpEF-I: LA1, and HFpEF-II: LA1.....	51
Table 4. 4: LA contractility parameter (End-systolic elastance, Ees (Pa/ml)) values used for Normal and HFpEF patients.	52
Table 4. 5: Hemodynamic and functional indices of LV for Normal and HFpEF models with varying LA contractility (End-systolic elastance parameter, Ees).....	59
Table 4. 6: LA stiffness parameter (scaling factor A_{LA} of EDPVR) values used for Normal and HFpEF patients.	60
Table 4. 7: Hemodynamic and functional indices of LV for Normal and HFpEF models with varying LA stiffness (Scaling factor, A_{LA} of EDPVR).....	66
Table 4. 8: Variation of parameters of LA time varying elastance model for Normal, HFpEF-I, and HFpEF-II cases.....	68
Table 4.9: Hemodynamic and functional indices of LV for Normal and HFpEF models for different LA time varying elastance model parameters	77

ACKNOWLEDGEMENT

I would like to express my deepest gratitude and indebtedness to my supervisor Dr. Sheikh Mohammad Shavik, Assistant Professor, Department of Mechanical Engineering, BUET for his kind supervision, constant guidance, encouragement, support, and thoughtful discussion throughout the entire research. Without his guidance, it was impossible to complete the thesis work.

I wish to thank my parents, spouse, brother, relatives, colleagues, friends and well-wishers for their help and mental support during the research.

Finally, I wish to thank almighty for everything in my entire life.

Author

ABSTRACT

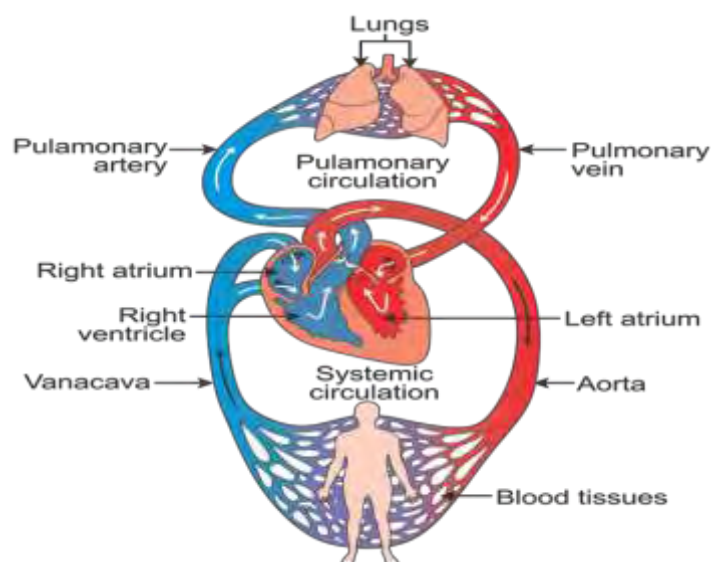
Heart Failure with preserved ejection fraction (HFpEF) has emerged as a prevalent heart disease which has high risk of short-term and long-term mortality rate. The progression of HFpEF along with the key factors which contributes to this process is an area of active research. Since the structural and functional changes of Left Ventricle (LV) governs the progression of HFpEF, computational models have emerged as a robust tool to study the features of HFpEF as well as to develop effective treatment plan in recent years. Though the ejection fraction is preserved apparently, the proper understanding of the left ventricular function in HFpEF patients is not well understood. Moreover, the synergy between the left atrium (LA) and the left ventricle (LV) is also disrupted in HFpEF. The malfunction and remodeling of LA frequently occur in the HFpEF patients, as a result of which the proper functioning of the LV is also affected due to having the direct connection between the LV and the LA through the mitral valve. In the present study a coupled left ventricular finite element-lumped parameter systemic circulatory modeling framework has been used to assess the effect of left atrial malfunction on the performance of left ventricle in HFpEF patients. The model was calibrated using the measurements taken from the literature for a healthy person and patients with HFpEF. To account for the wide range of LV geometry reported in HFpEF patients in the literature, two distinct LV geometries have been used in this study, one with a smaller LV cavity (HFpEF I) and one with a slightly dilated LV cavity (HFpEF II) in comparison to the healthy LV geometry. Both HFpEF geometries had a thicker wall and higher mass than the healthy case. Simulations were performed using the normal, HFpEF-I, and HFpEF-II LV models to quantify the effects of the variation of LA contractility (90% and 110% of healthy contractility) and LA stiffness (90%, and 110% healthy stiffness) on LV function. Increased LA contractility produced elevated pressure and enlarged volume in LA and as a consequence, the LV function gradually improved as indicated by higher ejection fraction and higher peak longitudinal and circumferential strains in both HFpEF cases. In case of increased LA stiffness, similar results have been found for both HFpEF cases where LV ejection fraction and peak longitudinal and circumferential strains have gradually increased. Finally, combinations of both LA contractility and stiffness were used which also showed a gradual improvement of LV function as indexed by the ejection fraction and the peak longitudinal and circumferential strains with elevated LA pressure for both HFpEF cases. The results of the study suggests that the enlargement of LA and elevated LA pressure improves the overall LV function. As enlargement

of LA with elevated LA pressure is a common feature found in HFpEF, the results suggest that this mechanism could be a possible way which aid LV to preserve its ejection fraction.

CHAPTER 1

INTRODUCTION

Pulmonary and systemic circuits functionally consist of the blood flow circulation in the human body. The human heart consists of four major muscular chambers: two ventricles, and two atria. The two ventricles and atria are divided into two distinct right and left heart pumps. The systemic circuit is related to the left two chambers and the pulmonary circuit is related to the right two chambers of the heart, respectively. The left ventricle (LV) and left atrium (LA) compose the left heart which pumps oxygen-rich blood through the systemic circulation. On the other hand, the right heart pump is composed of the right ventricle and the right atrium that pumps oxygen-poor blood through the pulmonary circulation [1]. The detailed representation of the human heart is depicted in Fig. 1.1.



Source: <http://surl.li/bjcf0>

Figure 1. 1: Human heart blood circulation circuits

Cardiovascular disorders are the leading cause of death worldwide, accounting for 30% of all fatalities [2]. Heart disease and stroke are responsible for the majority of these deaths (more than 75%) [2]. Smoking, being overweight, not getting enough exercise, having high cholesterol, having high blood pressure, and having poorly managed diabetes are all risk factors for cardiovascular disease. Cardiovascular disorders often go unnoticed since they don't show any

symptoms like chest discomfort or shortness of breath. The most common methods of diagnosing heart illness include collecting a medical history, listening to the patient's heart sounds using a stethoscope, doing an ECG, and using ultrasound equipment. Cardiologists use Ejection Fraction (EF) as a clinical marker for heart failure (HF) because it is the most important clinical parameter for HF detection. It is the percentage of each heartbeat's volume ejected from the left ventricle divided by the volume of blood in the left ventricle when it is maximally filled.

HF basically appears in two different common types such as HF with preserved ejection fraction (HFpEF) and HF with reduced ejection fraction (HFrEF). Nearly half of those who suffer heart failure have HFpEF, whereas the other half have heart failure with decreased ejection fraction (HFrEF). It is seen in the literature review, ejection fraction (EF) is more than 56 %, and less than 56 % for normal and HFpEF patients, respectively [3]. Echocardiography (ECG) and cardiac catheterization are the most appropriate methods to clinically measure the EF [4]. The key risk factors for HFpEF include hypertension, diabetes, hyperlipidemia, smoking, and obstructive sleep apnea [5]. Diastolic dysfunction is the most common symptom in HFpEF, and the left ventricle becomes more rigid in patients with HFpEF. Increased pressure and/or poor filling are the outcome when left ventricular relaxation is reduced during the diastolic phase [6]. Atrial fibrillation and pulmonary hypertension are frequently found in the patients with elevated HFpEF [7].

Computer heart models have made remarkable progress over the years in describing cardiac geometry and muscle architecture realistically [8]. The researcher is prompted by a computer model to look into the underlying causes of heart illness, which is something that would be impossible to study in a clinical context. Despite the substantial progress, there are still several open questions and areas that need to be improved. To find out more about one of these problems, researchers set out to uncover the underlying mechanics of heart failure with preserved ejection fraction (HFpEF) through this study.

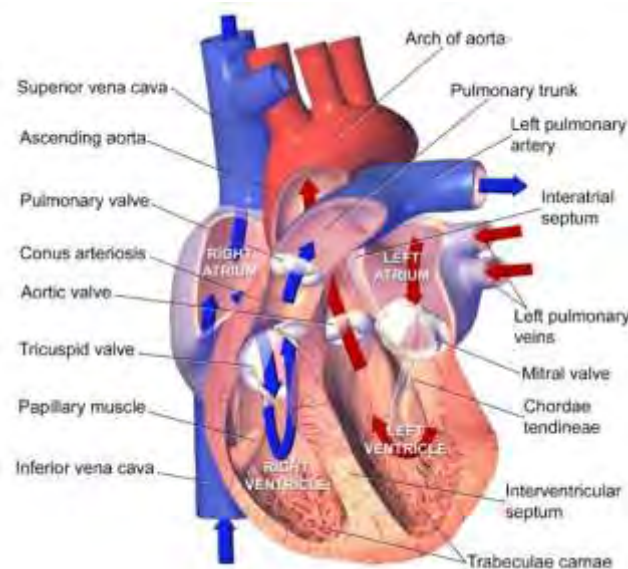
In this research, we have conducted a finite element modelling (FEM) analysis to investigate the influence of LA dysfunction on the function of LV using open-source solver FEniCS [9]. To the best of our knowledge, very limited number of studies has been conducted on the LA dysfunction- which is an important factor that adversely affects the LV function in HFpEF. In our study, we have focused to find out the effects of LA dysfunction by changing the LA

contractility and stiffness which have a direct influence on the variation of pressure and volume of the LV. This chapter discusses about basic anatomy and functioning of heart and the different viewpoints regarding progression of HFpEF, challenges as well as reliability concerns for impeding HFpEF progression.

1.1 Human Heart Anatomy in Brief

The heart is a muscle pump that is linked to the circulatory systems of the body as a whole as well as the lungs. The primary function of the heart and vasculature is to ensure that all of the tissues in the body receive an appropriate quantity of nutrients in the form of oxygenated blood and metabolic substrates under a variety of circumstances. There are two functionally different left and right heart pumps in an adult human heart, which is split into four distinct muscle chambers, two atria and two ventricles (Fig. 1.2). The left heart pumps blood from the pulmonary veins to the aorta through the left atrium and left ventricle. In humans, the left ventricle is a 1 cm thick axisymmetric truncated ellipsoid. Billions of cardiac muscle cells (myocytes) are joined end-to-end at their gap junctions to form a network of branching muscle fibers that wrap around the chamber in a very structured way. An atrium and ventricle make up a right heart, which is responsible for moving blood from the vena cavae to the lung arteries [10]. Myocardial fibers (the right ventricular free wall) create an approximately crescent-shaped structure in the right ventricle, where they interdigitate with the muscle fibers of the left ventricle's outer layer at the anterior and posterior insertion sites. The interventricular septum, which separates the right and left ventricles, is shared by both chambers [11]. Unlike the heart, which has a thick walled muscle structure, the atria have thin walls and receive their blood through low-pressure veins. The tricuspid valve in the right heart and the mitral valve in the left heart are two examples of valves that divide the atrium from the corresponding ventricle and guarantee one-way flow through the pump by preventing backward flow during the vigorous contraction of the ventricles. The free ends of these valves attach through chordae tendinae to the papillary muscles that arise from the ventricular walls via fibrous rings that encircle each valve annulus [1]. Ventricle-to-atrioventricular pressure gradient controls valve opening and closure primarily. The papillary muscles, on the other hand, contract in unison with the rest of the heart's muscles and assist keep the valve leaflets in the appropriate place during contraction, preventing regurgitant (backward) flow. In order to maintain unidirectional blood flow, the aortic and pulmonary valves separate

each ventricle from its associated arterial link. These valves prohibit blood from returning to the ventricle from the arteries they separate. The magnitude of the pressure difference across the valves determines whether or not they are open [12]. Heart and lungs are linked in a closed loop to form a cardiovascular system. The average human heart is around the size of a fist and weighs anywhere from 200 to 425 grams, depending on the individual. There are approximately 2,000 gallons (7,571 liters) of blood-flow occur every day on an average heartbeats of 100,000 per day [13]. Heartbeats take around 864 milliseconds to complete on average Heart and blood vessels (arteries, capillaries and veins) make up the circulatory system together with blood.



Source: <https://rb.gy/qldp1r>

Figure 1. 2: Simplified structure of the human heart, and direction of blood flow through the heart chambers and heart valves.

The circulatory system includes the heart as well as the arteries and veins that carry blood all over the body. To be alive, blood must be constantly pumped through the body. It is responsible for transporting oxygen from the air we breathe to all of the cells in our body. Circulation moves through arteries, capillaries, and veins because of heart pumping action. A single pair of blood veins carries oxygen-rich blood to and from the lungs [14]. Other blood veins provide energy for the organism as a whole. Pulmonary circulation and systemic circulation are both types of circulation. Blood is circulated between the heart and lungs via the lungs' pulmonary circulation system (Figure 1.1 and Figure 1.2). In order to absorb oxygen and expel carbon dioxide, it transfers deoxygenated blood to the lungs for re-oxygenation. After returning to the heart, the

oxygenated blood returns to the lungs. A person's blood is circulated throughout their body via systemic circulation. By returning deoxygenated blood to the heart, it helps keep cells healthy. To initiate systemic circulation, the heart pumps oxygenated blood from the left ventricle into the aorta. The blood returns deoxygenated blood to the right atrium of the heart after supplying oxygen and nutrients to cells all over the body. The right atrium delivers deoxygenated blood to the right ventricle. As a result, blood is pumped from the right ventricle into the pulmonary arteries, where it begins its journey through the body's circulatory system. Upon leaving the heart, blood travels to the lungs, where it picks up carbon dioxide and gives it back to the body as oxygen. In order to restart systemic circulation, oxygenated blood flows from the left atrium to the left ventricle below. Both the circulatory and respiratory systems operate in tandem to keep the body well-oxygenated and to eliminate waste products [15]. The passage of deoxygenated blood into the lungs is made possible by pulmonary circulation. Carbon dioxide is exhaled and is exchanged for oxygen in the alveoli, which are small air sacs in the lungs. Internal respiration is facilitated by systemic circulation. The remainder of the body receives oxygenated blood via capillaries. The blood transports oxygen throughout the body and removes carbon dioxide from the system. Deoxygenated blood leaves the right ventricle and travels via the pulmonary trunk in the pulmonary loop. The right and left pulmonary arteries emerge from the pulmonary trunk. Lung arterioles and capillary beds get deoxygenated blood from these arteries. There's a balance between releasing CO₂ and absorbing O₂. After that, oxygenated blood travels from the capillary beds to the pulmonary veins through venules [16] After passing through the lungs, it travels to the left atrium of the heart, where it is stored. Only the pulmonary arteries and veins transmit oxygenated blood and the deoxygenated blood across the body. The aorta, the body's biggest artery, pumps oxygenated blood from the left ventricle of the heart via the systemic loop. Blood travels from the aorta to the arterioles and capillary beds that nourish the body's tissues through the systemic arteries. During this process, nutrients and oxygen are exhaled while carbon dioxide and other waste products are taken in. Deoxygenated blood is subsequently transported to the systemic veins from the capillary beds through venules. There are systemic veins that feed into the larger body veins called the inferior and superior venae cavae. The venae cavae provide the right atrium of the heart with deoxygenated blood [17] (see Figure 1.3).

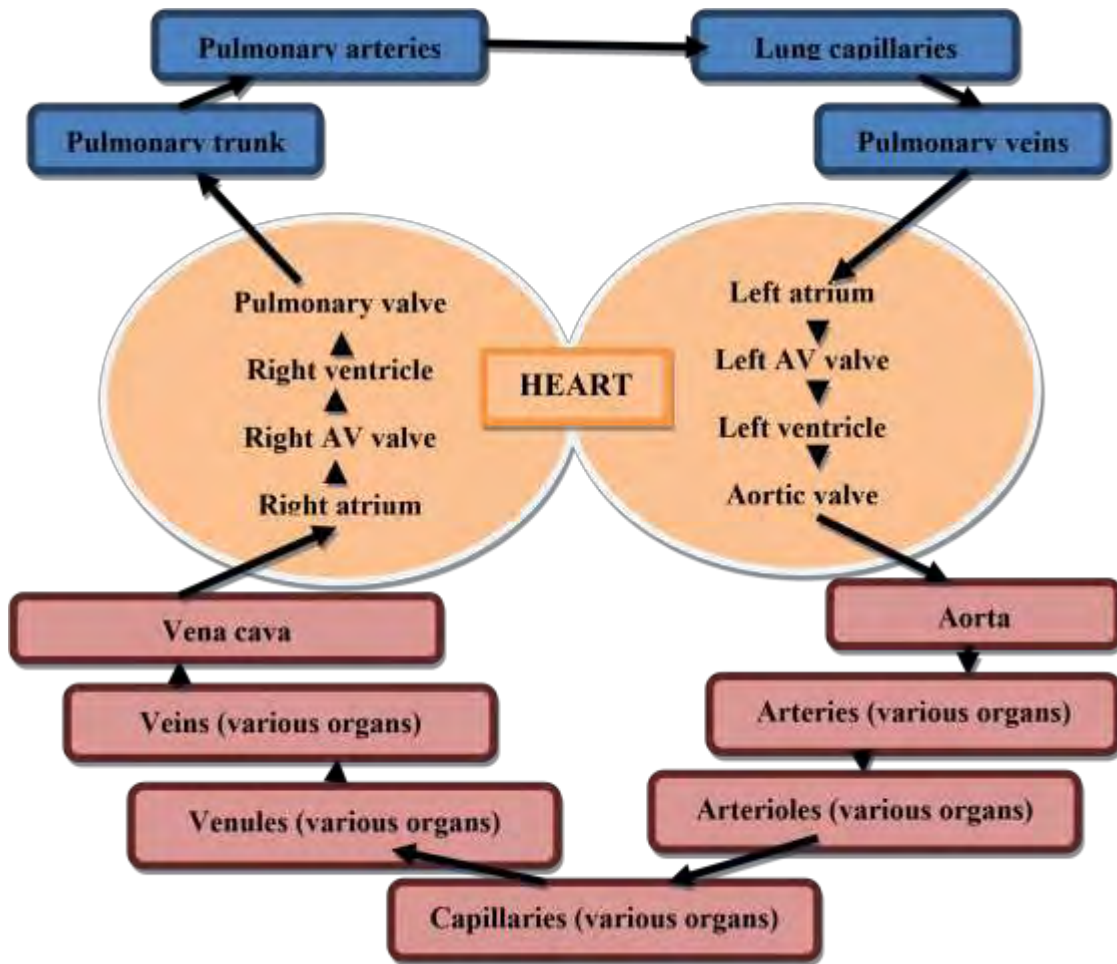


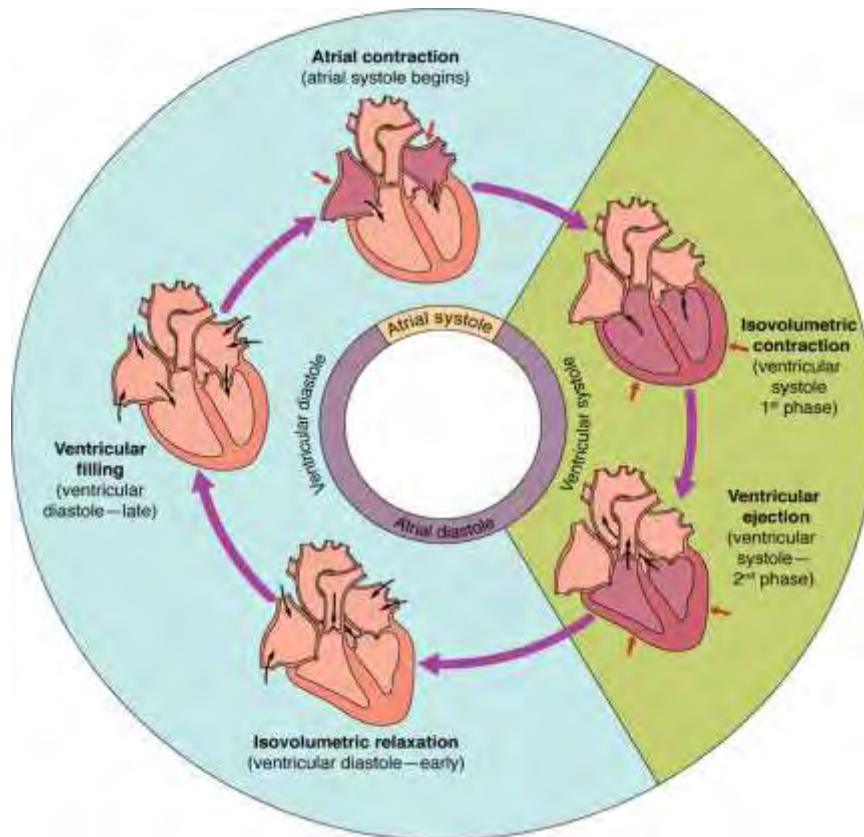
Figure 1. 3: Heart's circulatory relay during systemic and pulmonary circulatory processes [8]

The atria and ventricles are relaxed at the start of the cardiac cycle (diastole). The coronary sinus and the superior and inferior venae cavae provide blood to the right atrium. The four pulmonary veins supply the left atrium with blood. The tricuspid and mitral atrioventricular valves are both open, allowing blood to freely flow from the atria into the ventricles from the heart. This procedure fills the ventricles to a capacity of 70–80%. Closed pulmonary and aortic semilunar valves prohibit blood from flowing backward from the right pulmonary trunk and the left aorta into the heart's right and left ventricles, respectively [18].

1.2 Physiology of Left Ventricle (LV)

The depolarization of the ventricles is followed by ventricular systole (Figure 1.4 and Figure 1.6), which is indicated by the QRS complex on the ECG. It may be broken down into two halves, with each lasting 270 ms in length. A standing adult's ventricles hold around 130 mL of blood toward

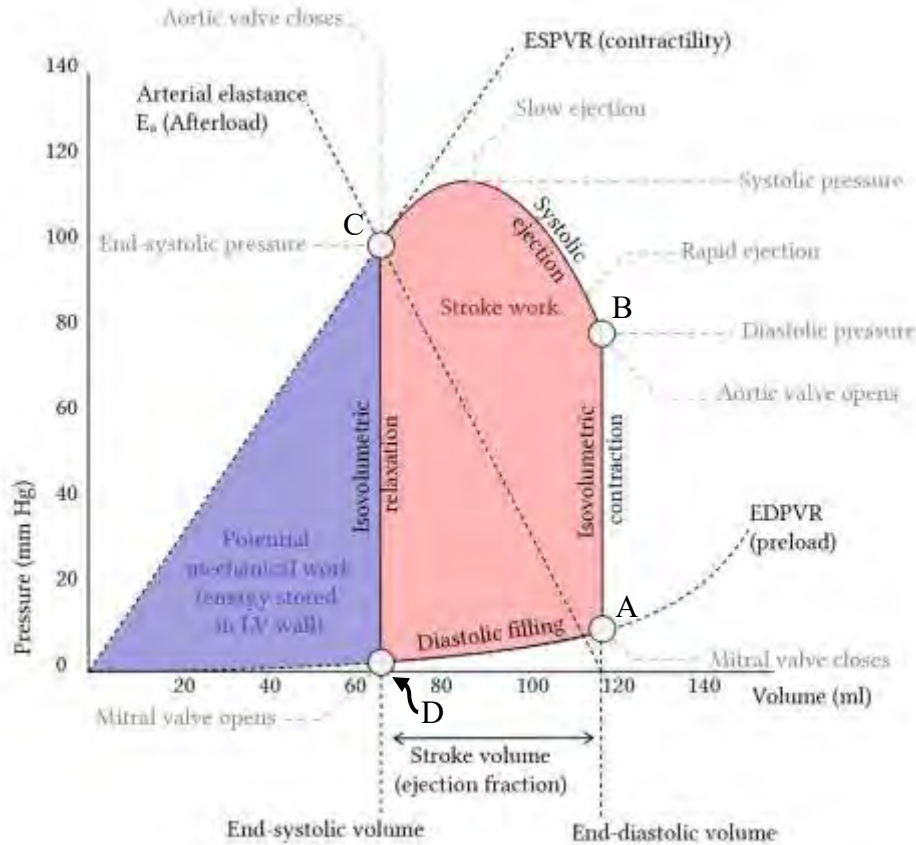
the end of atrial systole and immediately before atrial contraction. Also known as preload, EDV is the last volume of a heartbeat [19]. Although blood pressure increases initially when the ventricle's muscles contract, it is not high enough to open the heart's semilunar (pulmonary and aortic) valves and evacuate the blood. Nevertheless, the blood pressure rapidly exceeds that of the newly relaxed and diastolic atria, and cardiac arrest occurs [20]. As a result of the increased pressure, blood returns to the atria and the tricuspid and mitral valves close. At the early stage of the cycle, no blood is being evacuated from the ventricles hence the total amount of blood is not fluctuating much. When the heart begins to beat normally again, it begins a process known as isovolumetric contraction. At this stage, the pressure in the ventricle is larger than the pressures in the pulmonary trunk and the aorta because the ventricular muscle has been contracted throughout the second phase of systole. The pulmonary and aortic semilunar valves open as blood is pumped from the heart. Because the aortic pressure is so much higher, the pressure created by the left ventricle will be significantly more than the pressure generated by the right ventricle. Despite this, the volume of blood pumped by each ventricle is the same. Stroke volume is the term used to describe this amount of material. In most cases, the volume of a stroke will be between 70 and 80 mL. This suggests that 50–60 mL of blood remains in the ventricle after contraction since ventricular systole began with an EDV of around 130 mL of blood. The end systolic volume (ESV) is the medical term for this amount of blood flow [21].



Source: <https://rb.gy/5inbny>

Figure 1. 4: Cardiac Cycle Overview: The cardiac cycle begins with atrial systole and continues through ventricular systole, atrial diastole, and ventricular diastole before starting all over again. Correlations with the electrocardiogram (ECG) are emphasized

The ventricular wall muscles contract and relax during each cardiac cycle, causing the chamber to stiffen (to reach a peak stiffness at the end of systole) and then to become less rigid during the relaxation phase (to reach its minimal stiffness at the end of diastole). A heart's cyclic rhythm is reflected in the heart's mechanical characteristics, which change over time in a cyclic pattern (Figure 1.5). The pressure-volume diagram may be used to depict the heart's mechanical characteristics as they change over time. For our first step, we will focus at ventricular parameters during systole and diastole at their stiffest points, before moving on to study mechanical properties throughout the cardiac cycle.

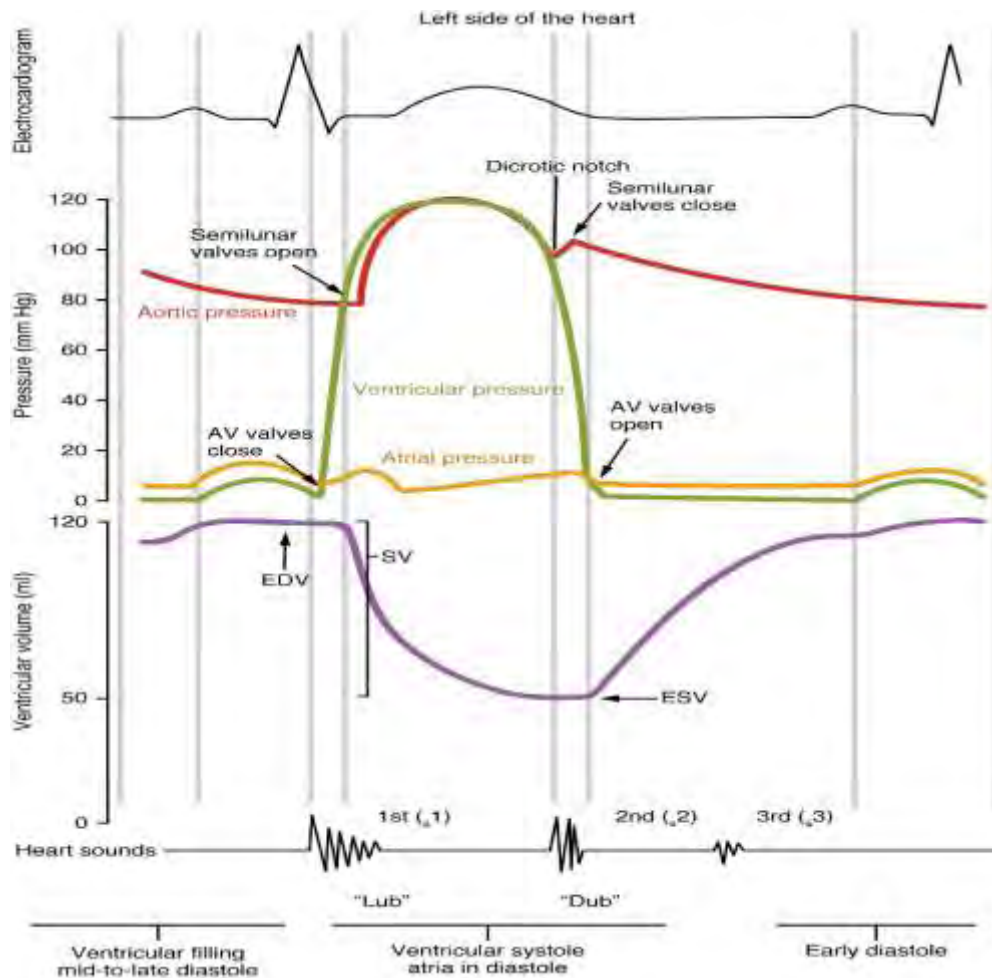


Source: <http://surl.li/apcix>

Figure 1. 5: A typical pressure – volume (PV) loop with identifiable physiological parameters, and ESPVR and EDPVR

Point A marks the end of diastole or, the beginning of systole, as seen in the diagram. The isovolumic contraction phase, where the ventricle contracts with both valves closed, occurs in the initial half of the cycle, where pressure rises but volume remains constant. Ejection commences, the aortic valve opens (B), and volume decreases throughout the ejection phase as the pressure in the ventricular chamber rises. The aortic valve shuts and isovolumic relaxation begins once the ventricular pressure decreases below aortic pressure (C, top left corner of PV loop). Finally, the filling process begins when the mitral valve opens (D, lower left corner) and ends when the valve shuts (A), with the cycle then repeating itself again and again. The PV loop may be used to determine a number of physiologically significant factors and variables (Figure 1.5). End-diastolic volume (EDV) is a terminology used to represent the maximal volume of the cardiac cycle, which may be calculated from point A. (Figure 1.5). Using point D, or the ventricular volume at the conclusion of the ejection phase (the ESV), one may obtain this value, which is known as the

minimum volume (ESV). To calculate how much blood is expelled during each cardiac cycle, EDV and ESV must be compared (SV). The moment at which the ventricle begins to expel (the point at which ventricular pressure barely surpasses aortic pressure and volume begins to decline) may be observed towards the upper right of the loop. Therefore, the diastolic blood pressure is a measure of the pressure in the aorta at the beginning of ejection (DBP). During the ejection phase, the aortic and ventricular pressures are nearly identical. Because of this, the point of maximum pressure on the loop represents the systolic blood pressure in the aorta (SBP). Perceived pressure in the left upper corner of a loop (Pes) indicates end-systolic pressure (Pes). It is the pressure in the ventricle that is at the conclusion of the cardiac cycle (point D in Figure 1.5) and is referred to as the end-diastolic pressure (EDP). During the end-diastolic pressure-volume relationship (EDPVR), the ventricle's passive filling curve occurs. An important factor in determining the line's curvature is how effectively the muscle can contract, as well as how well it can expand (e.g., wall thickness). Ventricle maximum pressure is determined by end systolic pressure-volume relation (ESPVR). PV loops that are limited by both the ESPVR and EDPVR are depicted in Figure 1.5. An end point (end systolic point) in the top left corner of each loop is shown on both the ESPVR and EDPVR. End-systolic elastance, abbreviated as Ees, is a measure of the ESPVR slope. The ventricular contractility is assessed with this test. An ECG, a phonocardiogram, and an aortic, left atrial, and left ventricular pressure and volume Wiggers diagram (Figure 1.5) are all shown in relation to heart cycle time [13].



Source: <https://rb.gy/5inbny>

Figure 1. 6: Wiggers diagram showing aortic, left atrial, left ventricular pressure; left ventricular volume; electrocardiogram; phonocardiogram with respect to heart cycle time [13]

1.3 Physiology of Left Atrium (LA)

There is no simple transport chamber in the left atrium (LA) because of the dynamic nature of its reaction to strain and the production of atrial neuropeptides. Natriuresis, vasodilatation, and suppression of the sympathetic and renin-angiotensin-aldosterone systems allow for partial correction of fluid and hemodynamic balance [22]. In addition, an increased risk of stroke, transient ischemic attack TIA, congestive heart failure (CHF), atrial fibrillation (AF), and other cardiovascular events can be predicted by an increased size of the LA. There are generally three integrated stages of left atrial function: reservoir, conduit, and booster-pump (Figure 1.7) [23-24]. During LV systole, the LA acts as a reservoir for pulmonary venous return, storing it during contraction and isovolumic relaxation. During ventricular diastole, the LA acts as a conduit for

blood to enter the LV. When atrioventricular rhythm is present, the LA actively contracts during the last part of diastole and contributes between 15% and 30% of the LV stroke volume [23-24]. Due to the fact that the LA empties into the LV, its size and function are heavily dependent on the LV's compliance during diastole. By boosting end-diastolic volume and pressures in patients with ventricular failure, the active contractile component of the LA plays a crucial role in enhancing ejection force. It's also a compensatory mechanism in people with less-than-perfect ventricular compliance. When atrial contraction is lost due to conditions such AF or unsynchronized ventricular pacing, cardiac output is reduced by 20% [25]. Due to improved reservoir function, the atrioventricular pressure gradient may be maintained during diastole and the LA booster function can be augmented by increased preload. According to the LA reservoir and booster functions as well as the conduit's conduit function is not supported. When there is a drop in LA compliance, the LA's conduit function rises. In reaction to changes in hemodynamics, the LA may be able to optimally allocate LV filling across reservoir, conduit, and booster-pump functions [26].

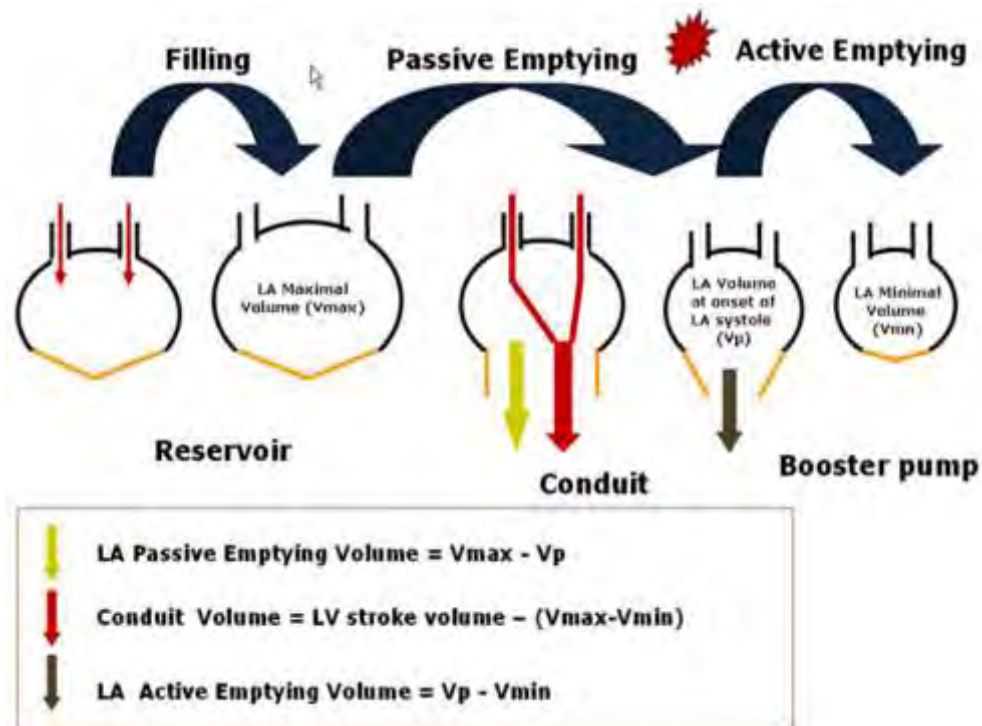


Figure 1. 7: Phases of left atrial function. During ventricular systole, the left atrial chamber operates as a reservoir for blood from the pulmonary vein, whereas during ventricular diastasis, the left atrial chamber serves as a conduit for pulmonary vein flow that empties into the ventricle once the mitral valve opens. During ventricular end diastole, the left atrium finally contracts and actively empties, completing ventricular filling. LV, left ventricle; V_p , left atrial volume before atrial contraction; V_{max} , maximum volume (measured at left ventricular end-systolic phase); and V_{min} , left atrial minimum volume (as defined at left ventricular end-diastolic phase) [27]

The LA pressure–volume loop is made up of an active (A) loop that represents the LA stroke work and a passive (V) loop that represents the entire passive elastic energy stored by the LA during reservoir phase. The slope of the end-systolic pressure–volume relationship quantifies changes in the inotropic condition of the lungs. The pressure–volume loop may test LA static compliance by measuring the slope of the line between the A loop's minimal LA pressure and the V loop's maximum LA pressure (Figure 1.12).

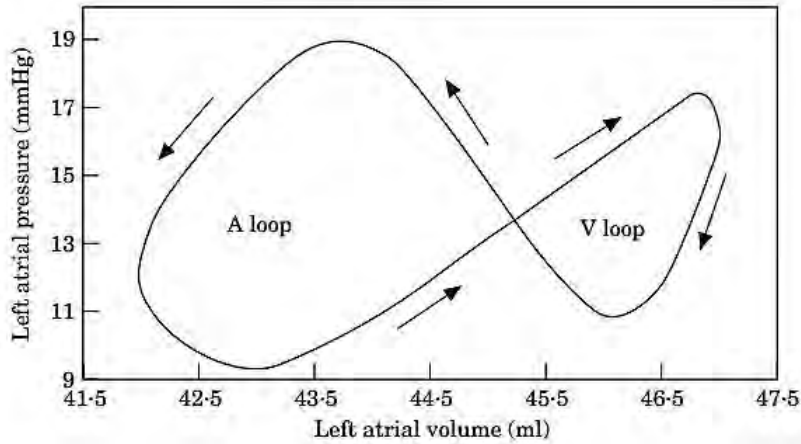


Figure 1. 8: Pressure volume loop of the left atrium (LA)

By changing the left atrium contractility, the ESPVR slope of both left atrium and left ventricle have been changed. By increasing the contractility the slope of the ESPVR has been increased and vice-versa.

1.4 Heart Failure and Ejection Fraction

Blood flow through the left ventricle (or right ventricle) is measured by the ejection fraction (EF). The quantity of blood pumped out of the left ventricle each time it contracts is commonly referred to as the EF (ejection fraction). The heart's primary pumping chamber is the left ventricle. End diastolic volume (EDV) is the unit used to measure EF. The lower the EF, the more likely it is that the heart is failing. Heart failure (HF_rEF) may be diagnosed based on an individual's EF, which indicates how serious their illness is. With each heartbeat, the left ventricle (the primary pumping chamber) pumps a portion of the heart's blood out of the left ventricle and into the rest of the body. This is the percentage of blood pumped from the right ventricle of the heart to the lungs for oxygenation. Most of the time, "ejection fraction" refers to the percentage of the left ventricle that pumps blood out of the heart.

The EF can be measured in several clinical ways such as echocardiogram (ECG), magnetic resonance image (MRI) scan of the heart, and nuclear medicine scan or multiple gated acquisition (MUGA) of the heart also called a nuclear stress test. Among these methods, the ECG is the most commonly used method to measure the EF. The EF is critical in determining whether or not a patient's heart is healthy or unwell. Having heart failure indicates that a person's heart isn't pumping as efficiently as it should be. From 55% to 70% of the heart's blood flow is considered normal [4]. As an example, having an LVEF of 65 percent indicates that 65 percent of the left ventricle's total blood volume is pumped out of the body with each pulse. Because of an individual's cardiac disease and how effectively their medication is working, one's EF might fluctuate wildly.

- Ejection Fraction (EF) %: 55% to 70%
 - ✓ Pumping Ability of the Heart: Normal
 - ✓ Level of Heart Failure/Effect on Pumping: Heart function may be normal or may have heart failure with preserved EF (HFpEF).
- Ejection Fraction (EF) %: 40% to 54%
 - ✓ Pumping ability of the heart: Slightly below normal
 - ✓ Level of heart failure/effect on pumping: less blood is available so less blood is ejected from the ventricles. There is a lower-than-normal amount of oxygen-rich blood available to the rest of the body. The patient may not have symptoms then.
- Ejection Fraction (EF) %: 35% to 39%
 - ✓ Pumping ability of the heart: Moderately below normal
 - ✓ Level of heart failure/effect on pumping: Mild heart failure with reduced EF (HFrEF).
- Ejection Fraction (EF) %: Less than 35%
 - ✓ Pumping ability of the heart: Severely below normal
 - ✓ Level of heart failure/effect on pumping: Moderate-to-severe HFrEF. Severe HFrEF increases the risk of life-threatening heartbeats and cardiac dyssynchrony/desynchronization (right and left ventricles do not pump in unison).

Patients with heart failure due to left ventricular dysfunction require regular consultations with their doctors to monitor their progress. A pacemaker or an implantable cardiac defibrillator may be recommended in some cases, depending on the underlying cause. Cardiac resynchronization

therapy or cardiac contractility modulation may be beneficial in some moderate or serious cases. If the disease persists despite all other treatments, a ventricular assist device (for the left, right, or both ventricles) or a heart transplant may be necessary. It is a prevalent, expensive, and possibly deadly condition known as heart failure. Adults have heart failure at a rate of 2 percent, but this rises to 6–10 percent among those over 65. Rates are predicted to rise. About 35 percent of people who are diagnosed die within the first year of their diagnosis, whether this number drops to fewer than 10 percent by the second year of the diagnosis [2].

Due to the overwork of the ventricle, a failing heart may have a lower contraction force. In a normal heart, increasing ventricular filling leads to an increase in contraction force, which results in an increase in cardiac output. Due to a dilated ventricle, this process begins to malfunction in heart failure patients, resulting in fewer effective cardiac muscle contractions.

By the side of the heart affected, a historical way of classifying heart failure has been used in the past (right heart failure versus left heart failure). It was formerly considered that the lungs were compromised by right heart failure, while the aorta was compromised by left heart failure, which affected the brain and all of the rest of the body's systemic circulation. Many patients have a combination of symptoms, including both right and left heart failure. Heart failure type may be more accurately classified by measuring ejection fraction, which is the percentage of blood pumped out of the heart during a single contraction. End-diastolic volume (EDV) is divided by stroke volume (SV) to get the ejection fraction (EF), which is the percentage of EDV that is expelled every beat.

$$EF(\%) = \frac{SV}{EDV} \times 100\%$$

Where the stroke volume is given by, $SV = EDV - ESV$

It is important to know that there are two forms of heart failure such as heart failure with reduced ejection fraction (HFrEF): HFrEF occurs when the ejection fraction falls below 40% [4]. This happens when the left ventricle contracts properly, but does not relax correctly during diastole, since the ventricle is stiff. This hampers filling, which results in heart failure with preserved ejection fraction (HFpEF).

Another type of heart failure is acute or chronic. Decompensated heart failure can cause acute breathing problems that aggravate chronic heart failure symptoms. An ongoing condition, chronic

heart failure is managed by addressing the symptoms. A rise in left ventricular diastolic pressure due to an increase in cardiac demand can cause high-output heart failure, which can lead to pulmonary congestion. Heart failure can be caused by a number of other conditions, however they should not be confused with HF. When the heart stops beating, it is called cardiac arrest or asystole. When left untreated, they might lead to an untimely death. Due to a lack of blood flow to the heart muscle, myocardial infarction (also known as "heart attack") occurs. Specifically, cardiomyopathy refers to the heart muscle's abnormalities, which can lead to heart failure. Myocardial infarction caused by ischemic cardiomyopathy shows that coronary artery disease is to blame. Having dilated cardiomyopathy indicates that the damage to the heart muscle has caused it to expand. Hypertrophic cardiomyopathy, on the other hand, is characterized by heart muscle expansion and thickening [28].

1.4.1 Heart Failure with Preserved Ejection Fraction (HFpEF)

HFpEF (heart failure with preserved ejection fraction) is a clinical condition in which individuals suffer heart failure symptoms while having an ejection fraction of the left ventricle of 50% or above [29]. A variety of diseases can contribute to HFpEF, making treatment more difficult. Hypertensive heart failure (HFpEF) is on the rise because of an aging population and rising risk factors such as hypertension, diabetes, and obesity (Figure 1.9). It has the potential to be a massive drain on already overstretched healthcare systems across the world.

However, the diagnosis of heart failure with an abnormal echocardiographic parameter might be difficult, as there is no one faulty echocardiographic parameter that can accurately identify it. There must be a careful evaluation of all the echocardiography data, including left ventricular mass and the volume of the left atrium [30].

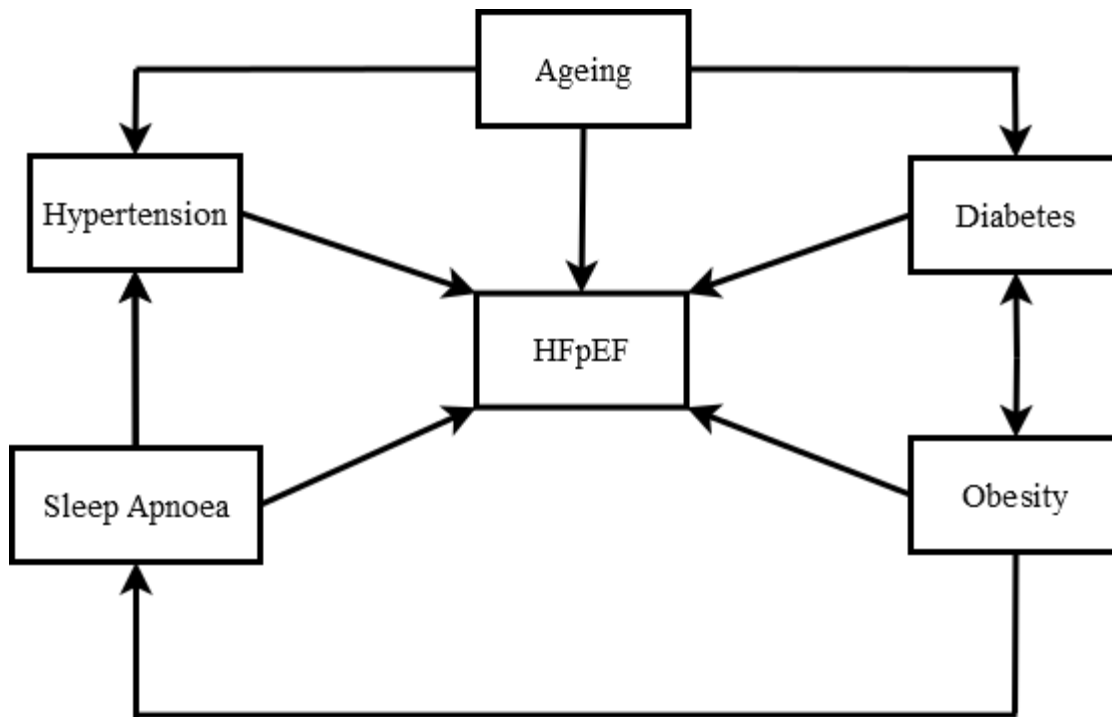


Figure 1. 9: HFpEF, or heart failure with preserved ejection fraction, as well as the risk factors associated with it (comorbid diseases)

When the heart pumps blood, two factors come into play: (a) the contraction of cardiac muscle, or how well the heart squeezes; and (b) the size of the blood vessels. A heart's ability to relax and reabsorb blood

A patient's heart failure is classified according to which of those two functions is impaired [13]. Heart failure with a low ejection fraction (HFrEF) occurs when the heart muscle is too weak. Heart failure with preserved ejection fraction (HFpEF) and heart failure with reduced ejection fraction (HFrEF) are two different terms for the same underlying condition.

Left ventricular diastolic dysfunction due to hypertrophy of the left ventricle is the most prevalent cause of HFpEF, which is characterized by high left ventricular filling pressures (Figure 1.2). LVH (left ventricular hypertrophy) is a classic example of this, in which prolonged systemic pressure overload induces an increase in left ventricular muscle mass. Hypertrophy induces myocardial ischaemia, which results in fibrosis and stiffness of the left ventricle as a result of myocardial blood supply being overwhelmed by hypertrophy. In certain individuals with HFpEF, concentric hypertrophy can shrink the left ventricle, resulting in a reduced stroke volume, even if the patient's ejection fraction may appear to be normal. In the same way that long-term high blood pressure causes LVH, significant aortic stenosis does the same.

1.4.2 Progression of HFpEF

Elderly people are more likely to suffer from heart failure (HF) because they are more likely to suffer from HFpEF, which has no effective treatment options. Heart failure with preserved ejection fraction (HFpEF) has emerged as a common heart illness with a significant risk of both short-term and long-term death [31]. Systolic function may be compromised in individuals with HFpEF, however, this has not been adequately studied so far. HFpEF, on the other hand, has been linked to an ever-decreasing impairment of the LV-systemic artery interaction [32]. In recent studies, it has shown that the evolution of HFpEF is influenced by LV diastolic dysfunction, ventricular remodeling, hypertension, myocyte stiffness, hypertrophy, fibrosis, and so on. HFpEF is a disease that progresses at a much slower rate in people with a wide range of genetic and environmental risk factors. Pre-clinical diastolic dysfunction (PDD) through the ultimate clinical phases of diastolic dysfunction (DDD) are poorly understood. HFpEF and other more complicated clinical models with multi-organ involvement, akin to heart failure with reduced ejection fraction (HFrEF), continue to advance clinically in a manner that is poorly understood in the subclinical stage of PDD. Patients with HFpEF need to be studied in order to understand the natural development of their condition and to determine the specific left ventricular remodeling, or other associated physiological variation, that explains this progression. There are several shortcomings in the design of the relevant clinical studies, and the therapy is empiric at best [33]. Multiple factors are thought to be involved in the pathophysiology of HFpEF [34]. A growing number of patients are being diagnosed with HFpEF because of diastolic LV dysfunction as a result of age and other comorbidities. When it comes to diastolic LV function and the emergence of clinical symptoms of heart failure (HF) syndrome, comorbidities play an important role [33]. In order to better understand how the HFpEF develops, it is likely that we need to better understand what causes it.

1.5 Finite Element Analysis of Human Heart

Combining imaging sciences with mathematics, informatics, and cardiovascular biology, computational modeling of the heart aims to increase mechanistic knowledge, inspired diagnostics, and novel therapeutics for cardiovascular illness. Since the emergence of high medical imaging, there has been an increase in the ability to create realistic three-dimensional (3D) computer models of blood arteries and the heart. Finally, an effective FEM (Finite Element Method) solver is used to solve the 3D model of the heart. Furthermore, the rise in clinical data has made cardiovascular

informatics a better discipline. A sophisticated patient-specific model of cardiovascular disease may be created using 3D computer models of heart architecture with function and clinical data. Cost-effectively, computational simulations may be used to develop the mechanical and biological properties of cardiovascular system components. For example, an electrical model of the myocardial may be simulated after the heart's anatomy, and structure have been established in 3D. Electromechanical heart models may also simulate the overall organ function to structures from the molecular level [35]. Electromechanical performance may be affected by pathological alterations in the heart structure and function. Researchers have devised ways to represent both forms of remodeling. There has been a significant advancement in the field of cardiovascular modeling, which is moving toward customized treatment. Cardiac and vascular hemodynamics are studied separately. The former includes blood flow in heart chambers, while the latter confers blood transport to/from these chambers via cardiac vessels. More advanced computational modeling focuses on the circulation of smaller arteries by combining more complex mathematical lumped-parameter models to simulate the heart's cycle. As boundary conditions play a substantial role in the validity of computational hemodynamic models, their accurate establishment is critical. Consequently, lumped-parameter models may be used in computational investigations of bigger vascular hemodynamics to adjust the boundary conditions of the external arteries. It has been widely accepted by both manufacturers and regulators that computational modeling is a cost-effective and reliable way to optimize device design. Virtual intervention/surgery planning is a viable next step for computational models, in which the type of device, size, and procedural guidelines might be adjusted in complex clinical circumstances [36]. Computational models of the heart confront a number of issues that must be solved before they can be used in clinical settings. Other co-morbidities such as diabetes and pulmonary edema are also associated with cardiovascular pathogenesis, which is launched and accompanied by a number of risk factors such as smoking and obesity. If these perplexing elements are taken into consideration, more accurate prognoses and diagnoses can be made. A significant increase in the usage of FEM approaches to model distinct cardiac compartments has been seen in the last few years [37] in order to accurately simulate the hemodynamic behavior of human physiology. Models of heart failure pathophysiology that may simulate physiological, hemodynamic, and functional characteristics of HFpEF are relatively recent in cardiovascular research, despite their efficacy in predicting pathogenesis to some extent.

1.6 Background and present state of the problem

Recently, heart failure with preserved ejection fraction (HFpEF) has gained clinical significance. When an echocardiogram shows normal or near-normal cardiac performance in the presence of heart failure (HF) symptoms, the term "HFpEF" is used. More than 55% of patients with a normal or preserved ejection fraction may develop heart failure and HFpEF has high mortality rate, both in the short and long term [38]. Though the ejection fraction is preserved apparently, the proper understanding of the left ventricular function in HFpEF patients is not well understood [39]. Moreover, the synergy between the left atrium (LA) and the left ventricle (LV) is also disrupted in HFpEF. The malfunction and remodeling of LA frequently occur in the heart failure patients, as a result of which the proper functioning of the LV is also adversely affected due to having the direct connection between the LV and the LA through the mitral valve [27, 40, 41]. Although numerous clinical studies have found the evidence of LA dysfunction and its adverse effect on LV in HFpEF, the underlying mechanics is not well understood, so far. Moreover, a few modeling studies have addressed this issue and overall, there is lack of modeling studies which aim to investigate the mechanics and pathophysiology of HFpEF patients [42]. Therefore, in the present study, a lumped-finite element modeling framework of left ventricle, left atrium and systemic circulation will be used to assess the significance of left atrial malfunction on the performance of left ventricle in HFpEF patients.

1.7 Objectives of the Study

Closed-loop lumped parameter circulatory model combined with finite element model of LV with realistic geometry and microstructures will be utilized to simulate the cardiac cycle in a normal subject and HFpEF patient. The models will be calibrated using data from the available literature review of a healthy subject and HFpEF patient.

The specific aims of this study are:

- i. To calibrate a lumped-finite element modeling framework of left ventricle, left atrium and systemic circulation to simulate HFpEF patients by matching the simulation results with the previously published clinical data.
- ii. To evaluate the effects of the alteration of left atrial contractility, stiffness, volume and pressure on the left ventricular function in HFpEF patients. The LV function will be quantified by estimating the PV loops, circumferential, longitudinal and radial strains.

CHAPTER 2

LITERATURE REVIEW

Heart disease is a leading cause of mortality worldwide. Understanding the mechanics of a healthy and sick heart is becoming easier due to computer models. FE modeling of the heart with realistic geometry and architectural construction of cardiac muscle fibers has improved dramatically over the past few decades. Using these models, researchers have been able to connect electrophysiology and mechanics and accomplish long-term remodeling of the heart. As opposed to animal and clinical research, computer models are increasingly being utilized to describe heart disease pathogenesis and treatment processes, such as cardiac resynchronization therapy and surgical ventricular restoration [43]. Because of their variety and low cost, computational models can augment animal and clinical investigations. Only a few factors may be modified in animal research without impacting the others. Distinguishing between distinct variables that may have an impact on the pathophysiology of heart disease is challenging as a result. Computer models that are verified using physiological principles are repeatable and may be used to explore the impact of individual parameters without having to consider the confounding effects of other parameters [44]. There are still a number of concerns that need to be addressed and aspects that need to be improved. The researchers will be able to address crucial outstanding concerns regarding human heart illnesses that can't be answered through experiments, according to realistic cardiac models. Models such as this allow for rapid development of a patient-specific medicine plan in the event of an emergency, which is time-consuming in the traditional treatment procedure.

Literature suggests that either a FE model of the heart or an electrical analog of the circulatory system was constructed separately or was connected to the FE model in open [43] or closed loop [37]. A simplified description of the heart's peripheral system, based on a time-varying elastance function, was used to build the coupled electrical analog. Open-loop circulatory modeling frameworks are commonly used in which outlet boundary constraints are combined with a Pulsatile model to simulate ejection of blood. Physiological factors constrain the process's outcomes. Isovolumic phases and expansion can be reproduced by expanding and constricting the ventricular cavity capacity. With the help of both of these approaches, the modeling framework's free parameters are optimized to simulate real-world heart function by creating a closed pressure volume loop. Since the entire amount of blood in the cardiovascular system is naturally preserved, a closed-loop circulatory modeling framework appears to be more physical. A highly idealized

electrical circuit, such as a resistor, capacitor, and voltage generator, is used to simulate the ventricular-arterial interactions and the peripheral cardiovascular system. The modeling of cardiac fiber contraction has been a key difficulty from the beginning of the mathematical modeling of the cardiovascular system. An early version of this concept relied on the forced contraction of heart muscle as a result of mechanical factors in the surrounding environment. However, this is a faulty representation of heart function. To ensure that model predictions are compatible with well-established physiological principles at the entire heart level, accurate description of ventricular active contraction activity is critical. Calcium ion association-dissociation, the amount of actin sites accessible to respond with myosin, classical kinetics, differential equation, etc. are all involved in the complex process of active contraction. In cardiac muscle, a variety of constitutive relationships [45] for active fiber stress were postulated. There are various parameters that may be used to match experimental data from the literature. Research on active contraction is ongoing and this definition is continually being refined.

Heart failure with preserved ejection fraction (HFpEF) affects approximately half of all chronic HF patients (HFpEF). With death rates equivalent to those of heart failure with reduced ejection fraction (HFrEF), the incidence of HFpEF is growing at a rate of around 1 percent per year [4]. Patients with HFpEF tend to be older and have higher levels of blood pressure [4]. No established therapy option exists for HFpEF patients, despite novel medicines being presented and identified. Cardiomyocyte stiffness, concentric hypertrophy, delayed LV relaxation, and other pathological characteristics hinder LV filling. Prior to this study, diastolic dysfunction, which was previously known as diastolic HF [46], was the only cause of HFpEF. Recently, research has shown that myocardial contractility may also be reduced in individuals with HFpEF. This raises doubts about the initial claim that systolic function is unaffected by the condition since EF remains unaffected. Normal or increased end-systolic elastance (E_{es}) has been seen in patients with HFpEF. This shows that global ventricular contractility may be maintained or perhaps increased. On the other hand, hearts with HFpEF diagnoses show reduced global longitudinal strain, indicating that myocardial contractility is impaired. By using clinical or experimental investigations, it is challenging to resolve these obvious contradicting observations. This condition is also associated with an increase in the patient's heart mass, as well as an increase in the patient's cardiovascular resistance (afterload). As a result, the relationship between myocardial contractility and longitudinal strain is obscured by these factors. However, computational modeling frameworks

automatically alleviate this challenge by identifying the parameters that influence LV function and development in HFpEF patients. Consequently, it is feasible to identify the specific roles and contributions of these components at various phases of HFpEF development. However, computer modeling has only been used in a few studies to better understand ventricular mechanics in heart failure with preserved ejection fraction (HFpEF). As understanding the mechanisms for progression of HFpEF provides the opportunity, to target these mechanisms in therapeutic or preventive strategies, the transition among stages of HFpEF is an area of intense research [34]. When it comes to understanding how HFpEF progresses, the usual approach is to focus on the structural remodeling of the left ventricle, which includes left ventricular hypertrophy, as well as variables such as hypertension, left ventricular diastolic dysfunction and left atrial dilation [47]. There have been just a few investigations to date on the mechanisms underlying the pathophysiology of HFpEF. Increased myocardial stiffness was found to have an impact on HFpEF development in a recent computational analysis [46].

The malfunction and remodeling of LA frequently occur in heart failure patients, as a result of which the proper functioning of the LV is also adversely affected due to having the direct connection between the LV and the LA through the mitral valve. The operation cycle of the LA comprises three different phases such as reservoir, conduit, and booster pump. In the reservoir phase, the LA gets blood from the pulmonary veins during the systole of LV. Mechanistically, the reservoir phase is determined by the relaxation and contraction of the LA and LV, respectively. The conduit phase vacates the LA while the booster pump phase is in its end-systolic condition and the LV is at its end-diastolic condition. In addition, due to the nature of the cardiac cycle, the LA acts as a turning point between the pulmonary circulation and the LV, flow oscillations, and pressure. Therefore, the impairment of LA can excessively accelerate the blood flow pressure on the vasculature circulation which in turn promotes the worsening and dysfunction of pulmonary hypertension (PH). The relaxation and contraction of chamber volumes can be characterized by the mechanical properties of the heart, for example, atrial compliance, elastance, stiffness, preload, afterload, scaling factor, passive stiffness, relaxation time etc. [1, 48].

Bytyçi and Bajraktari [4] have conducted a clinical study to investigate the effect of the changes of LA on the preliminary stages of patients with heart failure with preserved ejection fraction (HFpEF). The authors have implemented a complete M-mode, Doppler, and 2-dimensional echocardiographic analysis in consecutive 79 patients with different classes of HFpEF according

to NYHA standard. They have found that during the initial stages of diastolic dysfunction, the emptying fraction of LA has been decreased while the least LA volume and LA mass has been increased. A clinical study has been performed by M. Tamargo et al. [49] to make a comparison between the HFpEF patients with and without mitral regurgitation (MR). They have chosen 280 patients to conduct their experiment where 163 patients were non-MR-HFpEF and 117 were MR-HFpEF. They have found that the MR HFpEF patients possessed increased LA volume mitral annual dilatation, decreased LA compliance and strain. A similar investigation has been performed by A.B.S. Santos et al. [50] to make a comparison between healthy controls and the HFpEF patients. They have conducted their research on 175 members where 135 individuals are HFpEF patients and 40 individuals are healthy controls of the same gender and age. They have sought out that the patients with HFpEF have the surpassed conduit, reservoir, and booster pump function as compared to healthy individuals.

A computational study has been performed by Vedula et al. [51] to investigate the impacts of left atrial hemodynamics on the flow patterns in LV. They have utilized computed-dynamic tomographic images to model the heart geometry and have conducted simulations with the implementation of immersed boundary conditions. They have shown that the accelerated circulatory flow by the pulmonary veins (PVs) is the characterization of the hemodynamics in the left atrium. They have also found that the PVs form the complicated interaction of vortex flow which leads to vortex annihilation and vortex breakup, as a result of which, a smooth streamlined flow is produced at the annulus of the mitral valve. Pironet et al. [52] have investigated a numerical simulation study of LA function by utilizing a mathematical model of the cardiovascular circulatory system. They have utilized the cardiac pressure induced from the nature of sarcomere to model the multi-scale properties. They have computed the differences among eight different indices which have been validated with the experimental results. The authors have found the correlation of the accountability of three different stages (reservoir, conduit and pump) of LA volume with the pressure of the LA. A numerical simulation has been carried out by A. Zingaro et al. [53] to study the hemodynamic behavior of LA by using the multiscale Large Eddy Simulation (LES) method. They have focused on twofold purposes in their study such as, acquiring the knowledge of blood flow patterns in LA, and understanding the influence of turbulence effect in the blood flow. They have utilized Variational Multiscale (VMS) - Large Eddy Simulation (LMS) method in their investigation. They have found that the blood flow patterns in LA are transitional

flow from laminar to turbulent. Land and Niederer [54] have nicely presented an investigation regarding the impact of dynamics of left atrial contractility on cardio-vascular performance. The goal of their study is to develop and test a biophysical model of human atrial contraction that can be used to investigate the impact of atrial contraction on whole organ function as well as the implications of remodeling caused by atrial fibrillation on both the atrial and ventricular functions. In this research, we have conducted a multi-scale numerical finite element modelling (FEM) analysis to investigate the influence of LA dysfunction on the function of LV. Nowadays, the number of patients with cardiac disease is increasing rapidly. The most common cardiac disease is mainly due to heart failure with preserved ejection fraction (HFpEF) and heart failure with reduced ejection fraction (HFrEF). Due to the lack of proper clinical investigations and the limitation of research, the actual reason behind the HFpEF and HFrEF is still unresolved. To the best of our knowledge, very limited research has been conducted on the LA dysfunction - which has been clinically found to adversely affect the pressure -volume loop of the LV. As the clinical study is not feasible to perform directly on the human heart in most of cases, it is more suitable to utilize the computational modeling of the human heart. In our study, we have focused to find out the effects of LA dysfunction by changing the LA contractility and stiffness which have a direct influence on the variation of pressure and volume of the LV.

CHAPTER 3

MODELING THE LEFT VENTRICLE AND CIRCULATORY SYSTEM

A finite element model of the left ventricle which is coupled to a lumped parameter systemic circulation model are discussed in this chapter.

3.1 Modeling the Systemic Circulatory System

A LV finite element model was coupled with other systemic circulation compartments using a closed-loop lumped parameter circulatory model.

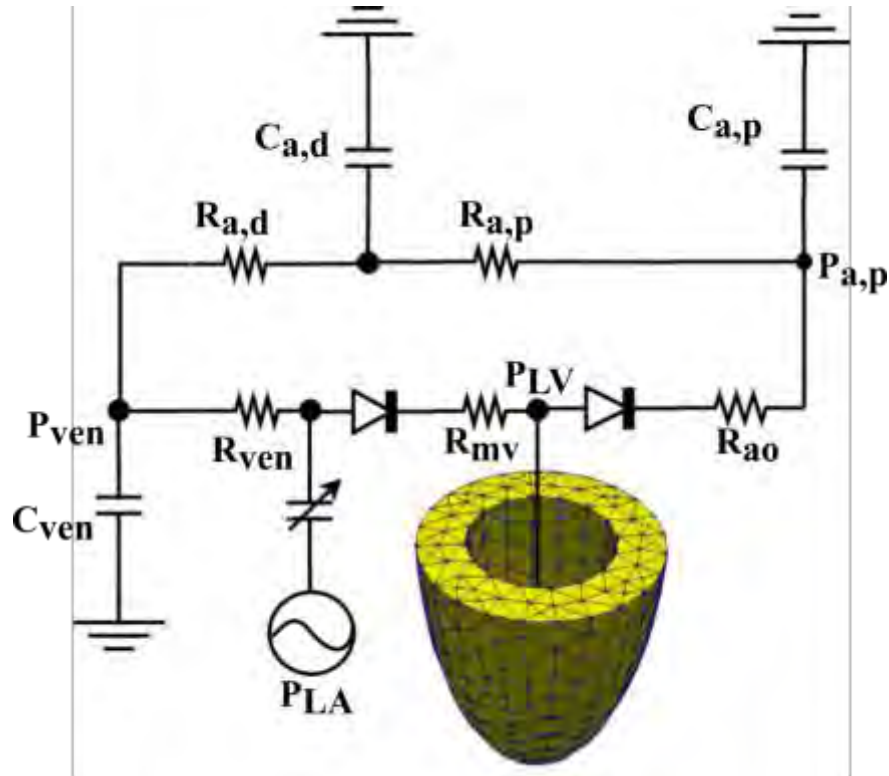


Figure 3. 1: Systemic circulatory compartments and their electrical analogs are shown in a schematic representation of the modeling framework [42]

Electrical analogues were used to model the other components of the systemic circulation (Fig. 3.1). The rate of volume change in each storage compartment of the circulatory system must be connected to the net change of inflow and outflow rates by the following equations (Eq. 1-4) [55] since the total mass of blood in the circulatory system must be conserved.

$$\frac{dV_{LV}(t)}{dt} = q_{mv}(t) - q_{ao}(t) \quad (1)$$

$$\frac{dV_{a,d}(t)}{dt} = q_{a,p}(t) - q_{a,d}(t) \quad (2)$$

$$\frac{dV_{LA}(t)}{dt} = q_{ven}(t) - q_{mv}(t) \quad (3)$$

$$\frac{dV_{ven}(t)}{dt} = q_{a,d}(t) - q_{ven}(t) \quad (4)$$

$$\frac{dV_{a,p}(t)}{dt} = q_{ao}(t) - q_{a,p}(t) \quad (5)$$

Where,

V_{LV} , $V_{a,d}$, V_{LA} , V_{ven} , and $V_{a,p}$ are volumes of LV, distal artery, LA, vein, and proximal artery, respectively, and q_{mv} , $q_{a,p}$, q_{ao} , q_{ven} , and $q_{a,d}$ are volumetric flow rates at various segments. The volumetric flowrates of different components of the circuit are the functions of the corresponding components flow resistances (R_{ven} , $R_{a,p}$, $R_{a,d}$, R_{ao} , and R_{mv}) and the pressure drop between the adjacent compartments. The flow rates are given by the following equations (Eq. 6-10).

$$q_{ven}(t) = \frac{P_{ven}(t) - P_{LA}(t)}{R_{ven}} \quad (6)$$

$$q_{a,p}(t) = \frac{P_{a,p}(t) - P_{a,d}(t)}{R_{a,p}} \quad (7)$$

$$q_{mv}(t) = \begin{cases} \frac{P_{LA}(t) - P_{LV}(t)}{R_{mv}} & \text{when, } P_{LA}(t) \geq P_{LV}(t) \\ 0 & \text{when, } P_{LA}(t) < P_{LV}(t) \end{cases} \quad (8)$$

$$q_{ao}(t) = \begin{cases} \frac{P_{LV}(t) - P_{a,p}(t)}{R_{ao}} & \text{when, } P_{LV}(t) \geq P_{ap}(t) \\ 0 & \text{when, } P_{LV}(t) < P_{a,p}(t) \end{cases} \quad (9)$$

$$q_{a,d}(t) = \frac{P_{a,d}(t) - P_{ven}(t)}{R_{a,d}} \quad (10)$$

The pressure drop in each component is characterized by its volume. The simplified relationships of pressure and volume were implemented for the veins, proximal, and distal arteries, respectively are given in Eq. 11-13.

$$P_{ven}(t) = \frac{V_{ven}(t) - V_{ven,0}}{C_{ven}} \quad (11)$$

$$P_{a,p}(t) = \frac{V_{a,p}(t) - V_{ap,0}}{C_{a,p}} \quad (12)$$

$$P_{a,d}(t) = \frac{V_{a,d}(t) - V_{ad,0}}{C_{a,d}} \quad (13)$$

Where,

$V_{ven,0}$, $V_{ap,0}$, and $V_{ad,0}$ are constant volumes at the rest of the veins, proximal, and distal arteries, respectively. C_{ven} , $C_{a,p}$, and $C_{a,d}$ are the total passive stiffness of the veins, proximal, and distal arteries, respectively. However, the following equations (Eq. 14-17), which explain the contraction of the left atrium using a time-varying elastance function, required that pressure in the left atrium $P_{LA}(t)$ be a function of its volume $V_{LA}(t)$.

$$P_{LA}(t) = e(t)P_{es,LA}(V_{LA}(t)) + (1 - e(t))P_{ed,LA}(V_{LA}(t)) \quad (14)$$

where,

$$P_{es,LA}(V_{LA}(t)) = E_{es,LA}(V_{LA}(t) - V_{0,LA}) \quad (15)$$

$$P_{ed,LA}(V_{LA}(t)) = A_{LA}(e^{B_{LA}(V_{LA}(t) - V_{0,LA})} - 1) \quad (16)$$

And

$$e(t) = \begin{cases} \frac{1}{2} \left(\sin \left[\left(\frac{\pi}{t_{max}} \right) t - \frac{\pi}{2} \right] + 1 \right); & 0 < t \leq 3/2 t_{max} \\ \frac{1}{2} e^{-(t - 3/2 t_{max})/\tau_{LA}}; & t > 3/2 t_{max} \end{cases} \quad (17)$$

In Eq. 15-16, $V_{0,LA}$ is the volume axis intercept of the end-systolic pressure-volume relationship (ESPVR), both A_{LA} and B_{LA} are parameters of the end-diastolic pressure-volume relationship (EDPVR) of the left atrium. EDPVR is depending on stiffness and can be changed by varying A_{LA} , and B_{LA} . $E_{es,LA}$ is the end-systolic elastance of the LA which is a measure of the LA contractility. The driving function $e(t)$ is given in Eq. (17) in which τ is the time constant of relaxation, and t_{max} is the point of maximal chamber elastance. The values of $E_{es,LA}$, $V_{0,LA}$, A_{LA} , B_{LA} , t_{max} , and τ_{LA} are listed in Table 3.1 and 3.2 for individual and combine cases.

Table 3. 1: LA time-varying elastance model parameters for all cases

<div style="display: flex; align-items: center; justify-content: center;"> <div style="text-align: right; margin-right: 5px;">↓</div> Parameter Case ID <div style="margin-left: 10px;">→</div> </div>	LA Contractility (End-systolic elastance, Ees (Pa/ml))		
	Ees1 (Case: A)	Ees2 (Case: B [baseline])	Ees3 (Case: C)
Normal: LA1	47.52	52.80	58.08
LA Stiffness (Scaling factor, A_{LA} (Pa))			
Normal: LA1	A _{LA1}	A _{LA2} (baseline)	A _{LA3}
	48.58	53.98	59.38
LA Contractility (End-systolic elastance, Ees (Pa/ml))			
HFpEF-I: LA1	Ees1	Ees2 (reference)	Ees3
	47.52	52.80	58.08
LA Stiffness (Scaling factor, A_{LA} (Pa))			
HFpEF-I: LA1	A _{LA1}	A _{LA2}	A _{LA3}
	48.58	53.98	59.38
LA Contractility (End-systolic elastance, Ees (Pa/ml))			
HFpEF-II: LA1	Ees1	Ees2	Ees3
	47.52	52.80	58.08
LA Stiffness (Scaling factor, A_{LA} (Pa))			
HFpEF-II: LA1	A _{LA1}	A _{LA2}	A _{LA3}
	48.58	53.98	59.38

Table 3. 2: LA time-varying elastance model for all cases (combine case)

<div style="display: inline-block; text-align: center;"> Parameter → </div> <div style="display: inline-block; text-align: center;"> ↓ Case ID </div>	Combine case				
	E _{es} (Pa/ml)	A _{LA} (Pa)	B _{LA} (/ml)	T _{max} (ms)	τ (ms)
Baseline	60	58.67	0.049	200	35
Normal: LA1	52.80	53.98	0.045	168	33
Normal: LA2	46.66	48.96	0.042	145	30
Normal: LA3	40.66	42.24	0.039	130	25
HFpEF-I: LA1	52.80	53.98	0.045	168	33
HFpEF-I: LA2	46.66	48.96	0.042	145	30
HFpEF-I: LA3	40.66	42.24	0.039	130	25
HFpEF-II: LA1	52.80	53.98	0.045	168	33
HFpEF-II: LA2	46.66	48.96	0.042	145	30
HFpEF-II: LA3	40.66	42.24	0.039	130	25

The LV pressure is a function of its corresponding volume that can be correlated by a non-closed form function

$$P_{LV}(t) = f^{LV}(V_{LV}(t)) \quad (18)$$

The FE method, as described below, was used to determine the functional connection between LV pressure and volume. Table 3.3 lists the parameter values for the closed-loop circulatory model.

Table 3. 3: Fixed values of the model parameters for all simulation cases

Parameter	Unit	Values
Aortic valve resistance, R_{ao}	Pa ms ml ⁻¹	500
Proximal aorta resistance, $R_{a,p}$	Pa ms ml ⁻¹	18000
Distal aorta resistance, $R_{a,d}$	Pa ms ml ⁻¹	145000
Venous resistance, R_{ven}	Pa ms ml ⁻¹	100
Mitral valve resistance, R_{mv}	Pa ms ml ⁻¹	200
Proximal aorta compliance, $C_{a,p}$	ml Pa	0.0032
Distal aorta compliance, $C_{a,d}$	ml Pa	0.033
Venous compliance, C_{ven}	ml Pa	0.28
Resting volume for proximal aorta, $V_{ap,0}$	ml	360
Resting volume for distal aorta, $V_{ad,0}$	ml	40

3.2 Formulation of The Left Ventricular Finite Element model

For the LV finite element formulation, the weak form was obtained via minimizing of these Lagrangian functionals [56, 57]:

$$\begin{aligned}
 & \mathcal{L}(\mathbf{u}, p, P_{cav}, \mathbf{c}_1, \mathbf{c}_2) \\
 &= \int_{\Omega_0} W(\mathbf{u}) dV - \int_{\Omega_0} p(J - 1) dV - P_{cav}(V_{cav}(\mathbf{u}) - V) - \mathbf{c}_1 \cdot \int_{\Omega_0} \mathbf{u} dV \\
 & - \mathbf{c}_2 \cdot \int_{\Omega_0} \mathbf{X} \times \mathbf{u} dV
 \end{aligned} \tag{19}$$

P_{cav} is the Lagrange multiplier used to limit the LV cavity volume $V_{cav}(u)$ to a certain value of V [58] when u is the displacement field, p multiplier enforces tissue incompressibility (i.e., Jacobian of the deformation gradient tensor $J = 1$), and both c_1 and c_2 are Lagrange multipliers that limit rigid body translation (i.e. zero mean translation) and rotation (i.e., zero mean rotation). Vacuum volume V_{cav} in the left ventricle is determined by

Where, Γ_{inner} is the inner surface, n is the normal unit vector, and Ω_{inner} is the enclosed volume by the inner and basal surface at $z = 0$.

The solution produced by minimizing the functional specified pressure-volume relationship of the left ventricular (LV) is necessary for the lumped parameter circulatory model [59]. Using Eq. (19)'s first functional variant, we get the following equation.

$$\begin{aligned}
\delta\mathcal{L}(\mathbf{u}, p, P_{\text{cav}}, \mathbf{c}_1, \mathbf{c}_2) &= \int_{\Omega_0} (\mathbf{P} - p\mathbf{F}^{-T}) \\
&: \nabla\delta\mathbf{u}dV - \int_{\Omega_0} \delta p(J - 1)dV - P_{\text{cav}} \int_{\Omega_0} \text{cof}(\mathbf{F}) \\
&: \nabla\delta\mathbf{u}dV - \delta P_{\text{cav}}(V_{\text{cav}}(\mathbf{u}) - V) - \delta\mathbf{c}_1 \cdot \int_{\Omega_0} \mathbf{u}dV - \delta\mathbf{c}_2 \cdot \int_{\Omega_0} \mathbf{X} \\
&\times \mathbf{u}dV - \mathbf{c}_1 \cdot \int_{\Omega_0} \delta\mathbf{u}dV - \mathbf{c}_2 \cdot \int_{\Omega_0} \mathbf{X} \times \delta\mathbf{u}dV
\end{aligned} \tag{21}$$

Where, F and P are the deformation gradient and first Piola Kirchhoff stress tensor, respectively. δP_{cav} , δc_1 , δc_2 , δu , and δp are the volume constraint, zero mean translation and rotation, variation of the displacement field, and Lagrange multipliers for enforcing incompressibility, respectively. The next step in the Euler-Lagrange equations is to discover $u \in H^1(\Omega_0)$, $p \in L^2(\Omega_0)$, $P_{\text{cav}} \in \mathbb{R}$, $c_1 \in \mathbb{R}^3$, $c_2 \in \mathbb{R}^3$ that satisfies Eq. (22).

$$\delta\mathcal{L}(\mathbf{u}, p, P_{\text{cav}}, \mathbf{c}_1, \mathbf{c}_2) = 0 \tag{22}$$

and $u(x, y, 0) \cdot \mathbf{n}|_{\text{base}} = 0$ (the deformation basal constraints to restrict in-plane) $\forall \delta u(\Omega_0)$, $\delta p \in L^2(\Omega_0)$, $\delta P_{\text{cav}} \in \mathbb{R}$, $\delta c_1 \in \mathbb{R}^3$, $\delta c_2 \in \mathbb{R}^3$.

3.3 The LV's constitutive law

The mechanical behaviour of LV has been described by using the formulation of active stress in the systemic circulation. As a result of this formulation, the stress tensor P may be divided into two parts: a passive one, P_p , and an active one, P_a . In order to calculate the passive stress tensor, we used the formula $P_p = dW/dF$, where W is the strain energy function [59], given by,

$$W = \frac{1}{2}C(e^Q - 1) \tag{23}$$

Where,

$$Q = b_{ff}E_{ff}^2 + b_{xx}(E_{ss}^2 + E_{nn}^2 + E_{sn}^2 + E_{ns}^2) + b_{fx}(E_{fn}^2 + E_{nf}^2 + E_{fs}^2 + E_{sf}^2) \quad (24)$$

C is a material property (unit is Pa) that may be changed to vary the material's stiffness (similar to Young's modulus). To provide polar anisotropic response, the values of material parameters b_{ff} , b_{xx} , and b_{fx} may be changed to modify the stiffness along the direction of myofibers and the plane perpendicular to the myofibers. The values of the material parameters b_{ff} , b_{xx} , and b_{fx} employed in this model are taken from earlier research [59]. The parameter C has been changed to match the normal and HFpEF patients' measured end-diastolic pressure (EDP).

E_{ij} is a component of the Green-Lagrange strain tensor E_{LV} in Equation (24), with $(ij) \in (f, s, n)$ designating the myocardial fiber, sheet, and sheet normal directions, respectively (Figure 3.2).

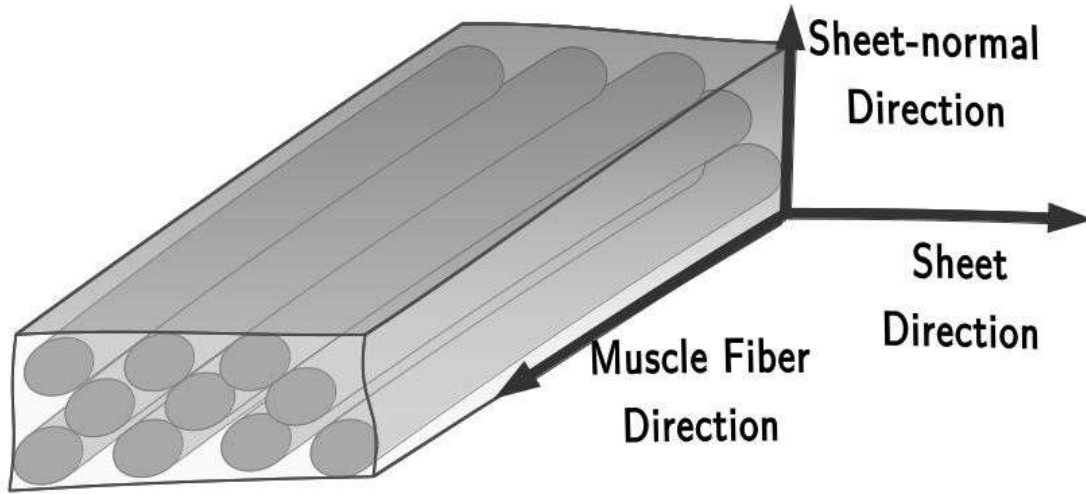


Figure 3. 2: Myocardial fiber direction f , sheet direction s and sheet normal direction n [60].

A modified time-varying elastance model is used to find the active stress P_a along the direction of the local fiber.

$$P_{LV,a} = T_{ref} \frac{Ca_0^2}{Ca_0^2 + ECa_{50}^2} C_t \mathbf{e}_f \otimes \mathbf{e}_{f_0} \quad (25)$$

This equation has four variables: \mathbf{e}_f , \mathbf{e}_{f_0} , T_{ref} , and Ca_0 , which stand for the local vectors describing muscle fiber direction in their present and reference configurations, respectively. The calcium sensitivity ECa_{50} , which varies with length, and the constant C_t are given by Eq. (26-27) [60].

$$ECa_{50} = \frac{(Ca_0)_{max}}{\sqrt{\exp(B(l - l_0)) - 1}} \quad (26)$$

$$C(t) = \begin{cases} \frac{1}{2} \left(1 - \cos \left(\pi \frac{t}{t_0} \right) \right) & t < t_t \\ \frac{1}{2} \left(1 - \cos \left(\pi \frac{t_t}{t_0} \right) \right) \exp \left(\frac{t - t_t}{\tau} \right) & t \geq t_t \end{cases} \quad (27)$$

As shown in Eq. (26), B is a constant, and $(Ca_0)_{max}$ is the highest intracellular calcium concentration, and l_0 is the length of sarcomere at which no active tension arises. As shown in Eq. (27), peak tension is reached in t_0 , isovolumic LV relaxation begins in t_t , and isovolumic relaxation has a time constant of τ . Tabulated in Table 3.3 are the LV model parameter values. Same values have been used for Normal, HFpEF-I and HFpEF-II cases.

Table 3. 4: Fixed parameter values of the LV FE model

Parameter	Unit	Values
Passive Stiffness, C	Pa	125
Exponent of strain energy function, b_{ff}	Unitless	29
Exponent of strain energy function, b_{xx}	Unitless	26.6
Exponent of strain energy function, b_{fx}	Unitless	13.3
Reference Tension (Contractility), T_{ref}	kPa	130
Maximum peak intracellular Ca concentration, $(Ca_0)_{max}$	μ M	4.35
Peak intracellular Ca concentration, Ca_0	μ M	4.35
Parameter for isometric tension-sarcomere relationship, B	μ m ⁻¹	4.75
Sarcomere length at zero-active tension, l_0	μ m	1.58
Time to peak tension, t_0	msec	275
Time to beginning of relaxation, t_t	msec	300

3.4 LV Geometry and Mesh

An idealized prolate ellipsoid has been used to create the LV geometry of normal, HFpEF-I and HFpEF-II cases. According to clinical investigations, individuals with HFpEF have a higher wall-to-cavity diameter ratio (internal dimension) and a longer apex-to-base distance than healthy controls [58, 61, 62]. There have been a few studies that show that in HFpEF patients, the LV cavity diameter is either not substantially different or slightly reduced (although both have a thicker ventricular wall). As a result of the wide range of LV geometry found in HFpEF patients, we applied two different LV geometries to the modelling framework to simulate HFpEF. HFpEF I had smaller LV cavity when compared to a normal LV geometry. HFpEF-II had slightly dilated LV cavity compared to normal case. There was an increase in wall thickness and mass in both HFpEF geometries compared to the typical scenario (Fig. 3.3). The corresponding geometrical parameters have been tabulated in Table 3.5. The LV's wall thickness was re-evaluated in light of prior research [10, 50]. The details of the modeling features of the LV heart geometry model have been illustrated in Figure 3.3.

Table 3. 5: Geometrical dimensions and mass

	Normal	HFpEF I	HFpEF II
WT (cm)	1.13	1.38	1.45
R (cm)	2.00	1.82	2.00
L (cm)	8.30	8.10	8.85
Mass (g)	108.9	127.5	160.2

The LV geometry was discretized (Figure 3.3) using 1100-1650 quadratic tetrahedral components, as indicated by the grid independence test (Section 3.6). Each quadratic element has ten nodes, each with three degrees of freedom (DOF) in three cartesian co-ordinate directions. As a result, each quadratic element has a total of 30 degrees of freedom. The heart's microstructure is fibrous. The left ventricle's myocardial fibers are organized helically across its length (Figure 3.5). Based on earlier experimental observations [62], the helix angle associated with the myofiber orientation in the LV was altered with a linear transmural variation from 60° at the endocardium to -60° at the epicardium in both normal and HFpEF patients (Figure 3.6).

Based on the data shown in Figure 3.3 (d), it has been determined that the origin (O (0, 0, 0)) of the LV model is located in the middle of the basal plane, with a total length of L cm between point O and point C and a thickness of WT cm between the two points A and B of the model. A variety of LV material characteristics, including LA contractility (end-systolic elastance ($E_{es,LA}$)) and LA stiffness (scaling factor for EDPVR (A_{LA})) have been investigated in this computational work. HFpEF of the heart has been achieved by performing geometrical variations in the heart wall thickness, length and the radius of the LV model. The wall thickness has been varied in the range of 1.13 cm to 1.45 cm along the X-axis, while the length of the left ventricular (LV) has been varied in the range of 8.10 cm to 8.85 cm along the Z-axis, in order to achieve the HFpEF of the heart. The inner radius of the LV has been altered in the range of 1.82 cm to 2.0 cm, respectively. The mass has also been varied in the range of 108.9 gm to 160.2 gm to achieve the HFpEF condition.

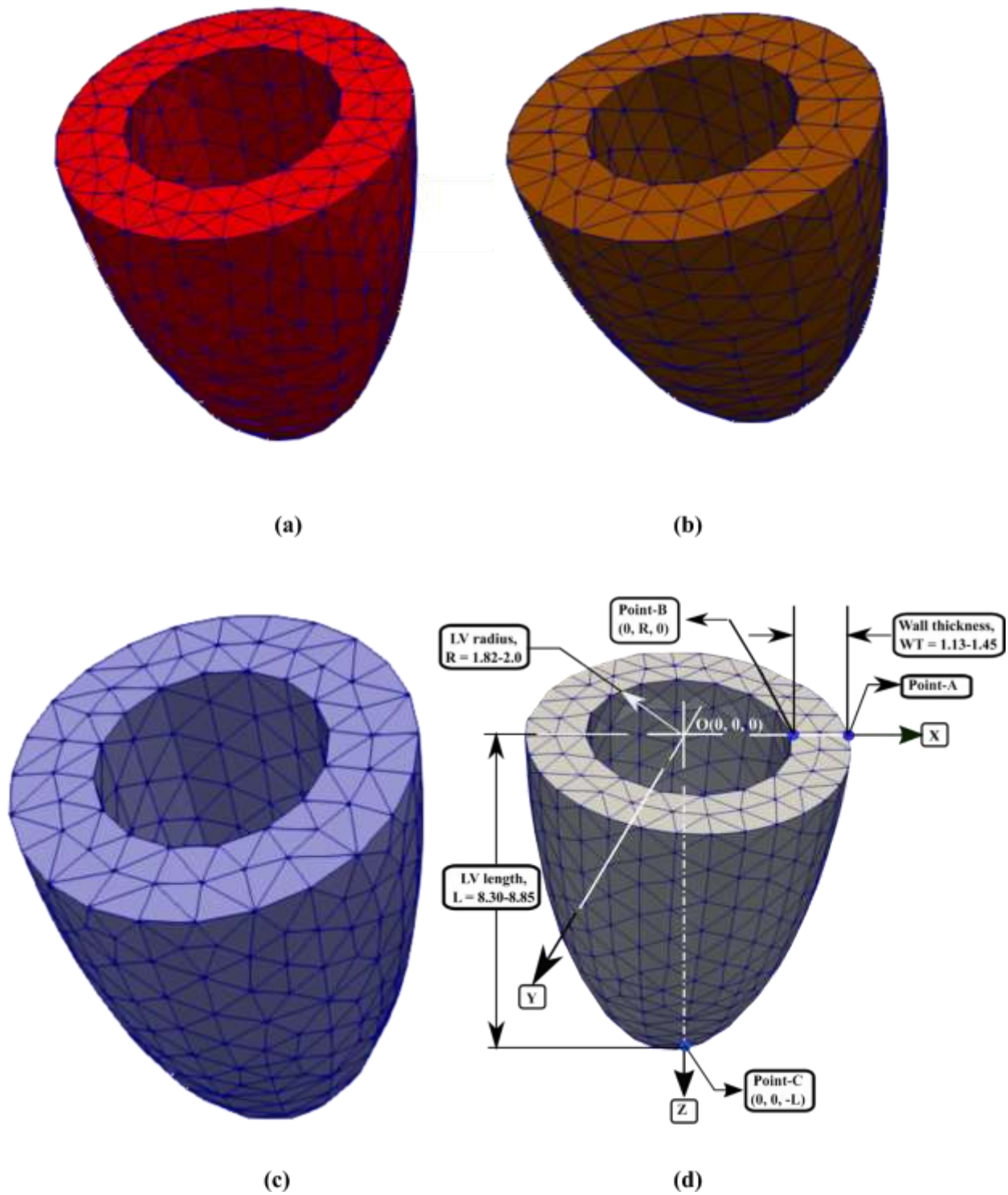


Figure 3. 3: LV geometry defined using a half prolate ellipsoid and discretized with quadratic tetrahedral elements constructed based on the acquired MRI images of (a) normal subject (b) HFpEF-I and (c) HFpEF-II (d) dimensioning of the ellipsoidal LV model of heart geometry

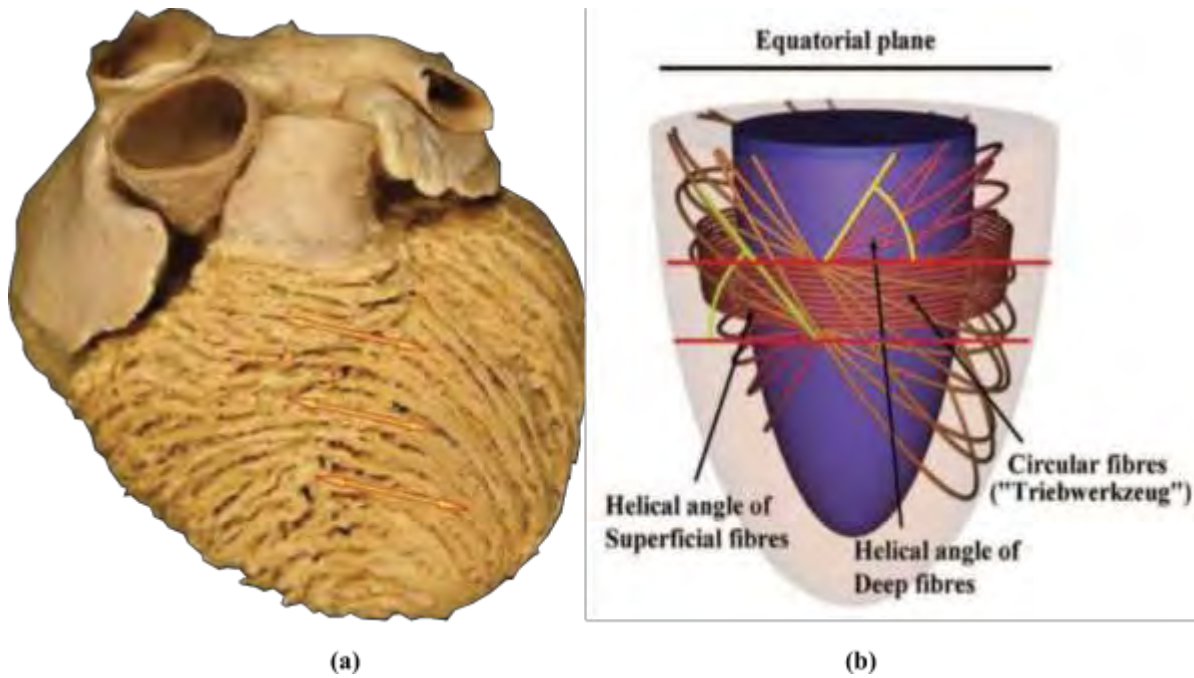


Figure 3. 4: Linear transmural variation of helix angle associated with the myofiber direction from endocardium to the epicardium shown in a (a) real heart image and (b) computational model [42]

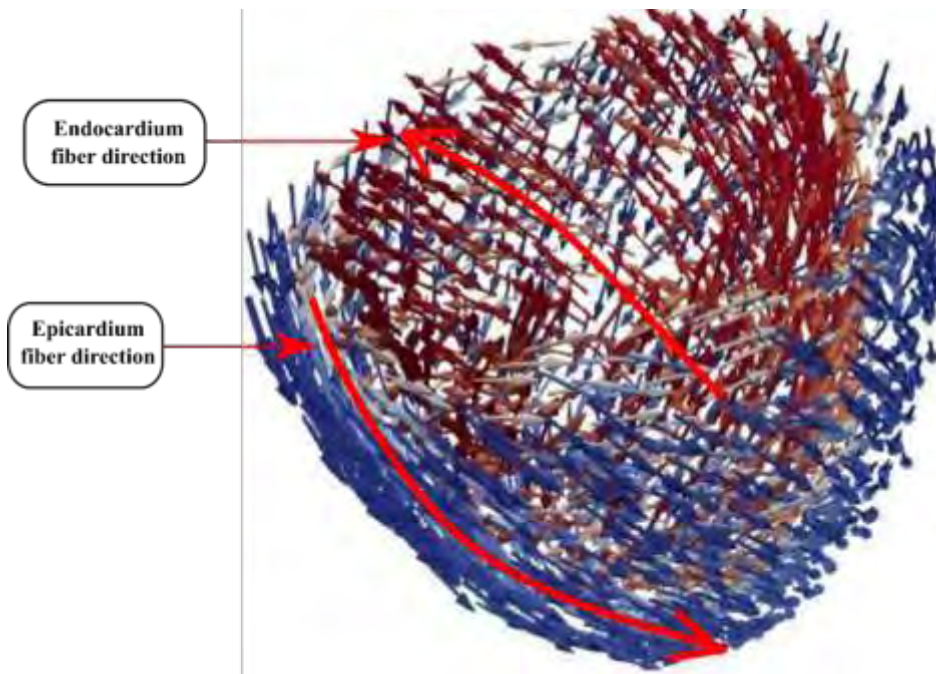


Figure 3. 5: Variation of the helix angle associated with the myofiber direction from the LV endocardium to the epicardium used in the FE model

The helix angle of the fiber directions across the LV wall has been varied from -60° at the epicardium to $+60^\circ$ at the endocardium based on the previous clinical study [63]. The LA contractility and stiffness have been varied based on the literature review [Table 3.1 and Table 3.2] to find out the nature of the LV behavior such as pressure-volume relationship, volume waveform, pressure waveform, radial, circumferential, and longitudinal strains etc. in all three cases of normal, HFpEF I, and HFpEF II.

3.5 Simulation Cases

First, a normal case was simulated, with end-diastolic and end-systolic LV geometrical features and hemodynamics, as well as global E_{cc} and E_{ll} (waveforms and peaks) close to values of the results of Gorcsan et al. [64], Hoit et al. [65] and Semiseth et al. [66]. After that, for HFpEF-I and HFpEF-II, we first determined the parameters for the typical scenario and then used those parameters on the two HFpEF geometries. In all three situations (normal, HFpEF I, and HFpEF II), the pressure and volume of the LA as well as the LV have been raised with the changing of LA contractility and LA stiffness.

This was done by simulating a variety of different scenarios using Normal: LA1, HFpEF-I: LA1 and HFpEF-II: LA1 as references, and then comparing the results to see how E_{cc} , E_{ll} and E_{rr} change in HFpEF based on the active tension produced by the tissue (i.e., myocardial contractility and stiffness). Because hypertension affects the majority of HFpEF patients, the time varying elastance model parameters' impact have been taken into account so that E_{cc} , E_{ll} , and E_{rr} fell within the range of values available in the literature review. These cases provided us with insights into how parameter values should be modified (to reflect a combination of these factors) in order to arrive at a combination that simultaneously fits all the conditions encountered by HFpEF patients in terms of both volume and ejection fraction (EF), strains and blood pressure. To simulate the HFpEF circumstances, the myofiber orientation (helix angle) has to be adjusted based on the available literature [42, 67]. As previously reported under resting settings [65, 68], the heart rate was kept constant for all simulations at 75 beats per minute (bpm). FEniCS [9], an open-source platform for solving PDEs, was used to create the modeling framework. Figure 3.9 is the simulation flow diagram for achieving a steady state solution using the specified model:

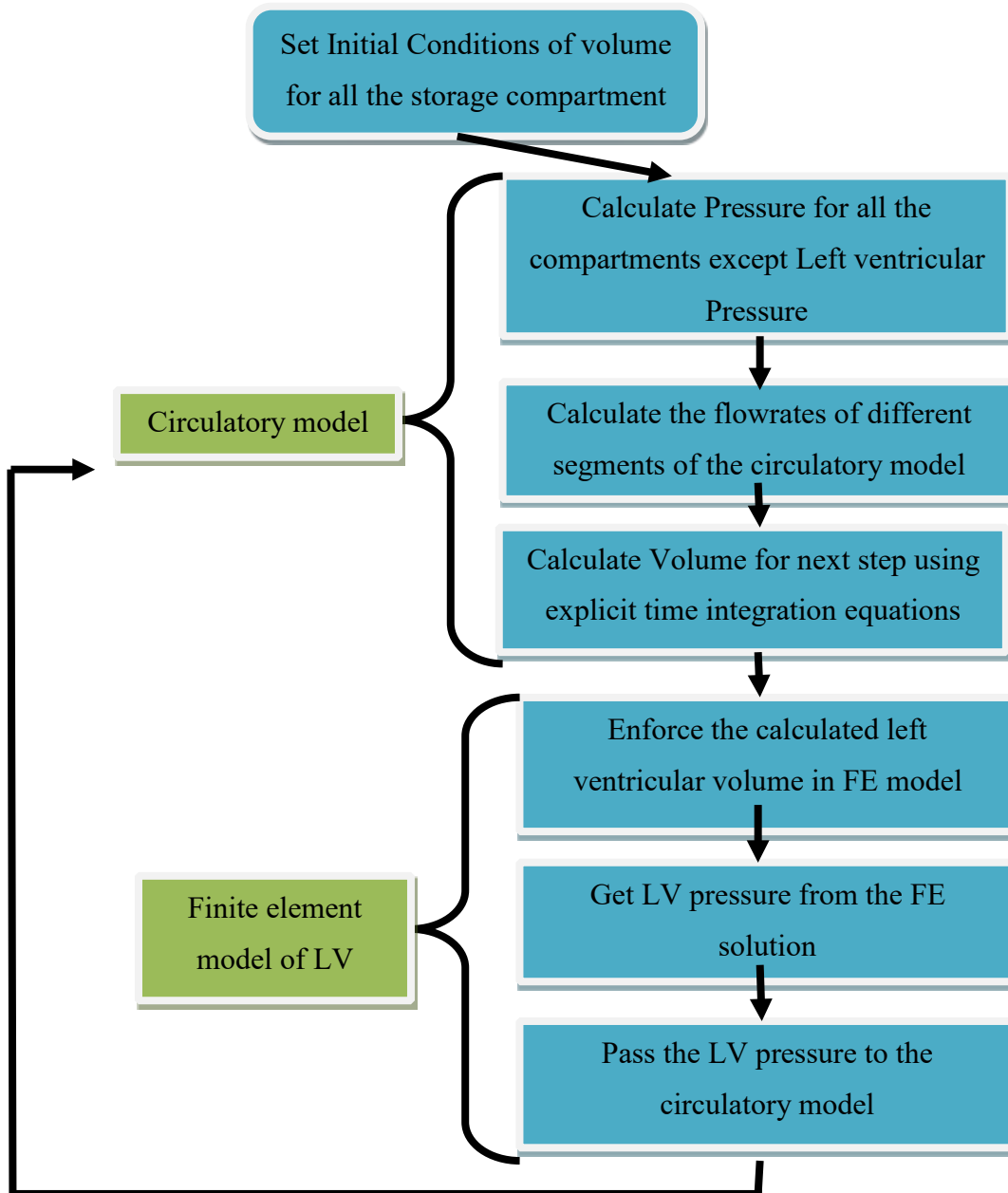


Figure 3. 6: Using the coupled LV FE lumped parameter systemic circulation model, a simulation flow diagram is shown to find the steady state solution.

3.6 Calculation of Myocardial Strain

End-diastole was used as the reference configuration to calculate regional three-dimensional stresses in the longitudinal and circumferential axes.

The myofiber stretch in these directions was calculated as follows:

$$\lambda_i = \sqrt{e_i \cdot C_{LV} e_i} \quad (28)$$

where, $C_{LV} = F_{LV}^T F_{LV}$ is the correct answer. The unit vectors in the longitudinal l and circumferential c directions, respectively, are e_i with $i \in (l, c)$ in the Cauchy-Green deformation tensor. The radial direction e_r is normal to the LV wall, according to the description. The circumferential direction e_c is said to be orthogonal to the apex-base direction and e_r . Finally, e_l is described as being orthogonal to both e_r and e_c in the longitudinal direction. As a result, this longitudinal axis is perpendicular to the LV hollow wall surface. The following definitions [37] were used to determine Euler-Almansi strains:

$$\varepsilon_i = \frac{1}{2} \left(1 - \frac{1}{\lambda_i^2} \right) \quad (29)$$

For each time step, the spatially averaged strain was calculated by,

$$\varepsilon_{i,avg} = \frac{1}{V} \int_{\Omega_{0,LV}} e_i dV \quad (30)$$

3.7 Grid Independence Test

A grid independence study was carried out to establish consistency in finite element outcomes when element counts varied. A simulation study was performed for quadratic tetrahedral components with sizes ranging from 230 to 1760. The results do not vary substantially as the number of pieces increases after 730. Figure 3.10 (A), (B), and (C) display the PV loop, LV volume, and pressure waveforms for a common LV model as well as (D) shows the PV loops of the left atrium for the same LV model with varied numbers of quadratic tetrahedral sections. We can note that the highest variation between the pressure measurements for 1531 and 1760 components is merely around 1.84 percent since pressure varies more than volume. However, running the model with 1760 components increases the simulation duration substantially. As a consequence, 1150 - 1550 elements were chosen for numerical simulation of the various examples in this study to efficiently duplicate the cases in terms of simulation time. We may conclude from this discussion that the outcomes reported in this study are mesh independent.

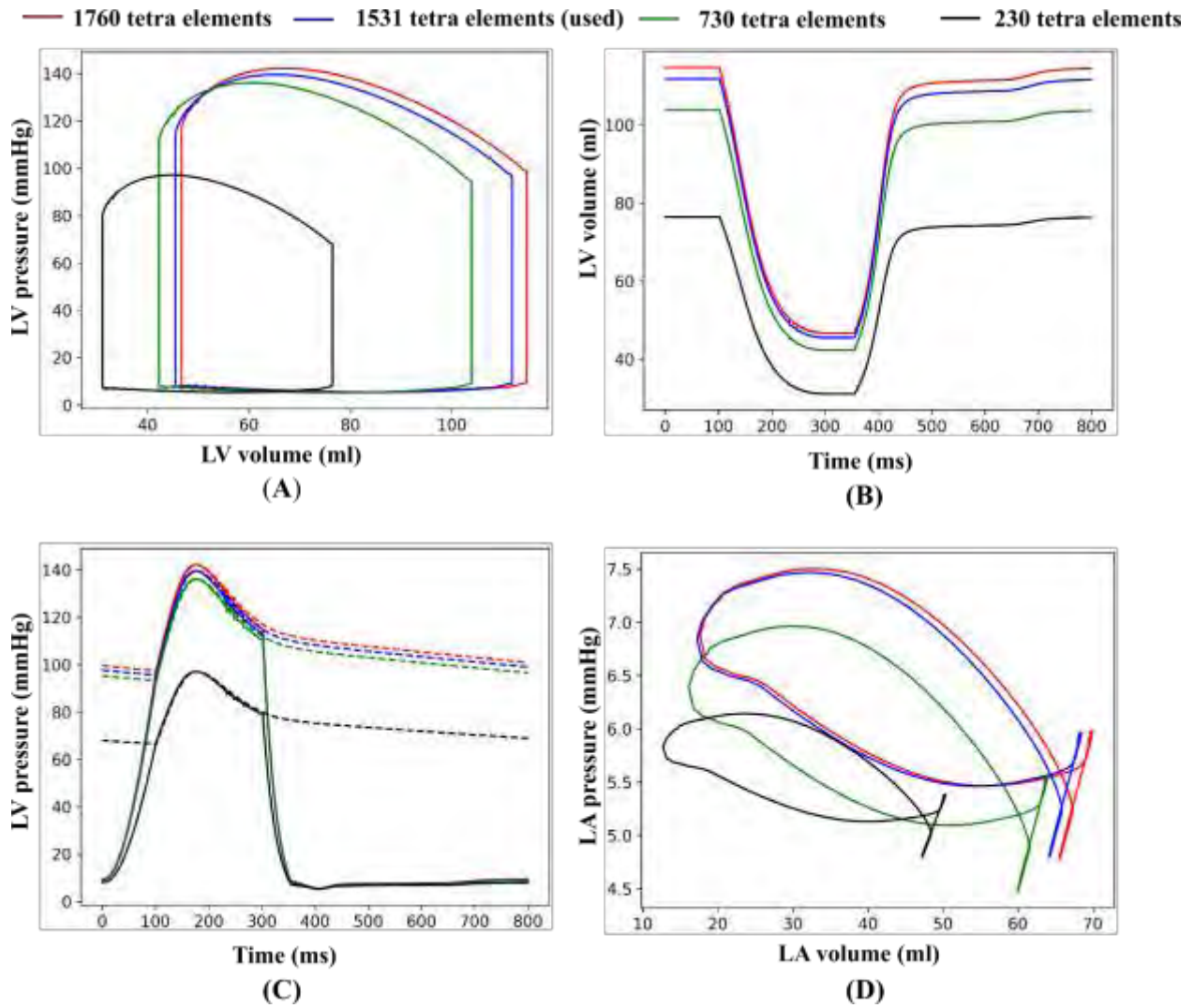


Figure 3. 7: Comparison of steady-state LV (A) PV loop, (B) volume waveforms, (C) pressure waveforms and LA (D) PV loops for normal case for different number of quadratic tetrahedral elements.

CHAPTER 4

RESULTS AND DISCUSSION

For patients with HFpEF, computational modeling can be used to better understand the role and contribution of many elements that impact LV functions. The model was calibrated using data from the literature review of normal subjects and HFpEF patients [37, 42, 56]. To predict the LV behavior due to the dysfunction of LA, the relevant model parameters of LA time varying elastance model has been altered on the three different cases: normal, HFpEF - I, and HFpEF – II. The model parameters that correspond to the LA contractility and stiffness namely, end-systolic elastance, scaling factor for EDPVR, and exponent for EDPVR were changed for different cases. The results (hemodynamics and overall mechanical behaviors) obtained from these normal and HFpEF models with isolated and combined change in LA contractility and stiffness were compared with the baseline normal and HFpEF models.

4.1 Comparison of the Models: Normal, and HFpEF-I, and HFpEF-II Cases

4.1.1 Comparison of the PV loops, volume waveforms, and pressure waveforms among the Normal, HFpEF-I, and HFpEF-II cases

The PV loops, volume and pressure waveforms of the LV and LA for the normal subject that have been found have been compared with the literature data (Gorcsan et al. [66], Hoit et al. [67] and Semiseth et al. [68]., Shavik et al. [42] and S. Land and S. A. Niederer [54]) as shown in Figure 4.1 and Figure 4.2. The model has an EDV of around ~114 ml and ESV of around ~47 ml. The normal range of the EDV is approximately 85.2 ± 24.5 ml and ESV of 34.9 ± 13.6 ml [8], respectively. Finally, the EF for the model came in at 59% that is near to the reference EF of 60% (normal range of EF for the healthy heart is more than 55% [6]). However, for Normal case, the peak pressure that has been found is slightly elevated (141 mmHg). The normal range of peak pressure around 90-140 mmHg [71]. There were likewise strong matches between the LV pressure and volume waveforms exhibited in Figure 4.1 (b) and Figure 4.1 (c) respectively with the clinical measurement. All the LV parameters have been matched within the normal range of aortic pulse pressure of 38 mmHg.

Fig. 4.1 (d) shows the PV loop for left atrium. The model has a LA peak pressure of around 7.5 mmHg which is close to the reference of around 8 mmHg. Moreover, the EDV of model is 69 ml

and ESV is 18 ml and which is close to the clinical reference of EDV of 67 ml and ESV of 15 ml. The normal range of peak pressure of LA is approximately 8.1 ± 2.8 mmHg and the volume is around EDV ($\sim 60 \pm 12$ ml) and ESV ($\sim 16 \pm 6.3$ ml) [40] respectively. Therefore, it can be said that the model has an LA peak pressure within the normal range as well as the EDV and ESV within the normal range and match with the clinical measurement.

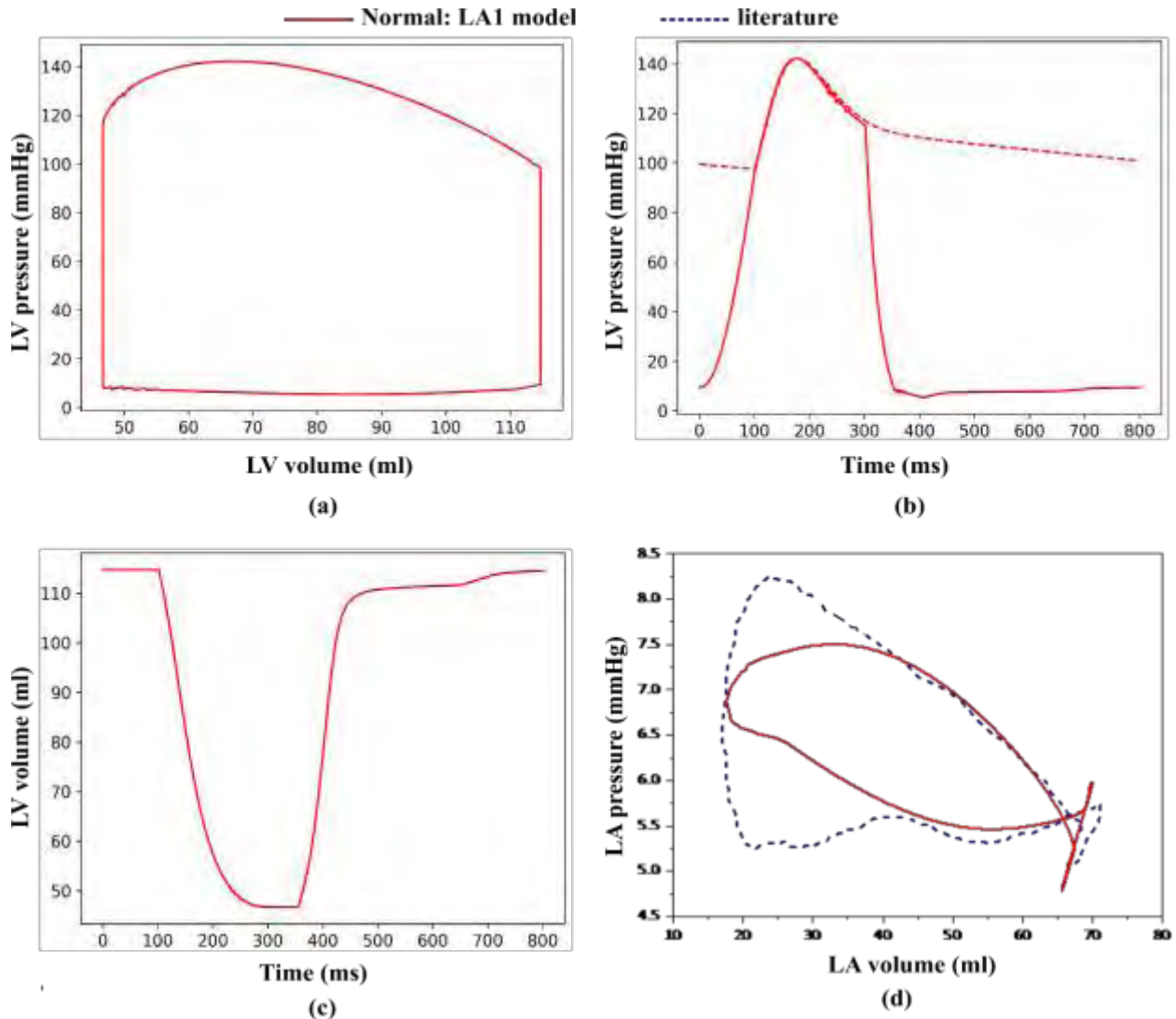


Figure 4. 1: The Normal: LA1 LV's (a) PV loop (b) pressure waveform (c) volume waveform (d) LA's PV loop matched with the literature [54]

Table 4. 1: Hemodynamic indices of LV and LA for Normal: LA1 case.

LV		
Index	Unit	Value
EDV	ml	114
ESV	ml	47
EF	%	59
Peak Pressure	mmHg	141
LA		
Index	Unit	Value
EDV	ml	70
ESV	ml	18
EF	%	74.3
Peak Pressure	mmHg	7.5

The PV loops, volume, and pressure waveforms of the LV for the HFpEFI: LA1 and HFpEFII: LA1 condition predicted by the model were satisfactorily matched with the clinical range [40, 42, 54], similar to the normal case. The HFpEFI: LA1 model yielded EDV of 104.6 ml and ESV of 41.3 ml. As a consequence, the model projected a 60.5% LV ejection fraction (EF) for HFpEFI: LA1 which is within the HFpEF range (EF = 58% to 68% [72]). Likewise, HFpEFII: LA1 model yielded EDV of 129 ml and ESV of 48 ml. As a result, the LV ejection fraction (EF) predicted by the model for HFpEFII: LA1 was 63.3% which is also within the HFpEF range (EF = 58% to 68% [72]). The HFpEFI: LA1 patient has a normal systolic pressure of 121 mmHg as seen by aorta pressure waveforms (Figure 4.2 (b)). The Figure 4.3 (b) shows the hypertensive systolic pressure of 175.8 mmHg for HFpEFII: LA1 patient. The HFpEF systolic pressure range is approximately 117-178 mmHg [72, 73].

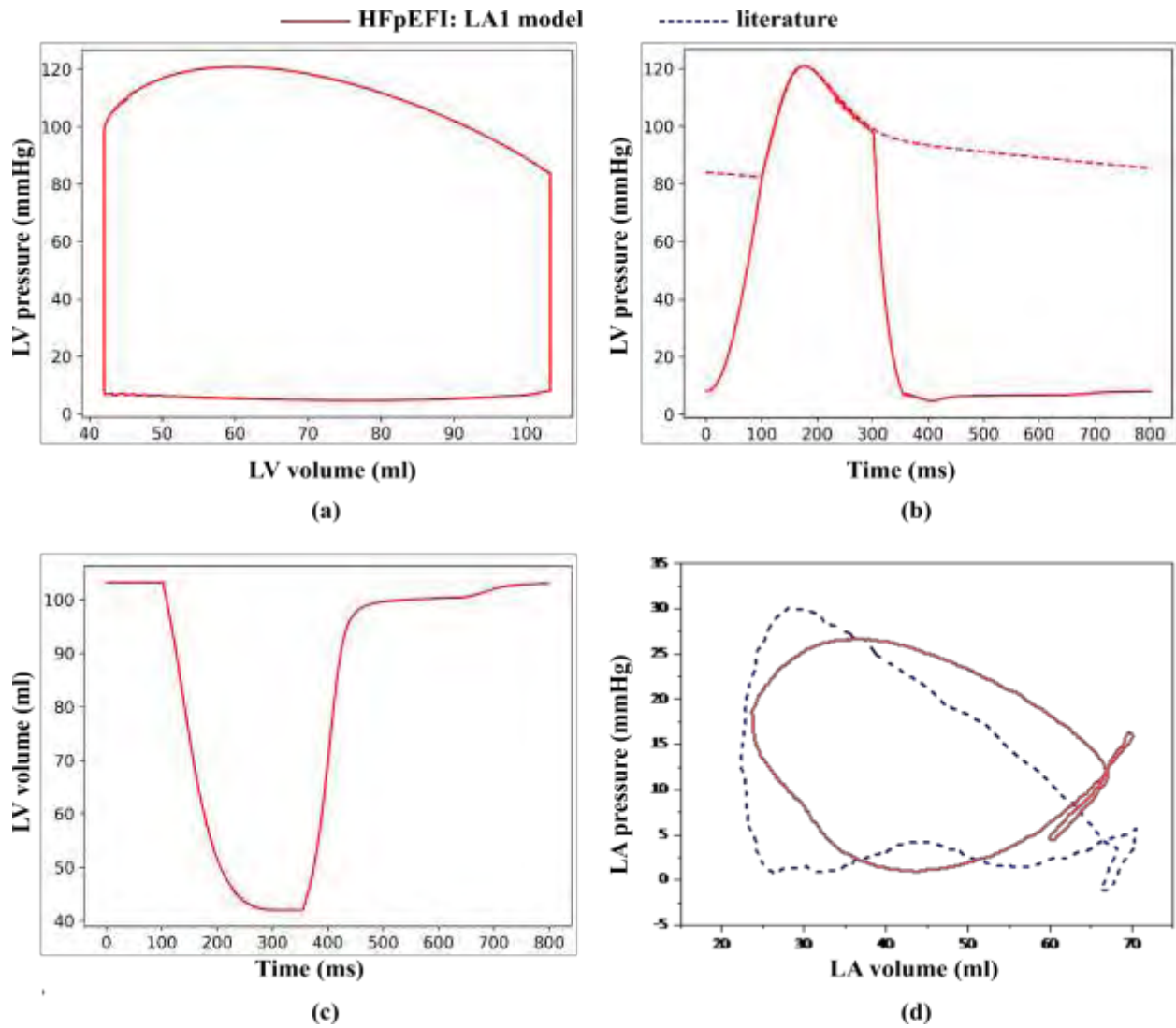


Figure 4. 2: The HFpEF-I: LA1 LV's (a) PV loop (b) pressure waveform (c) volume waveform (d) LA's PV loop matched with the literature [54]

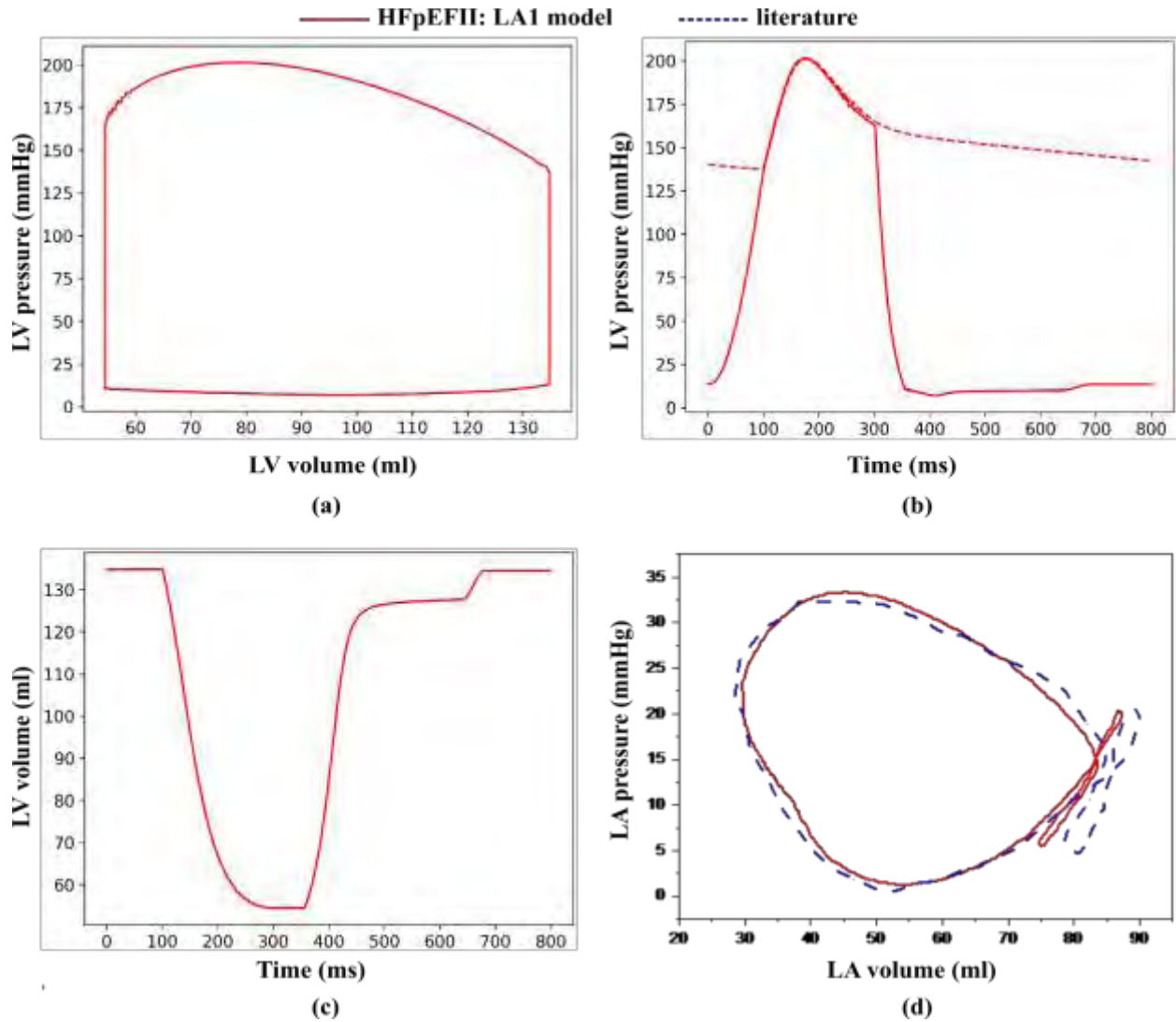


Figure 4. 3: The HFpEF-II: LA1 LV's (a) PV loop (b) pressure waveform (c) volume waveform (d) LA's PV loop matched with the literature [40]

Figure 4.2 (d) and Figure 4.3 (d) show the PV loop of left atrium for HFpEFI: LA1 and HFpEFII: LA1 cases. The HFpEFI: LA1 model has a peak pressure of around 26.7 mmHg which is close to the reference of around 31 mmHg. Moreover, the EDV of model is 70 ml and ESV is 24 ml and the reference has an EDV of 77 ml and ESV of 25 ml. The peak pressure of the HFpEFII: LA1 model is approximately 33.4 mmHg, which is similar to the clinical range of around 32.3 mmHg. Furthermore, the EDV of the model is 87.3 ml and the ESV is 29.6 ml, whereas the EDV of the reference is 90 ml and the ESV is 28.3 ml. The clinical range of LA peak pressure is approximately 20 ± 6.1 mmHg and the volume is around EDV ($\sim 85 \pm 28$ ml) and ESV ($\sim 54 \pm 27$ ml) [40]

respectively. Therefore, it can be said that the model has an LA peak pressure within the range as well as the EDV and ESV within the range.

Table 4. 2: Hemodynamic indices of LV and LA for HFpEF-I: LA1, and HFpEF-II: LA1 case.

HFpEFI: LA1		
LV		
Index	Unit	Value
EDV	ml	104.6
ESV	ml	41.3
EF	%	60.5
Peak Pressure	mmHg	121
LA		
Outcome Parameter	Unit	Value
EDV	ml	67
ESV	ml	23
EF	%	64.2
Peak Pressure	mmHg	27
HFpEFII: LA1		
LV		
Outcome Parameter	Unit	Value
EDV	ml	129
ESV	ml	48
EF	%	63.3
Peak Pressure	mmHg	175.8
LA		
Outcome Parameter	Unit	Value
EDV	ml	87.3
ESV	ml	29.6
EF	%	66.1
Peak Pressure	mmHg	33.4

4.1.2 Comparison of Strains among the Normal, HFpEF-I and HFpEF-II Cases

For the Normal: LA1, HFpEFI: LA1, and HFpEFII: LA1 patients, the circumferential strain, E_{cc} (Figure 4.4), and the longitudinal strain, E_{ll} (Figure 4.5) profiles were produced. In clinical practice, longitudinal and circumferential stresses in the left ventricle (LV) are often assessed using 2D-Doppler and speckle tracking echocardiography (STE) [64-66]. Figure 4.4 and Figure 4.5 depict typical strain patterns for normal persons measured in clinics. For circumferential strain, the model predicted patterns of Normal: LA1, HFpEFI: LA1, and HFpEFII: LA1 patients that matched well with the clinical data [66,67]. The simulated circumferential strains of both normal and HFpEF cases peak at around 350 ms during systole, which falls within the clinical measurement range of 300 - 450 ms. In addition, comparable to clinical findings, a fast shift in circumferential strain occurs at late diastole at roughly 650 ms in both cases due to left atrial contraction. Furthermore, the rate of relaxation during the isovolumic relaxation phase is very close to clinical values in both situations (Figure 4.4). The absolute peak values of circumferential and longitudinal stresses in the Normal: LA1 case are 20.1 percent and 19.1 percent, respectively, which are quite comparable to clinical measures [74]. When compared to the HFpEF conditions to the normal scenario, the peak circumferential strain is reduced to ~18.9 percent for HFpEFI: LA1, and ~17.6 percent for HFpEFII: LA1 which have been reduced by ~7 percent and ~15 percent, respectively compared to the Normal: LA1 case. Similarly, the peak longitudinal strain is reduced to ~17.4 percent for HFpEFI: LA1, and ~15.9 percent for HFpEFII: LA1, respectively which have been reduced by ~10 percent and ~20 percent, respectively compared to the Normal: LA1 case. It has been found in clinical studies that the peak longitudinal and circumferential strains become impaired due to HFpEF. For both HFpEF models, the peak longitudinal and circumferential strains were significantly reduced compare to the normal cases which agrees with the clinical findings.

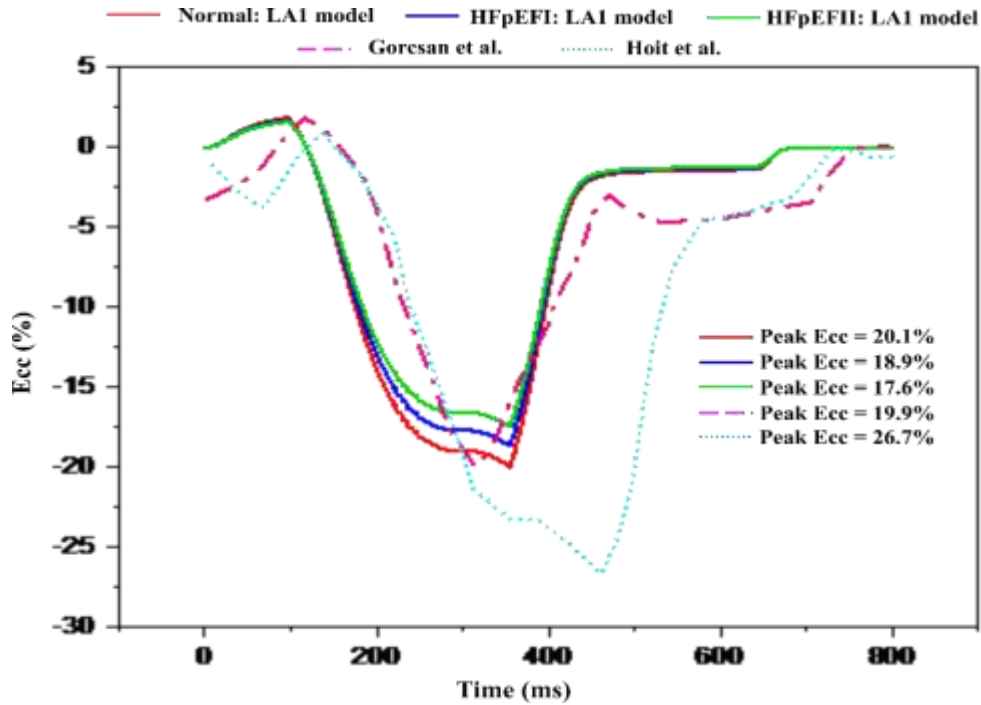


Figure 4. 4: Circumferential strain waveform calculated by the model for Normal: LA1, HFpEFI: LA1, and HFpEFII LA1 cases compared with echo measurements (dashed magenta color [66] and dotted cyan color [67] lines)

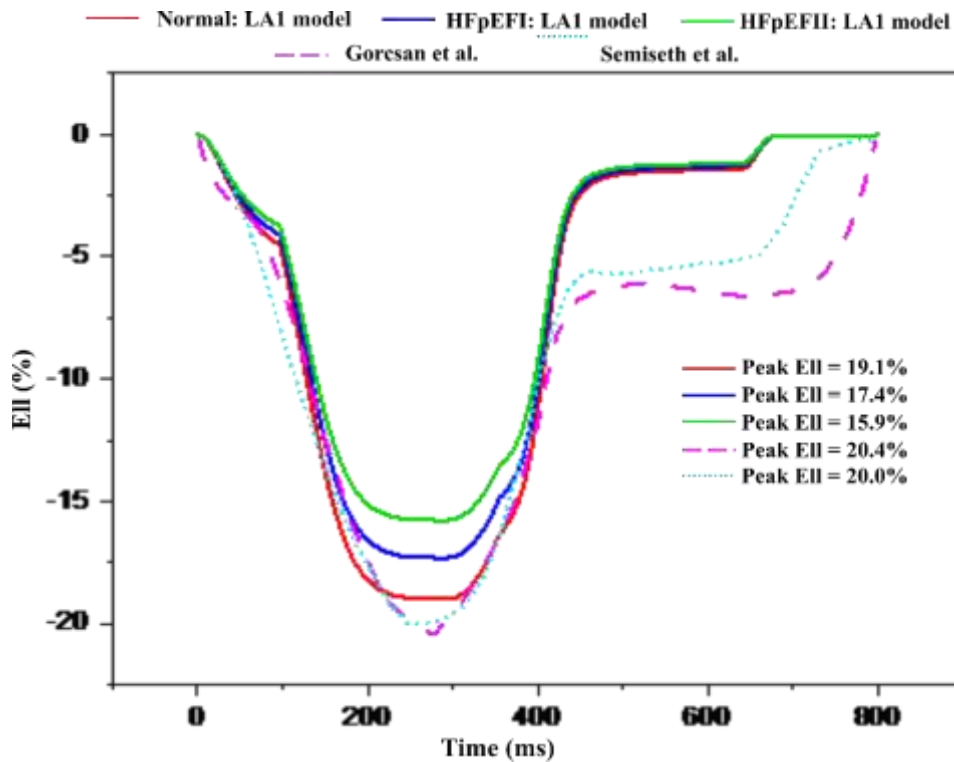


Figure 4. 5: Longitudinal strain waveform calculated by the model for Normal: LA1, HFpEFI: LA1, and HFpEFII LA1 cases compared with echo measurements (dashed magenta color [66] and dotted cyan color [68] lines)

4.1.3 Summary

The different hemodynamic and functional indices predicted by the model for Normal: LA1, HFpEFI: LA1, and HFpEFII: LA1 are shown in Table 4.1, and Table 4.2. The LA contractility and LA stiffness along with the time courses have been varied from the baseline case (Table 3.2) in such a way that the left atrium PV loops have been matched with the clinical measurement for all the cases. The EF is within the normal range for all cases. Furthermore, the EDV (104.6 ml) and ESV (41.3 ml) of the HFpEFI: LA1 case were lower than the normal case (114 ml EDV and 47 ml ESV) and the EDV (129 ml) and ESV (48 ml) of the HFpEFII: LA1 case were higher than the normal case (114 ml EDV and 47 ml ESV), indicating LV remodeling. The HFpEFI: LA1 patient exhibits lower end-diastolic pressure (EDP) than Normal: LA1 (8.6 mmHg in HFpEFI: LA1 vs. 9.6 mmHg in Normal: LA1), implying that the HFpEFI: LA1 patient's LV is stiffer than the normal LV. On the other hand, The HFpEFII: LA1 patient exhibits greater end-diastolic pressure (EDP) than Normal: LA1 (12 mmHg in HFpEFII: LA1 vs. 9.6 mmHg in Normal: LA1). EDP greater than 10 mmHg is regarded clinically to be a symptom of diastolic dysfunction, which is a frequent characteristic in HFpEF [72]. Furthermore, the absolute peak Ecc and Ell were considerably lower in HFpEF patients compared to normal cases, indicating LV dysfunction due to the presence of dysfunction heart failure of preserved ejection fraction (HFpEF). The results of both situations are described in Table 4.3.

Table 4. 3: Model predicted hemodynamic and functional indices for Normal: LA1, HFpEFI: LA1, and HFpEFII: LA1

Parameters	Normal: LA1 case	HFpEFI: LA1 case	HFpEFII: LA1 case
End-Diastolic Volume (ml)	114	103	127
Ejection fraction (%)	59 (reference 60 [42])	60.5 (reference 60.5 [42])	63.3 (reference 63.5 [42])
End-Diastolic Pressure (mmHg)	9.6 (normal range 7-10.6 [72])	8.6 (HFpEF range 8-18 [72])	12 (HFpEF range 8-18 [72])
Systolic Blood Pressure (mmHg)	141	120.8	175
Diastolic Blood Pressure (mmHg)	98.6	83.8	121
Peak Circumferential Strain (%)	20	18	17
Peak Longitudinal Strain (%)	19	17	15

4.2 Effects of the variations of LA contractility (end-systolic elastance parameter (E_{es})) on LV function for Normal, HFpEF-I, and HFpEF-II cases

The slope of a line through the end-systolic pressure-volume point (the left upper corner of the P-V loop) is termed End-Systolic Elastance (E_{es}) and is a measure of atrial contractility. E_{es} is an index of the LA contractility of the left atrium. In this study, to find out the effect of the contractility, two different cases have been simulated with respect to the baseline data (for normal, Normal: LA1 (Case:B) is considered as baseline and for HFpEF, HFpEFI: LA1 (Case:B) is considered as baseline for HFpEFI, and HFpEFII: LA1 (Case:B) is considered baseline for HFpEFII cases). The value of E_{es} has been decreased by 10 percent for Case A, and increased by 10 percent for Case: C from the reference value (considering Normal: LA1, HFpEFI: LA1, and HFpEFII: LA1 as reference for E_{es}). Figure 4.6 (A), Figure 4.7 (A), and Figure 4.8 (A) show the pressure and volume loop of LV for Normal: LA1, HFpEFI: LA1, and HFpEFII: LA1 cases and Figure 4.9, Figure 4.10, and Figure 4.11 show the pressure and volume loop of LA, respectively considering the variation of only the end-systolic elastance parameter (E_{es}). From these figures, it is seen that the end-systolic pressure (ESP), the end-diastolic pressure (EDP), and ejection fraction (EF) have increased with the higher value of E_{es} (Case: C) and have decreased with the lower value of E_{es} (Case: A) with respect to the baseline cases (Case: B) for both normal and HFpEF cases. On the other hand, the end-systolic volume (ESV), and the end-diastolic volume (EDV) have decreased with the higher value of E_{es} (Case: C) and increased with the lower value of E_{es} (Case: A) with respect to the baseline cases (Case: B) for normal as well as HFpEF cases. The EF and the slope of ESPVR have also been increasing along with the increased contractility. Tables 4.4 shows the contractility (end-systolic elastance parameter (E_{es})) parameter values used for different cases.

Table 4. 4: LA contractility parameter (End-systolic elastance, E_{es} (Pa/ml)) values used for Normal and HFpEF patients.

Parameter ↓ Case ID →	End-systolic elastance, E_{es} (Pa/ml)		
	Ees1 (Case: A)	Ees2 (Case: B [baseline])	Ees3 (Case: C)
Normal: LA1	47.52	52.80	58.08
HFpEF-I: LA1	47.52	52.80	58.08
HFpEF-II: LA1	47.52	52.80	58.08

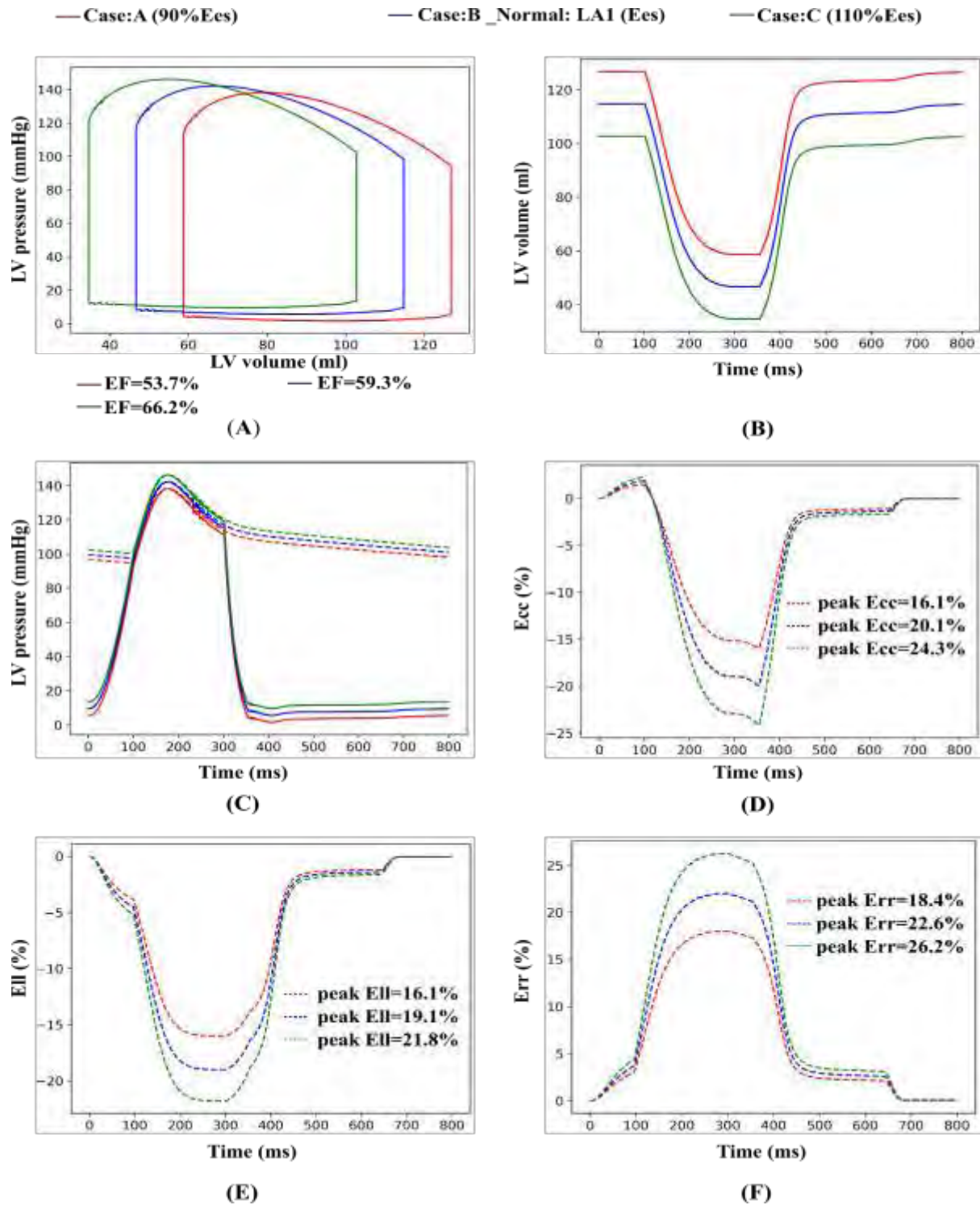


Figure 4. 6: Comparison among Normal LV of (A) PV loops, (B) volume waveforms, (C) pressure waveforms, (D) circumferential strains, (E) longitudinal strains, and (F) radial strains by varying end-systolic elastance (Ees) parameter

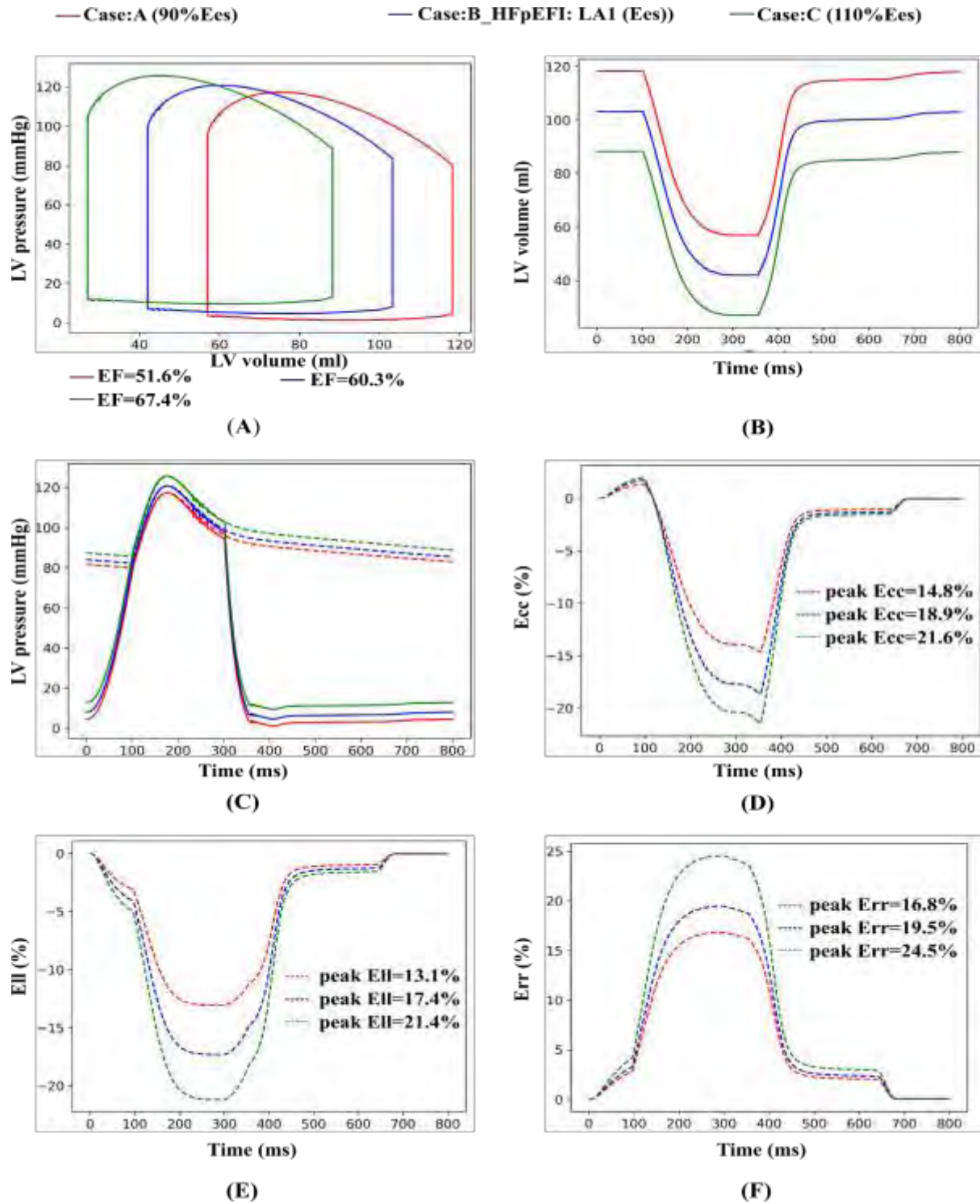


Figure 4. 7: Comparison among HFpEF-I LV of (A) PV loops, (B) volume waveforms, (C) pressure waveforms, (D) circumferential strains, (E) longitudinal strains, and (F) radial strains by varying end-systolic elastance (Ees) parameter

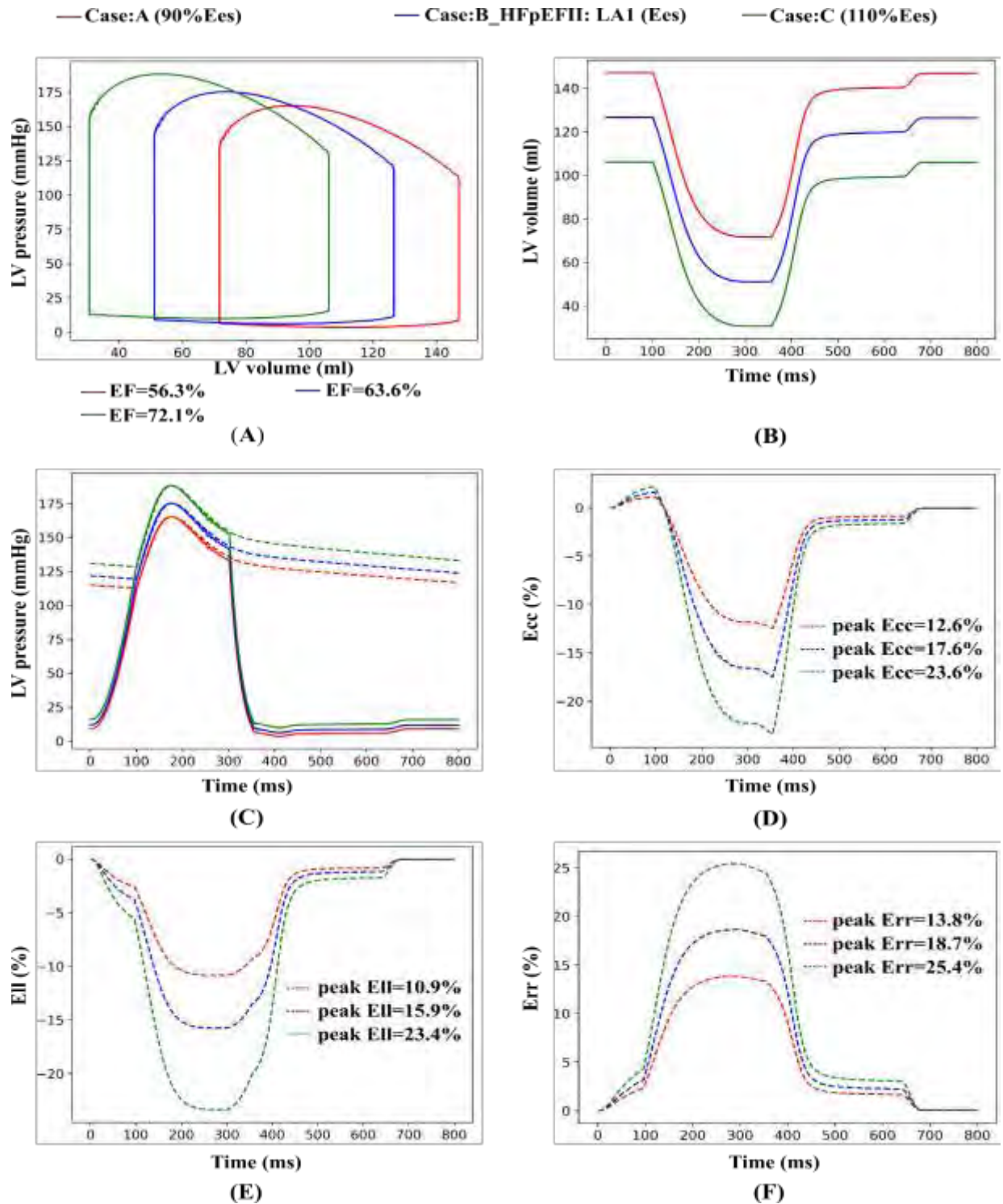


Figure 4. 8: Comparison among HFpEF-II LV of (A) PV loops, (B) volume waveforms, (C) pressure waveforms, (D) circumferential strains, (E) longitudinal strains, and (F) radial strains by varying end-systolic elastance (Ees) parameter

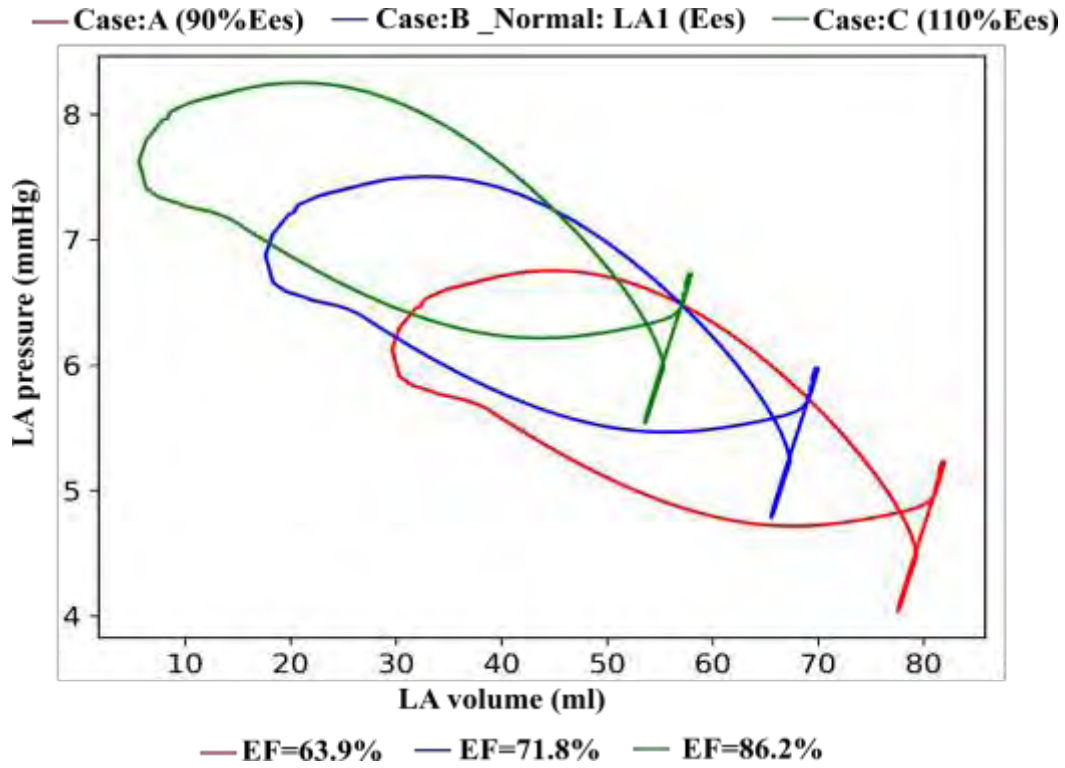


Figure 4. 9: Comparison among Normal LA of PV loops by varying end-systolic elastance (Ees) parameter

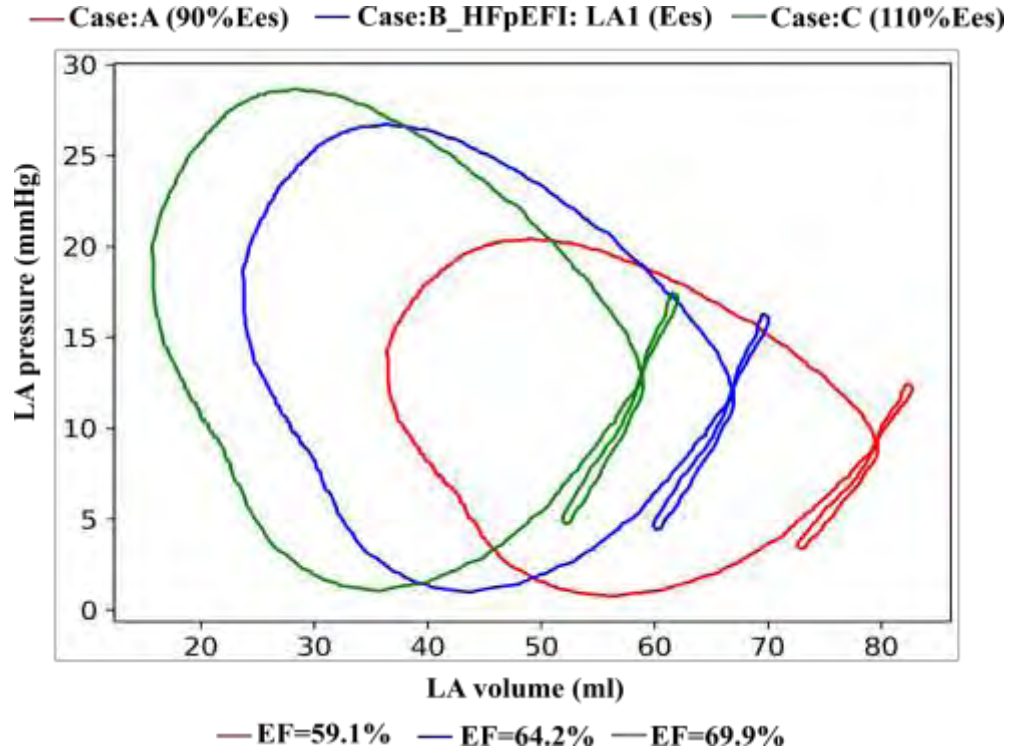


Figure 4. 10: Comparison among HFpEF-I LA of PV loops by varying end-systolic elastance (Ees) parameter

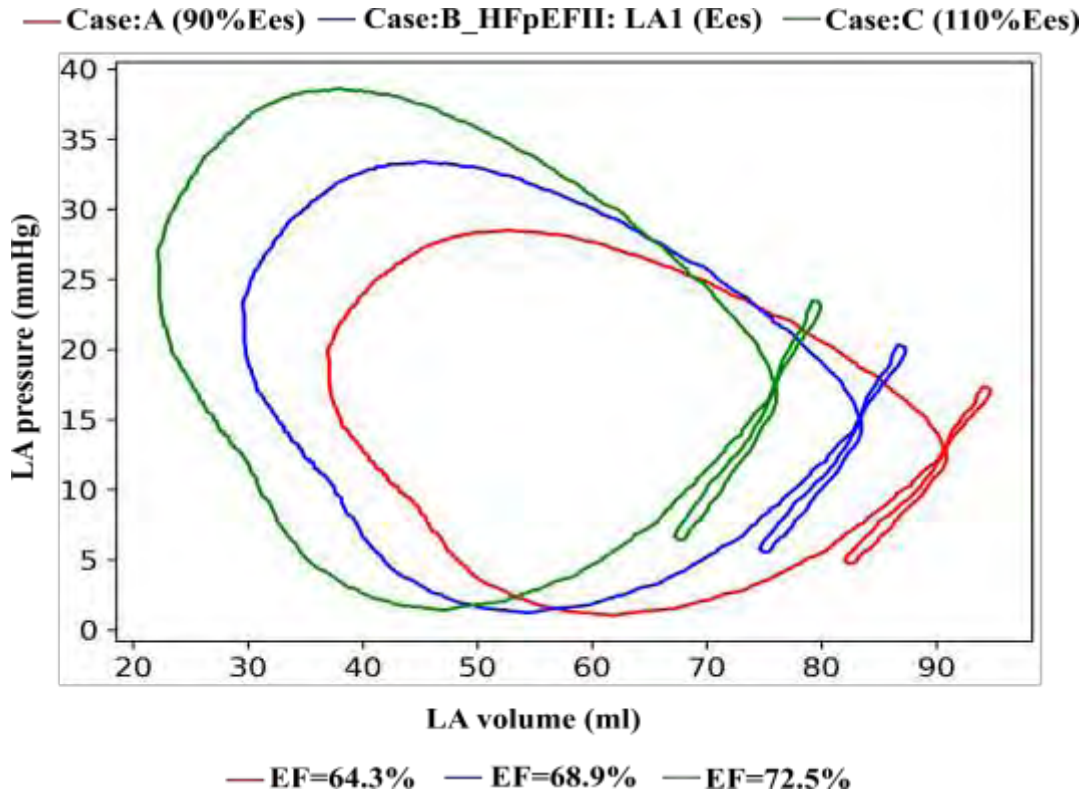


Figure 4. 11: Comparison among HFpEF-II LA of PV loops by varying end-systolic elastance (Ees) parameter

4.2.1 Effects of change of LA contractility on LV PV Loops

Figure 4.6 (A), Figure 4.7 (A), Figure 4.8 (A), and Figure 4.9, 4.10, Figure 4.11 depict the PV loops for LV and LA respectively of Normal: LA1, HFpEFI: LA1, and HFpEFII: LA1; Figure 4.6 (B), Figure 4.7 (B) and Figure 4.18 (B) show volume waveforms for LV of Normal: LA1, HFpEFI: LA1, and HFpEFII: LA1 and Figure 4.6 (C), and Figure 4.7 (C) and Figure 4.8 (C) represent pressure waveforms with varying LA contractility (end-systolic elastic parameter (Ees)). PV loops show that when LA Ees increases, both EDV and ESV of the LV dropped, however EDP and ESP increased for all cases of normal and HFpEF. As a result, when LA Ees increases, so does the EF along with the increasing slope of the ESPVR. By decreasing the Ees, the EF of LV decreased from 59.3 percent (Case: B) to 53.7 percent and by increasing the Ees, the EF has been increasing to 66.2 percent for normal cases. Similarly, for HFpEFI, by increasing the Ees, the EF has been increasing to 67.4 percent from 60.3 percent and on the other hand, by decreasing the Ees, the EF has been decreasing to 51.6 percent. Same trend has also found in HFpEFII where by increasing the Ees, the EF has been increasing to 72.1 percent from 63.6 percent and decreasing to 56.3

percent by decreasing the LA contractility. Furthermore, the LA contractility may create high pressure; systolic pressure increases as the LA contractility increases and the same trend was found in all cases. For normal, Case: B has a SBP of 141 mmHg. By decreasing the Ees from baseline, the SBP has decreased to 135 mmHg and by increasing the SBP has increased to 145 mmHg. The same trend has been found for HFpEF cases. From the above observation, it can be said that with increasing LA contractility, the HFpEF patients LV functions have been improved gradually as indicated by the increased EF. These findings are compatible with clinical data, which indicate comparable changes in the LV PV loop [32].

4.2.2 Effects of change of LA contractility on LV Strains

Figures 4.6 (D), 4.7 (D), Figure 4.8 (D), and Figure 4.6 (E), 4.7 (E), Figure 4.8 (E) and 4.6 (F), 4.7 (F), Figure 4.8 (F) depict changes in circumferential strain (Ecc), longitudinal strain (Ell), and radial strain (Err) waveforms with varying LA contractility for Normal: LA1, HFpEFI: LA1, and HFpEFII: LA1, respectively. The main takeaway from these results is that the peak values of Ecc, Ell, and Err have increased with the increase of LA contractility (Ees) (Case: A to Case: C) for both normal and HFpEF cases. The absolute peak Ecc is 16 percent, 20 percent, and 24 percent for Case: A (Ees = 47.52 Pa/ml), Case: B (52.80 Pa/ml), and Case: C (58.08 Pa/ml), respectively for Normal: LA1 (Figure 4.6 (D)). Likewise, the absolute peak Ecc is 15 percent, 19 percent, and 22 percent for Case: A (Ees = 47.52 Pa/ml), Case: B (52.80 Pa/ml), and Case: C (58.08 Pa/ml), respectively for HFpEFI: LA1 (Figure 4.7 (D)). Correspondingly, the absolute peak Ecc is 13 percent, 18 percent, and 24 percent for Case: A (Ees = 47.52 Pa/ml), Case: B (52.80 Pa/ml), and Case: C (58.08 Pa/ml), respectively for HFpEFII: LA1 (Figure 4.8 (D)). The absolute peak Ell is 16 percent, 19 percent, and 22 percent for Normal: LA1 (Figure (4.6 (E))), 13 percent, 17 percent, and 21 percent for HFpEFI: LA1 (Figure 4.7 (E)), and 11 percent, 16 percent, and 23 percent for HFpEFII: LA1 (Figure 4.8 (E)) for Ees of 47.52 Pa/ml, 52.80 Pa/ml, and 58.08 Pa/ml, respectively. Higher peak LV longitudinal (Ell) and circumferential (Ecc) strains in both HFpEF cases were found which indicates the improvement of LV function. The results are summarized in table 4.5 and compared with the clinical data [74, 76, 77].

Table 4. 5: Hemodynamic and functional indices of LV for Normal and HFpEF models with varying LA contractility (End-systolic elastance parameter, Ees)

Index	Normal: LA1			Clinical Range
	Case: A (Ees = 47.52)	Case: B (Ees = 52.80)	Case: C (Ees = 58.08)	
End-diastolic volume, EDV (ml)	126	114	103	84.1-132 [8, 72]
End-systolic volume, ESV (ml)	57	47	34	34.7-68.6 [8, 72]
Ejection fraction, EF (%)	54	59	66	52-71 [3, 8, 72]
End-diastolic pressure, EDP (mmHg)	8	10	13	7-16 [72, 73]
End-systolic pressure, ESP (mmHg)	110	116	123	101-124 [72]
Absolute peak Ecc (%)	16	20	24	13.45-24 [74, 76, 77]
Absolute peak Ell (%)	16	19	22	14-24 [74, 76, 77]
Absolute peak Err (%)	19	23	26	17-28 [74, 76, 77]
Index	HFpEFI: LA1			Clinical Range
	Case: A (Ees = 47.52)	Case: B (Ees = 52.80)	Case: C (Ees = 58.08)	
End-diastolic volume, EDV (ml)	118	103	88	114±28.1 [8]
End-systolic volume, ESV (ml)	58	41	39	47±16.7 [8]
Ejection fraction, EF (%)	51.6	60.3	67.4	59±7 [8]
End-diastolic pressure, EDP (mmHg)	7.4	8.6	14	7-18 [72, 73]
End-systolic pressure, ESP (mmHg)	108	115	119	104-153 [72]
Absolute peak Ecc (%)	15	19	22	13.45-24 [74, 76, 77]
Absolute peak Ell (%)	13	17	21	14-24 [74, 76, 77]
Absolute peak Err (%)	17	22	25	17-28 [74, 76, 77]

Index	HFpEFII: LA1			Clinical Range
	Case: A (Ees = 47.52)	Case: B (Ees = 52.80)	Case: C (Ees = 58.08)	
End-diastolic volume, EDV (ml)	149	129	105	114±28.1 [8]
End-systolic volume, ESV (ml)	69	48	29	47±16.7 [8]
Ejection fraction, EF (%)	56.3	63.3	72.1	58-75 [8, 72]
End-diastolic pressure, EDP (mmHg)	9	12	16	11.9±4.6 [8]
End-systolic pressure, ESP (mmHg)	137	151	168	123-178 [72, 73]
Absolute peak Ecc (%)	13	18	24	13.45-24 [74, 76, 77]
Absolute peak Ell (%)	11	16	23	14-24 [74, 76, 77]
Absolute peak Err (%)	14	19	26	17-28 [74, 76, 77]

4.3 Effects of the variations of LA stiffness (Scaling Factor (A_{LA})) on LV function for Normal, HFpEF-I, and HFpEF-II cases

The LA stiffness has been altered by changing the scaling factor A_{LA} of EDPVR of LA. The scaling factor, A_{LA} values used for different cases are tabulated in table 4.6.

Table 4. 6: LA stiffness parameter (scaling factor A_{LA} of EDPVR) values used for Normal and HFpEF patients.

Parameter ↓ Case ID →	LA stiffness (Scaling factor for EDPVR, A_{LA} (Pa))		
	Ees1 (Case: A)	Ees2 (Case: B [baseline])	Ees3 (Case: C)
Normal: LA1	52.80	58.67	64.54
HFpEF-I: LA1	52.80	58.67	64.54
HFpEF-II: LA1	52.80	58.67	64.54

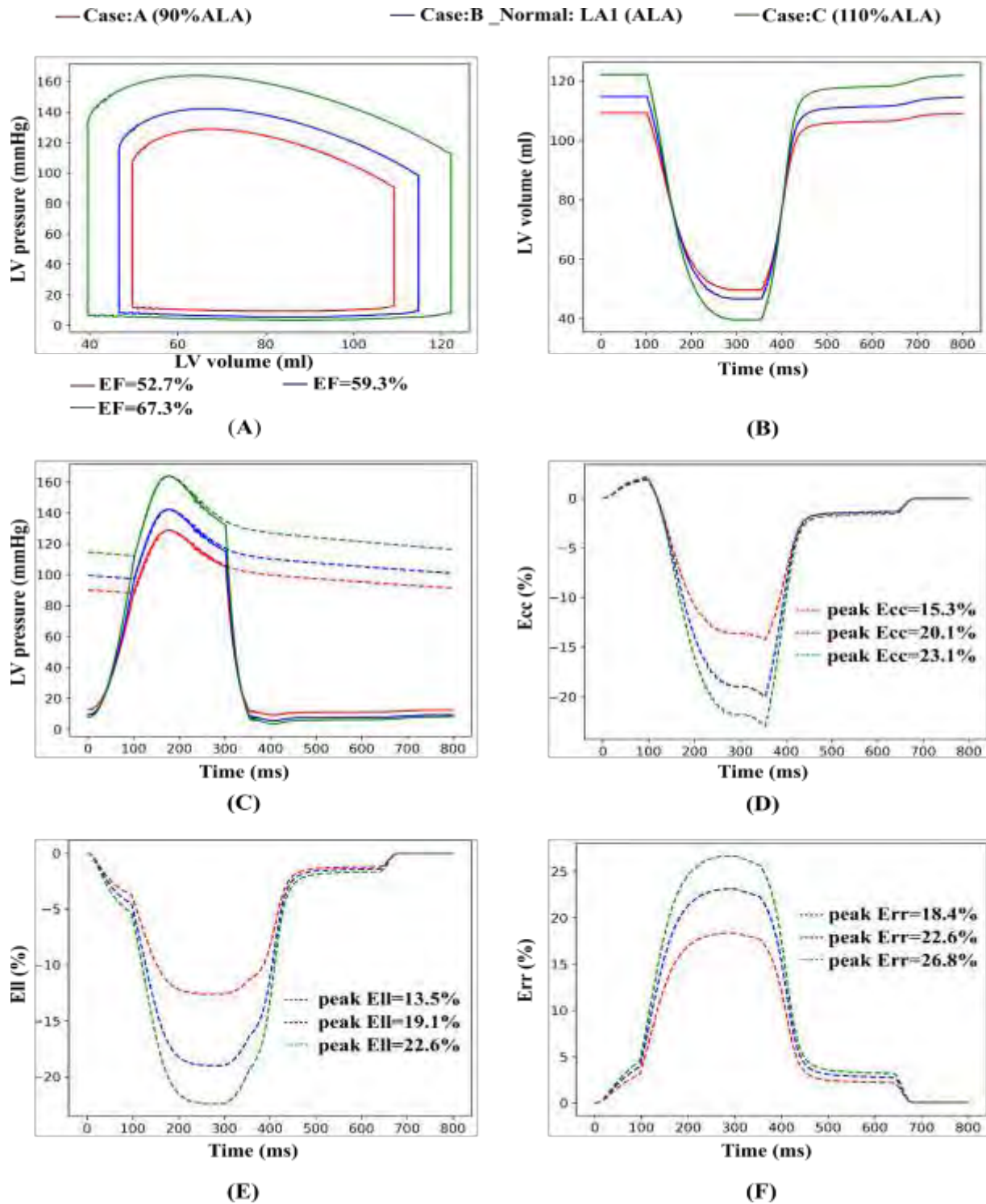


Figure 4. 12: Comparison among Normal LV of (A) PV loops, (B) volume waveforms, (C) pressure waveforms, (D) circumferential strains, (E) longitudinal strains, and (F) radial strains by varying scaling factor (ALA) for EDPVR

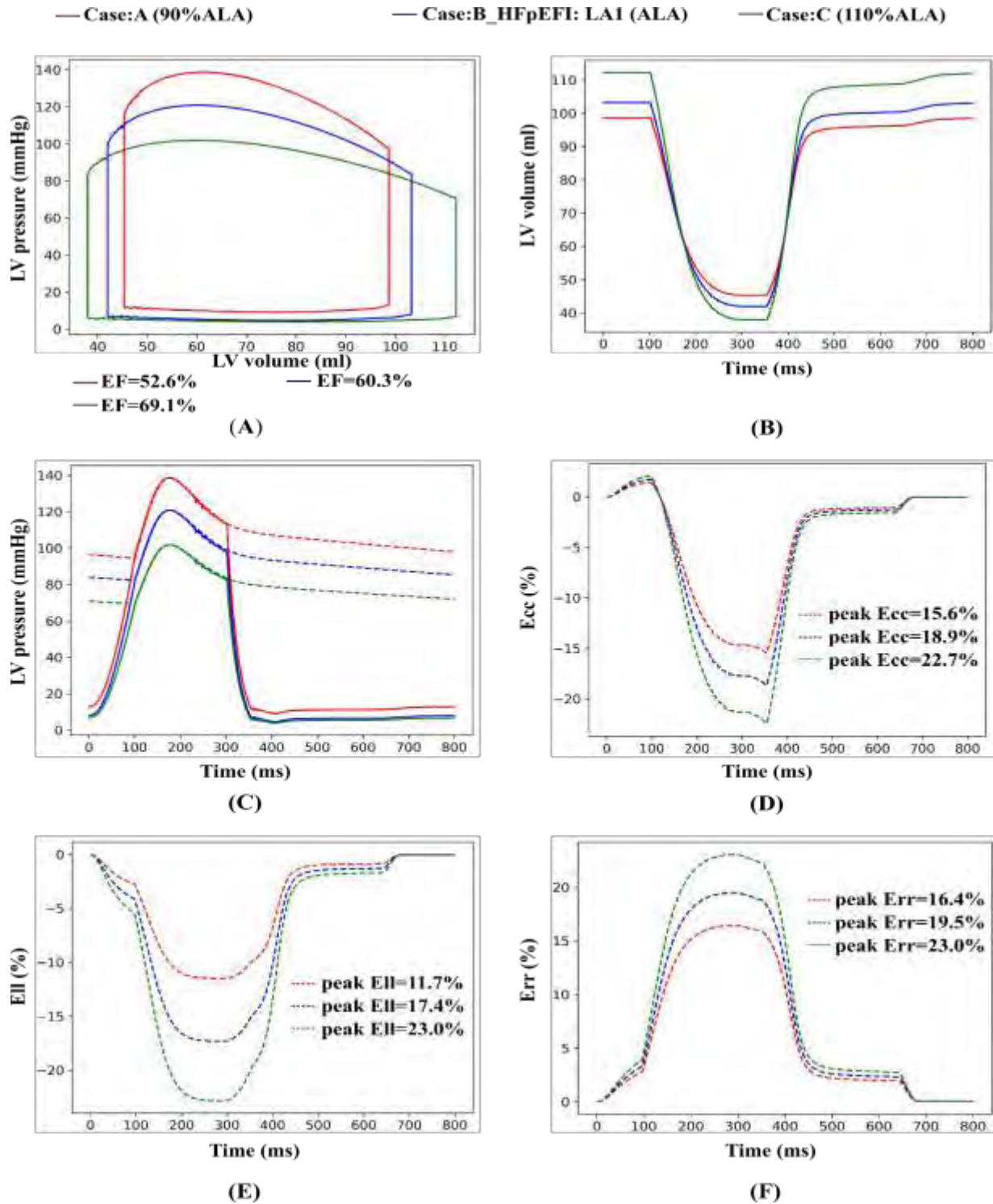


Figure 4. 13: Comparison among HFpEF-I LV of (A) PV loops, (B) volume waveforms, (C) pressure waveforms, (D) circumferential strains, (E) longitudinal strains, and (F) radial strains by varying scaling factor (ALA) for EDPVR

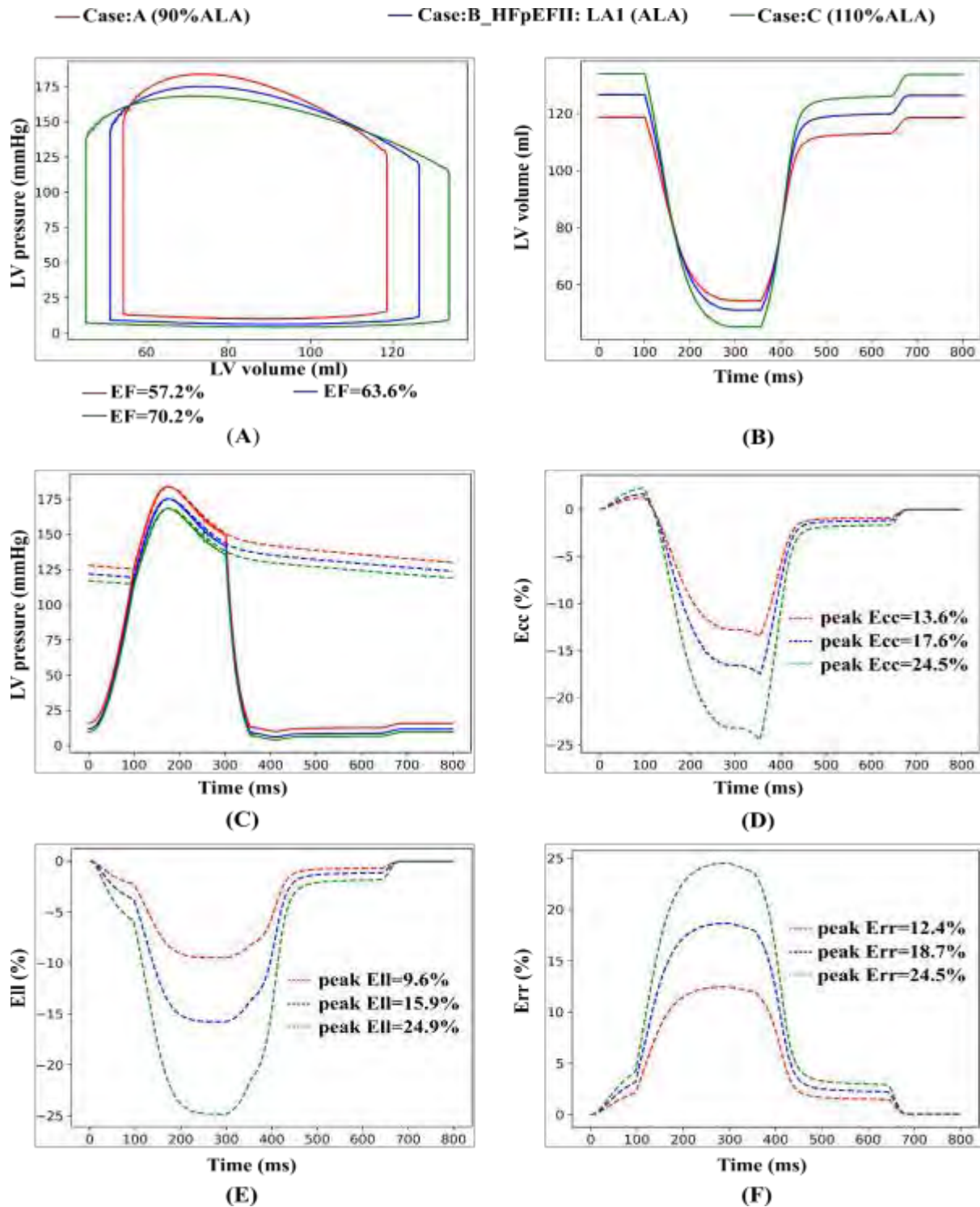
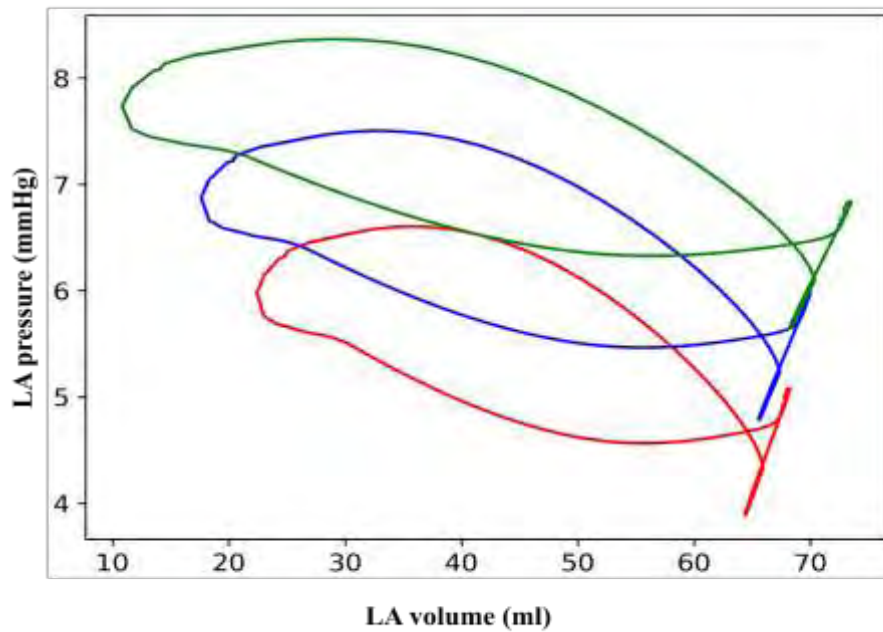


Figure 4. 14: Comparison among HFpEF-II LV of (A) PV loops, (B) volume waveforms, (C) pressure waveforms, (D) circumferential strains, (E) longitudinal strains, and (F) radial strains by varying scaling factor (ALA) for EDPVR

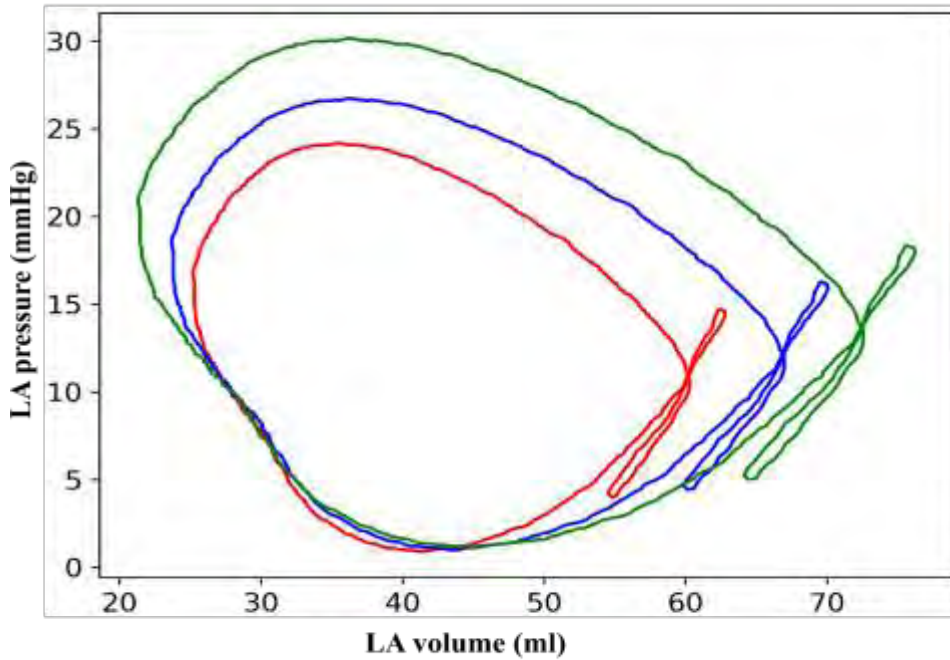
— Case:A (90%ALA) — Case:B_Normal: LA1 (ALA) — Case:C (110%ALA)



— EF=63.2% — EF=71.8% — EF=84.2%

Figure 4. 15: Comparison among Normal LA of PV loops by varying scaling factor (ALA) for EDPVR

— Case:A (90%ALA) — Case:B_HFpEFI: LA1 (ALA) — Case:C (110%ALA)



— EF=56.1% — EF=64.2% — EF=73.9%

Figure 4. 16: Comparison among HFpEF-I LA of PV loops by varying scaling factor (ALA) for EDPVR

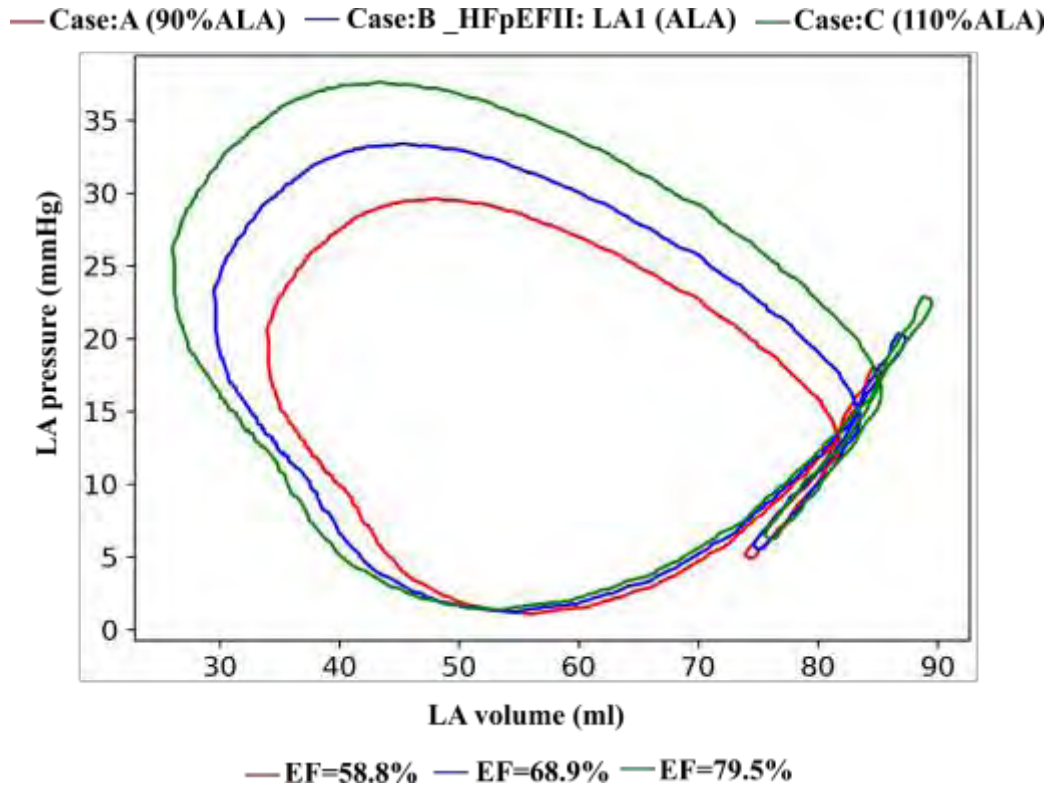


Figure 4. 17: Comparison among HFpEF-II LA of PV loops by varying scaling factor (ALA) for EDPVR

4.3.1 Effects of change of LA stiffness on LV PV Loops

The effects of changing the LA stiffness (Scaling Factor (A_{LA}) of EDPVR) (as indicated in Table 4.6) on the pressure and volume of LV have been demonstrated in Figure 4.12 (A), Figure 4.13 (A), and Figure 4.14 (A) for Normal: LA1, HFpEFI: LA1, and HFpEFII: LA1, respectively, and the pressure and volume of LA have been demonstrated in Figure 4.15, Figure 4.16, and Figure 4.17, respectively, using PV loops. Figure 4.12 (B), 4.13 (B), and Figure 4.14 (B) represented volume waveforms for LV. Figure 4.12 (C), 4.13 (C), and Figure 4.14 (C) illustrated pressure waveforms for LV respectively. The LA volume and pressure have been changed and as a consequence, the EDV of the LV has been increased as the A_{LA} have increased, however ESV has been decreased with the increased A_{LA} as can be seen in PV loops for all cases, as the compliance has been increased. Moreover, the EF have been increased, and the end-diastolic pressure (EDP) has been decreased by increasing the A_{LA} parameter for Normal: LA1, HFpEFI: LA1, and HFpEFII : LA1 cases.

4.3.2 Effects of change of LA stiffness on LV Strains

Figures 4.12 (D), 4.13 (D), Figure 4.14 (D), and Figure 4.12 (E), 4.13 (E), Figure 4.14 (E) and 4.12 (F), 4.13 (F), Figure 4.14 (F) depict changes in circumferential strain (Ecc), longitudinal strain (Ell), and radial strain (Err) waveforms with varying LA stiffness for Normal: LA1, HFpEFI: LA1, and HFpEFII: LA1, respectively. Peak Ecc, Ell, and Err have increased in increasing order as A_{LA} increases (Case: A to Case: C) in all cases. The absolute peak Ecc is 15 percent, 20 percent, and 23 percent for Case: A ($A_{LA} = 52.8$ Pa), Case: B ($A_{LA} = 58.67$ Pa), and Case: C ($A_{LA} = 64.54$ Pa), respectively For Normal: LA1 (Figure 4.12 (D)). Likewise, the absolute peak Ecc is 16 percent, 19 percent, and 23 percent for Case: A ($A_{LA} = 52.8$ Pa), Case: B ($A_{LA} = 58.67$ Pa), and Case: C ($A_{LA} = 64.54$ Pa), respectively for HFpEFI: LA1 (Figure 4.13 (D)). Correspondingly, the absolute peak Ecc is 14 percent, 18 percent, and 25 percent for Case: A ($A_{LA} = 52.8$ Pa), Case: B ($A_{LA} = 58.67$ Pa), and Case: C ($A_{LA} = 64.54$ Pa), respectively for HFpEFII: LA1 (Figure 4.14 (D)). The absolute peak Ell is 14 percent, 19 percent, and 23 percent for Normal: LA1 (Figure (4.12 (E))), 12 percent, 17 percent, and 23 percent for HFpEFI: LA1 (Figure 4.13 (E)), and 10 percent, 16 percent, and 25 percent for HFpEFII: LA1 (Figure 4.14 (E)) for A_{LA} of 52.8 Pa, 58.67 Pa, and 64.54 Pa, respectively. The absolute peak Err is 18 percent, 23 percent, and 27 percent for Normal: LA1 (Figure (4.12 (F))), 16 percent, 20 percent, and 23 percent for for HFpEFI: LA1 (Figure 4.13 (F)), and 12 percent, 19 percent, and 25 percent, respectively for HFpEFII: LA1 (Figure 4.14 (F)) whereas in healthy cases the peak Ecc, Ell and Err are 24 percent, 22 percent, and 26 percent, respectively [42]

Table 4. 7: Hemodynamic and functional indices of LV for Normal and HFpEF models with varying LA stiffness (Scaling factor, A_{LA} of EDPVR)

Index	Normal: LA1			Clinical Range
	Case: A ($A_{LA} = 52.8$)	Case: B ($A_{LA} = 58.67$)	Case: C ($A_{LA} = 64.54$)	
End-diastolic volume, EDV (ml)	109	114	123	84.1-132 [8, 72]
End-systolic volume, ESV (ml)	51	47	40	34.7-68.6 [8, 72]
Ejection fraction, EF (%)	53	59	67	52-71 [3, 8, 72]
End-diastolic pressure, EDP (mmHg)	15	10	7	7-16 [72, 73]

End-systolic pressure, ESP (mmHg)	107	122	138	101-124 [72]
Absolute peak Ecc (%)	15	20	23	13.45-24 [74, 76, 77]
Absolute peak Ell (%)	14	19	23	14-24 [74, 76, 77]
Absolute peak Err (%)	18	23	27	17-28 [74, 76, 77]
Index	HFpEFI: LA1			Clinical Range
	Case: A (ALA = 52.8)	Case: B (ALA = 58.67)	Case: C (ALA = 64.54)	
End-diastolic volume, EDV (ml)	97	103	114	114±28.1 [8]
End-systolic volume, ESV (ml)	47	41	36	47±16.7 [8]
Ejection fraction, EF (%)	52	60.3	69	59±7 [8]
End-diastolic pressure, EDP (mmHg)	14	8.6	7.2	7-18 [72, 73]
End-systolic pressure, ESP (mmHg)	118	101	87	80-153 [72]
Absolute peak Ecc (%)	16	19	23	13.45-24 [74, 76, 77]
Absolute peak Ell (%)	12	17	23	14-24 [74, 76, 77]
Absolute peak Err (%)	16	20	23	17-28 [74, 76, 77]
Index	HFpEFII: LA1			Clinical Range
	Case: A (ALA = 52.8)	Case: B (ALA = 58.67)	Case: C (ALA = 64.54)	
End-diastolic volume, EDV (ml)	119	129	141	114±28.1 [8]
End-systolic volume, ESV (ml)	51	48	42	47±16.7 [8]
Ejection fraction, EF (%)	57	63.3	70	58-75 [8, 72]

End-diastolic pressure, EDP (mmHg)	18	12	8.5	11.9±4.6 [8]
End-systolic pressure, ESP (mmHg)	162	147	137	123-178 [72, 73]
Absolute peak Ecc (%)	14	18	25	13.45-24 [74, 76, 77]
Absolute peak Ell (%)	10	16	25	14-24 [74, 76, 77]
Absolute peak Err (%)	12	19	25	17-28 [74, 76, 77]

4.4 Combined effects of varying LA contractility and stiffness on LV function for normal, HFpEF-I, and HFpEF-II cases

By varying the time varying elastance parameters of LA such as, end-systolic elastance parameter (Ees), scaling factor for EDPVR (A_{LA}), exponent for EDPVR (B_{LA}), time to end systole (T_{max}), time constant of relaxation (τ) the LA contractility and stiffness have been simultaneously changed to observe their combined effect on LV function. The parameters are listed in Table 4.8.

Table 4. 8: Variation of parameters of LA time varying elastance model for Normal, HFpEF-I, and HFpEF-II cases

Cases	Case ID	End-systolic elastance (Ees) (Pa/ml)		Scaling Factor A_{LA} for EDPVR (Pa)		Exponent for EDPVR, B_{LA} (per ml)		Tmax (ms)		τ (ms)	
		Pa/ml	% of baseline	Pa	% of baseline	per ml	% of baseline	ms	% of baseline	ms	% of baseline
Normal, HFpEF-I and HFpEF-II	Baseline	60.0	-	58.67	-	0.049	-	200	-	35	-
	LA 1	52.80	88.0	53.98	92.0	0.045	92.0	168	84.0	33	94.0
	LA 2	46.66	77.77	48.96	83	0.042	85.0	145	72.5	30	85.7
	LA 3	40.66	67.77	42.24	72	0.039	80.0	130	65	25	71.43

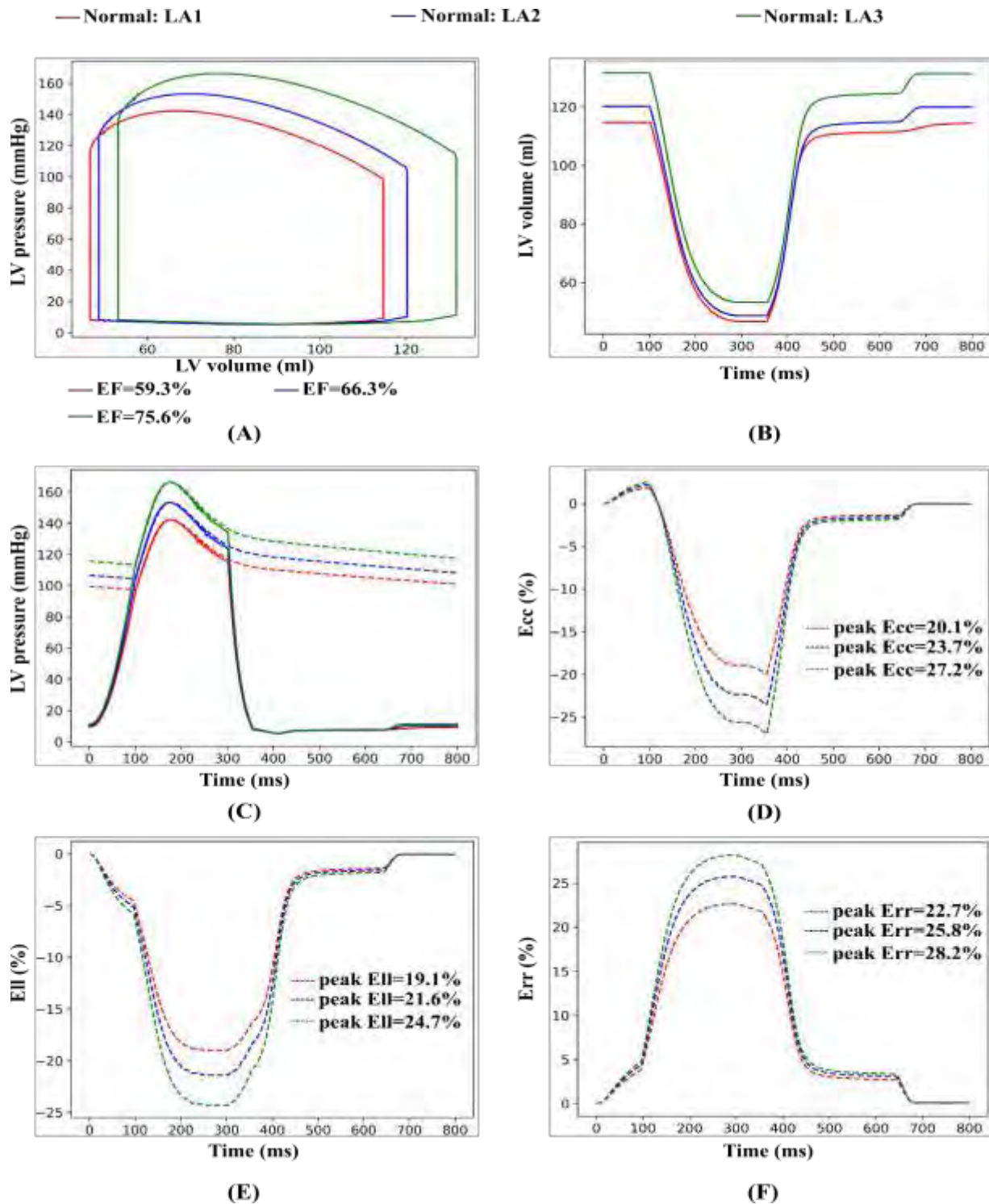


Figure 4.18: Comparison among Normal LV (A) PV loops, (B) volume waveforms, (C) pressure waveforms, (D) circumferential strains, (E) longitudinal strains, and (F) radial strains by varying LA time varying elastance parameters (E_{es} , A_{LA} , B_{LA} , T_{max} , τ)

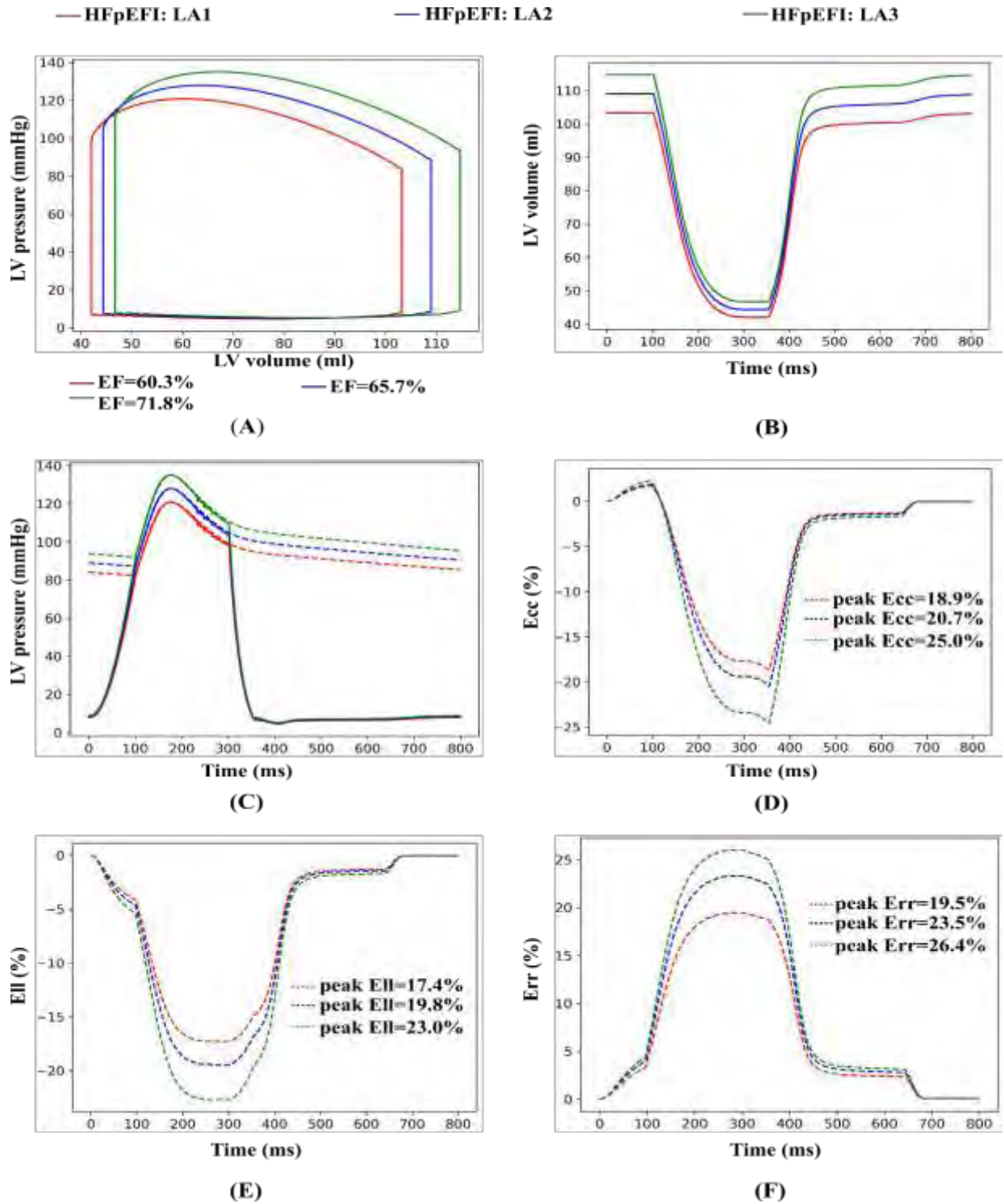


Figure 4. 19: Comparison among HFpEF-I LV (A) PV loops, (B) volume waveforms, (C) pressure waveforms, (D) circumferential strains, (E) longitudinal strains, and (F) radial strains by varying LA time varying elastance parameters (E_{es} , A_{LA} , B_{LA} , T_{max} , τ)

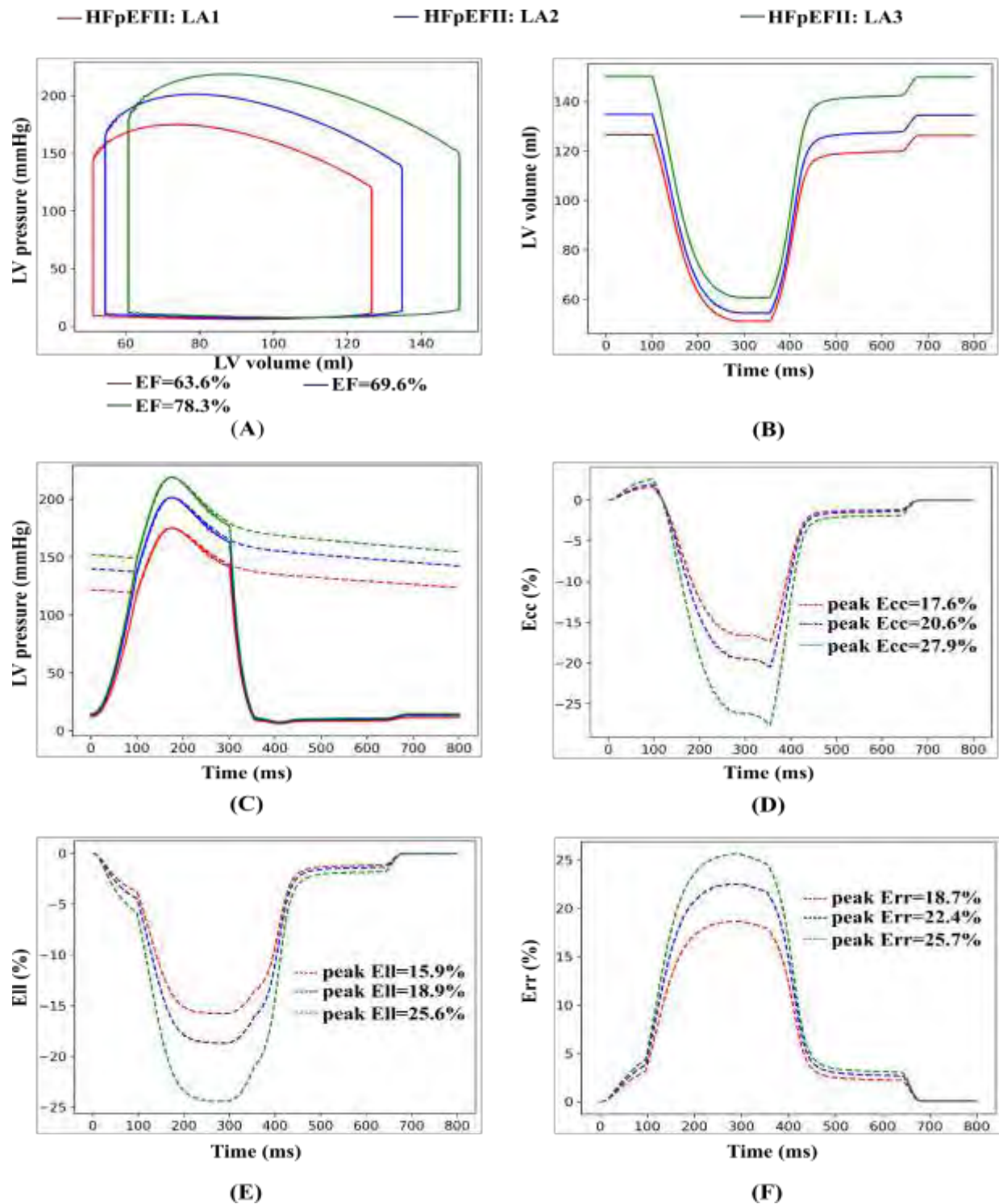


Figure 4. 20: Comparison among HFpEF-II LV (A) PV loops, (B) volume waveforms, (C) pressure waveforms, (D) circumferential strains, (E) longitudinal strains, and (F) radial strains by varying LA time varying elastance parameters (E_{es} , A_{LA} , B_{LA} , T_{max} , τ)

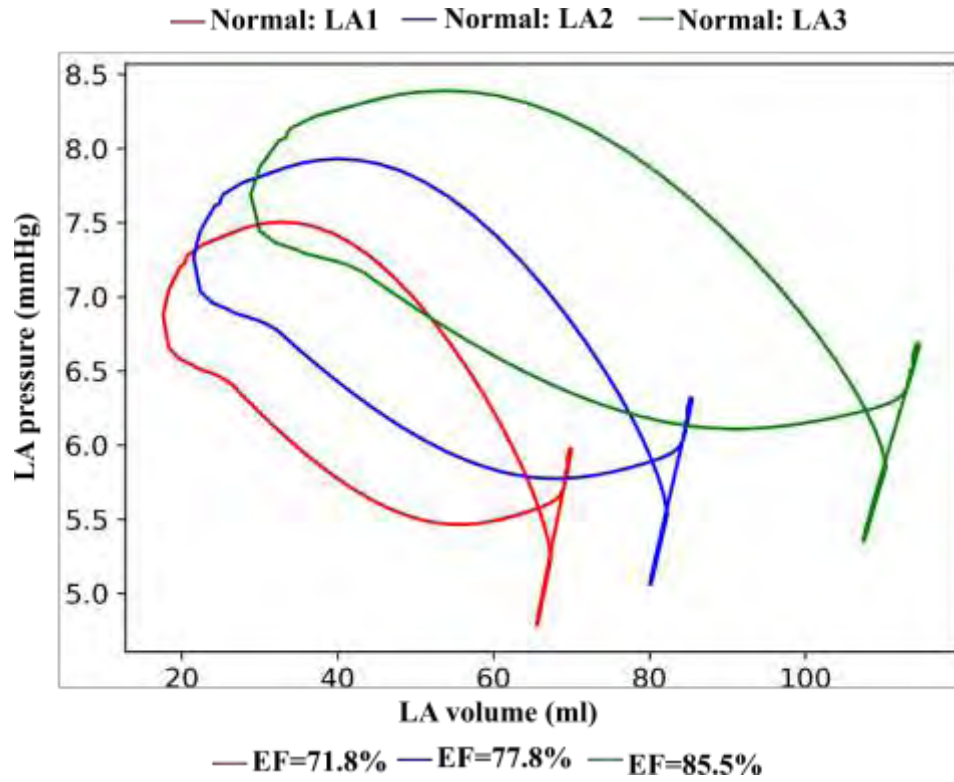


Figure 4. 21: Comparison among Normal LA PV loops by varying LA time varying elastance parameters (E_{es} , A_{LA} , B_{LA} , T_{max} , τ)

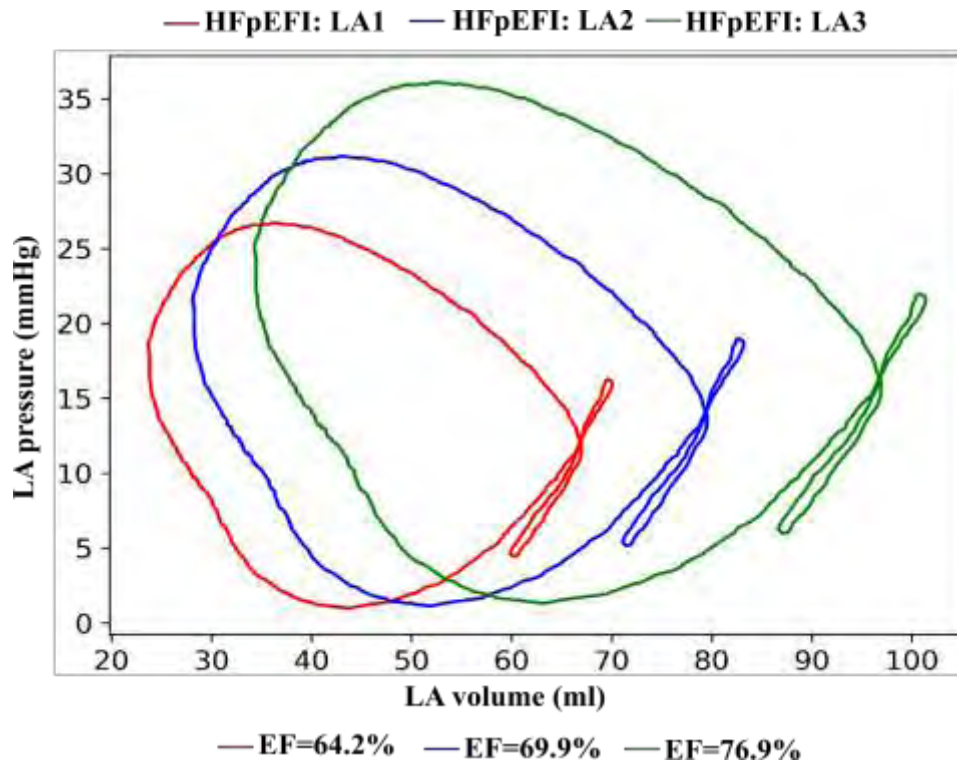


Figure 4. 22: Comparison among HFpEF-I LA PV loops by varying time varying elastance parameters (E_{es} , A_{LA} , B_{LA} , T_{max} , τ)

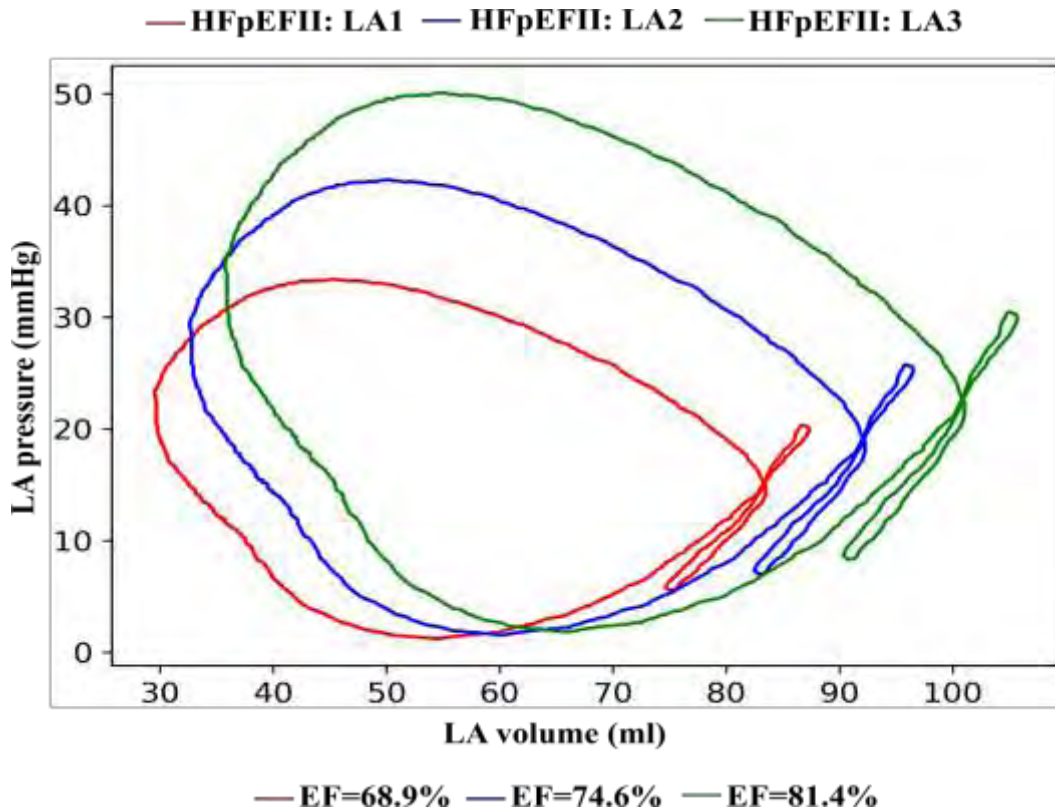


Figure 4. 23: Comparison among HFpEF-II LA PV loops by varying time varying elastance parameters (E_{es} , A_{LA} , B_{LA} , T_{max} , τ)

4.4.1 Effects of change of LA time varying elastance parameters on LV PV loop for Normal, HFpEF-I, and HFpEF-II cases

The effects of changing LA time varying elastance parameters (as indicated in Table 4.12) on the pressure and volume of LV have been demonstrated in Figure 4.18 (A), Figure 4.19 (A), and Figure 4.20 (A), respectively, and the pressure and volume of LA have been shown in Figure 4.21, Figure 4.22, and Figure 4.23, respectively, for Normal, HFpEFI, and HFpEFII, respectively. Figure 4.18 (B), 4.19 (B), and Figure 4.20 (B) represents volume waveforms for LV, respectively. Figure 4.18 (C), 4.19 (C), and Figure 4.20 (C) illustrates pressure waveforms for LV, respectively. By decreasing the E_{es} by 88%, A_{LA} by 92%, B_{LA} by 92%, T_{max} by 84% and τ by 94% from the baseline, the LA volume has been increased with the slightly increased of SBP of LA. As a result of which, EDV and ESV have been increased and the SBP has also increased. By decreasing the E_{es} by 78 percent (46.66 pa/ml), A_{LA} by 83 percent, B_{LA} by 85 percent T_{max} by 72.5 percent and τ by 85.7 percent (Normal: LA2 case) from the baseline, the LA EDV and ESV has been increased along with the increased SBP. As a consequences, the LV EDV and ESV has been increased. The SBP

has also been increased. The EF has also been increased from the Normal: LA1 case. Moreover, by decreasing the Ees by 67.8 percent (40.66 Pa/ml, range of varying Ees (29-80 Pa/ml [23]), A_{LA} by 92 percent, B_{LA} by 92 percent T_{max} by 84 percent and τ by 94 percent (Normal: LA3 case) from the baseline, the LA EDV and ESV have been increased at a very high rate. The corresponding LV EDV and ESV have also been increased rapidly. As the EF has been increased, the heart function improves.

From figure 4.21, the LA EDV for Normal: LA1 (red) is around 70 ml, and ESV is 20 ml (normal range of LA is 45 ± 12 ml [40], for HFpEF 85 ± 28 ml [40]). The SBP is 7.5 mmHg (normal range approximately 8.1 ± 2.8 mmHg [40]), and the EF is 71.8 percent. For Normal: LA2 (blue), the EDV has been increased to 91 ml. Corresponding ESV has been increased to 23 ml. The SBP has been increased to 7.9 mmHg. The EF has been increased to 77.8 percent. For Normal: LA3 (green), the EDV has been increased to 122 ml, and the ESV has been increased to 27 ml. The SBP has been increased to 8.4 mmHg. The EF has been increased to 85.5 percent. From figure 4.18 (A), it can be seen that the LV EDV for Normal: LA1 (red) is around 114 ml, and ESV is 47 ml. The SBP is 141 mmHg, and the EF is 59.3 percent. For Normal: LA2 (blue), the EDV has been increased to 126 ml. Corresponding ESV has been increased to 48 ml. The SBP has increased to 149 mmHg. The EF has been increased to 66.3 percent. For Normal: LA3 (green), the EDV has been increased to 153 ml, and the ESV has been increased to 51 ml. The SBP has increased to 163 mmHg. The EF has been increased to 75.6 percent.

From figure 4.22, the LA EDV for HFpEFI: LA1 (red) is around 67 ml, and ESV is 23 ml (normal range of LA is 45 ± 12 ml [40], for HFpEF 85 ± 28 ml [40]). The SBP is 26 mmHg (HFpEF range approximately 20 ± 6.1 mmHg [40]), and the EF is 64.2 percent. For HFpEFI: LA2 (blue), the EDV has been increased to 85 ml. Corresponding ESV has been increased to 27 ml. The SBP has increased to 31 mmHg. The EF has been increased to 69.9 percent. For HFpEFI: LA3 (green), the EDV has been increased to 110 ml, and the ESV has been increased to 32 ml. The SBP has increased to 36 mmHg. The EF has been increased to 76.9 percent. From figure 4.19 (A), it can be seen that the LV EDV for HFpEFI: LA1 (red) is around 104.6 ml, and ESV is 41.3 ml. The SBP is 121 mmHg, and the EF is 60.3 percent. For HFpEFI: LA2 (blue), the EDV has been increased to 110 ml. Corresponding ESV has been increased to 41.9 ml. The SBP has increased to 129 mmHg. The EF has been increased to 65.7 percent. For HFpEFI: LA3 (green), the EDV has been

increased to 137 ml, and the ESV has been increased to 43 ml. The SBP has increased to 138 mmHg. The EF has been increased to 71.8 percent.

Again, from figure 4.23, it can be seen that the LA EDV for HFpEFII: LA1 (red) is around 87.3 ml, and ESV is 29.6 ml (normal range of LA is 45 ± 12 ml [40], for HFpEF 85 ± 28 ml [40]). The SBP is 33.4 mmHg (HFpEF range approximately 20 ± 6.1 mmHg [40]), and the EF is 68.9 percent. For HFpEFII: LA2 (blue), the EDV has been increased to 99 ml. Corresponding ESV has been increased to 32 ml. The SBP has increased to 41 mmHg. The EF has been increased to 74.6 percent. For HFpEFII: LA3 (green), the EDV has been increased to 117 ml, and the ESV has been increased to 33 ml. The SBP has increased to 49 mmHg. The EF has been increased to 81.4 percent. From figure 4.20 (A), it can be seen that the LV EDV for HFpEFII: LA1 (red) is around 129 ml, and ESV is 48 ml. The SBP is 175.8 mmHg, and the EF is 63.6 percent. For HFpEFII: LA2 (blue), the EDV has been increased to 139 ml. Corresponding ESV has been increased to 49 ml. The SBP has increased to 197 mmHg. The EF has been increased to 69.6 percent. For HFpEFII: LA3 (green), the EDV has been increased to 168 ml, and the ESV has been increased to 61 ml. The SBP has increased to 227 mmHg. The EF has been increased to 78.3 percent. The EF range for the HFpEF patients is around 67 ± 8 percent [73]. For the EDV of 69-151 ml [72, 73], the heart is considered as HFpEF. From the above-mentioned cases, it can be concluded that the time varying elastance parameters have significant impact on the remodeling of LA as well as the LV and due to the changes of these values from the baseline case, improves the LV function as measured by the ejection fraction and peak longitudinal and circumferential strains with increased LA pressure. The study's findings show that enlarging the LA and increasing LA pressure improves overall LV function.

4.4.2 Effects of change of LA time varying elastance parameters on LV Strains for Normal, HFpEF-I, and HFpEF-II cases

Waveforms of circumferential strain (Ecc), longitudinal strain (Ell), and radial strain (Err) as a function due to varying LA time varying elastance parameters are depicted in Figures 4.18 (D), 4.18 (E), and 4.18 (F), respectively for Normal case. With varying LA time varying elastance parameters i.e. E_{es} , A_{LA} , B_{LA} , T_{max} , and τ of LA, the peak Ecc, peak Ell, and peak Err have all increased. In the Normal: LA1 (red), Normal: LA2 (blue), and Normal: LA3 (green), the absolute peak Ecc is 20 percent, 24 percent, and 27 percent, respectively (Figure 4.18 (D)), whereas the healthy heart has a peak Ecc of 24 percent [42]. The absolute peak Ell for the cases is 19 percent,

22 percent, and 25 percent (Figure 4.18 (E)), and the absolute peak Err is 23 percent, 26 percent, and 28 percent (Figure 4.18 (F)), respectively, whereas the peak Ell and Err for healthy patients are 22 percent and 26 percent [42].

Similarly, Waveforms of circumferential strain (Ecc), longitudinal strain (Ell), and radial strain (Err) as a function due to varying LA time varying elastance parameters are depicted in Figures 4.19 (D), Figure 4.20 (D), 4.19 (E), Figure 4.20 (E), and 4.19 (F), Figure 4.20 (F), respectively for HFpEF-I, and HFpEF-II cases. With varying LA time varying elastance parameters i.e. E_{es} , A_{LA} , B_{LA} , T_{max} , and τ of LA, the peak Ecc, peak Ell, and peak Err have all increased. In the HFpEFI: LA1 (red), HFpEFI: LA2 (blue), and HFpEFI: LA3 (green), the absolute peak Ecc is 18 percent, 20 percent, and 24 percent, respectively (Figure 4.19 (D)), whereas the healthy heart has a peak Ecc of 24 percent [42]. The absolute peak Ell for the cases is 17 percent, 19 percent, and 22 percent (Figure 4.26 (E)), and the absolute peak Err is 19 percent, 23 percent, and 26 percent (Figure 4.19 (F)), respectively, whereas the peak Ell and Err for healthy patients are 22 percent and 26 percent [42].

In the HFpEFII: LA1 (red), HFpEFII: LA2 (blue), and HFpEFII: LA3 (green), the absolute peak Ecc is 17 percent, 20 percent, and 27 percent, respectively (Figure 4.20 (D)), whereas the healthy heart has a peak Ecc of 24 percent [42]. The absolute peak Ell for the cases is 15 percent, 18 percent, and 25 percent (Figure 4.20 (E)), and the absolute peak Err is 18 percent, 22 percent, and 26 percent (Figure 4.20 (F)), respectively, whereas the peak Ell and Err for healthy patients are 22 percent and 26 percent [42].

As a consequence, it can be said that due to varying time varying elastance parameters the Ecc Ell and Err strains have been increased for all three cases i.e. Normal, HFpEF-I, and HFpEF-II. As the strain of the heart increases gradually, the LV function has been improved as indicated by the increased strain values. The pressure, volume, Ecc, Ell, and Err variations due to combined variation of time varying elastance parameters are tabulated in Table 4.9 for LV and LA. The results show that expanding the LA and increasing LA pressure improve overall LV function. Because LA expansion with increasing LA pressure is a common feature of HFpEF, the results suggest that this mechanism may assist the LV to maintain its ejection fraction.

Table 4.9: Hemodynamic and functional indices of LV for Normal and HFpEF models for different LA time varying elastance model parameters

Index	Normal			Clinical Range
	Normal: LA1	Normal: LA2	Normal: LA3	
	LV			
End-diastolic volume, EDV (ml)	114	126	135	84.1-132 [8, 72]
End-systolic volume, ESV (ml)	47	48	51	34.7-68.6 [8, 72]
Ejection fraction, EF (%)	59.3	66.3	75.6	52-71 [3, 8, 72]
End-diastolic pressure, EDP (mmHg)	10	11	11.5	7-16 [72, 73]
End-systolic pressure, ESP (mmHg)	121	133	143	101-124 [72]
Absolute peak Ecc (%)	20.076	23.693	27.226	13.45-24 [74, 76, 77]
Absolute peak Ell (%)	19.105	21.584	24.743	14-24 [74, 76, 77]
Absolute peak Err (%)	22.638	25.753	28.183	17-28 [74, 76, 77]
	LA			
End-diastolic volume, EDV (ml)	70	91	122	45±12 [40]
End-systolic volume, ESV (ml)	20	23	27	16±6.3 [40]
Ejection fraction, EF (%)	71.8	77.8	85.5	-
Systolic Blood Pressure (mmHg)	7.5	7.9	8.4	8.1±2.8 [40]
Index	HFpEFI			Clinical Range
	HFpEFI: LA1	HFpEFI: LA2	HFpEFI: LA3	
	LV			
End-diastolic volume, EDV (ml)	103	110	114	114±28.1 [8]
End-systolic volume, ESV (ml)	41	41.9	36	47±16.7 [8]
Ejection fraction, EF (%)	60.3	65.7	69	59±7 [8]
End-diastolic pressure, EDP (mmHg)	8.6	9.1	9.5	7-18 [72, 73]

End-systolic pressure, ESP (mmHg)	101	112	119	80-153 [72]
Absolute peak Ecc (%)	18.874	20.713	24.954	13.45-24 [74, 76, 77]
Absolute peak Ell (%)	17.427	19.773	22.937	14-24 [74, 76, 77]
Absolute peak Err (%)	19.477	23.485	26.413	17-28 [74, 76, 77]
	LA			
End-diastolic volume, EDV (ml)	67	85	110	85±28 [40]
End-systolic volume, ESV (ml)	23	27	32	23±5 [40]
Ejection fraction, EF (%)	64.2	69.9	76.9	-
Systolic blood pressure (mmHg)	26	31	36	20±6.1 [40]
Index	HFpEFII			Clinical Range
	HFpEFII: LA1	HFpEFII: LA2	HFpEFII: LA3	
	LV			
End-diastolic volume, EDV (ml)	129	139	168	114±28.1 [8]
End-systolic volume, ESV (ml)	48	49	61	47±16.7 [8]
Ejection fraction, EF (%)	63.6	69.6	78.3	58-75 [8, 72]
End-diastolic pressure, EDP (mmHg)	12	13.5	13.9	11.9±4.6 [8]
End-systolic pressure, ESP (mmHg)	147	168	182	123-178 [72, 73]
Absolute peak Ecc (%)	17.575	20.568	27.893	13.45-24 [74, 76, 77]
Absolute peak Ell (%)	15.929	18.914	25.573	14-24 [74, 76, 77]
Absolute peak Err (%)	18.648	22.375	25.693	17-28 [74, 76, 77]
	LA			
End-diastolic volume, EDV (ml)	87.3	99	117	85±28 [40]
End-systolic volume, ESV (ml)	29.6	32	33	54±27 [40]

Ejection fraction, EF (%)	68.9	74.6	81.4	-
Systolic blood pressure (mmHg)	33.4	41	49	34±13 [40]

4.5 Summary

Heart failure with preserved ejection fraction (HFpEF) is a life-threatening illness that leads in heart failure (HF) and premature death. We recreated important elements of ventricular geometry, chamber size, blood pressure, LV EF, and circumferential and longitudinal strain reported in normal, and HFpEF patients using a FE computational model. To the best of our knowledge no such research has been done yet which focus on the inter-relation between left atrium and left ventricle and quantify the effects of change of the LA properties on the LV function in HFpEF patients. In this study, the LA contractility and stiffness have been varied individually and at a time by varying relevant model parameters namely, end-systolic elastance (E_{cs}), scaling factor for the EDPVR (A_{LA}), exponent for EDPVR (B_{LA}), Time to end-systole (T_{max}) and time constant of relaxation (τ) of LA for HFpEF cases.

An isolated increase in LA contractility creates a steeper ESPVR i.e. the slope of the ESPVR increases. If the preload and afterload stay constant, the stroke volume increases. As a result, the ESV and EDV have been decreased, however the ESP and EDP have been increased. This is because by increasing the LA contractility, the contractile force has been increased and due to this force, more blood has been ejected from the LA to the LV chamber as indicated by the increased EF. The corresponding circumferential (E_{cc}), longitudinal (E_{ll}), and radial (E_{rr}) strains of LV also increased, and the overall LV function improved by isolated increasing of the LA contractility.

Scaling factor for EDPVR (A_{LA}) has been altered to change the LA stiffness. The compliance of the ventricle determines the pressure and volume that come from filling when the ventricle fills with blood. Compliance curves are often displayed as the change in volume (V) versus the change in pressure (P). However, for the ventricle, it is usual to plot P against V . As a result, the slope of the connection is the reciprocal of the compliance, which is also known as ventricular "stiffness." The pressure within the ventricular chamber gradually increases as the ventricle fills with blood and its volume grows. Because the compliance of the ventricular wall diminishes ("stiffness" rises) when the ventricular wall is stretched, the relationship is not linear, especially at greater volumes. This happens in the majority of biological tissues. The structural features of the heart muscle (e.g., muscle fibers and their orientation, and connective tissue) as well as the state of ventricular

contraction and relaxation define the ventricle's compliance. For example, with ventricular hypertrophy, ventricular compliance decreases (i.e., the ventricle becomes "stiffer") when ventricular wall thickness grows; as a result, ventricular end-diastolic pressure (EDP) rises at any given end-diastolic volume (EDV). Other heart disease states, such as various types of restrictive cardiomyopathy, can cause a reduction in ventricular compliance. Alternatively, a less compliant ventricle would have a smaller EDV at a given EDP (i.e., filling will be impaired). If ventricular relaxation is disrupted (as in some cases of diastolic cardiac failure), functional ventricular compliance is diminished (due to residual active tension), impairing ventricular filling. The ventricle becomes extremely dilated in a pathological condition such as dilated cardiomyopathy, with no discernible thickening of the wall. The dilated ventricle will have higher compliance; hence, while the EDV may be quite high, the EDP may not be much elevated. Decreased ventricular compliance results in higher pressure at a given volume, clinically results in lower end-diastolic volume associated with higher end-diastolic pressure etc. On the other hand, compliance increased by systolic dysfunction due to the dilated cardiomyopathy, and chronic volume overload due to valve regurgitation. Increased ventricular compliance results in lower pressure at a given volume, clinically results in larger end-diastolic volumes, and end-diastolic pressure which depends on both compliance and blood volume status.

Isolated increase in LA stiffness results increase of LV ESP, however LV EDP has been decreased, the LV SBP has also been increased. The LV EF is increased. Corresponding Ecc, Ell, and Err have also increased with the increasing LA stiffness for both normal and HFpEF cases. Thus, we can conclude that isolated increase in the LA stiffness increases the LV EF, peak Ecc, peak Ell and peak Err which indicates the improvement of the heart function.

By varying both the LA contractility, and stiffness, at a time, the LA pressure and volume have been increased. The slope of the LV's ESPVR has been decreased, however the EDP increased along with the increasing EDV. As a result of which the EF has been increased for both Normal and HFpEF patients for both HFpEF-I, and HFpEF-II cases which indicates the improvement of LV. The peak circumferential strain, longitudinal strain and radial strain have also increased which indicates the improvement of the LV function. Similar results have been found in cases of increased LA contractility and increased LA stiffness individually. By decreasing the LA time varying elastance parameters from the baseline, the LV EDV as well as the ESV increases. HFpEF patient usually has increased EDV which is a symptom of remodeling and increased systolic blood

pressure which is symptom of hypertension. HFpEF patient has higher end-diastolic pressure (EDP) than normal which suggests HFpEF patient's LV is stiffer than the normal LV. Clinically, EDP higher than 15 mmHg is considered as sign of diastolic dysfunction which is a common feature in HFpEF. However, by varying the LA time varying elastance parameters, the EF have been increased with a very little rise of the EDP which is a good sign for the LV. Therefore, it can be concluded that, the isolated change in the LA time varying elastance parameters have an impact on the improvement of LV which imply that this mechanism might help the LV to preserve its ejection fraction.

CHAPTER 5

CONCLUSION

5.1 Conclusion

In this thesis, a coupled left ventricular finite element-lumped parameter systemic circulatory model has been used to quantify the effect LA malfunction on the LV function. The model was calibrated using the clinical measurements from the literature review of a normal subject and HFpEF patients. Following that, the LA contractility and stiffness were varied individually and at a time to simulate the effects of these parameters on the LV function for HFpEF patients. The findings of this study are summarized below:

- With increased LA contractility, the peak pressure and volume of LA have been increased. As a consequence, the LV function gradually improved as indicated by higher ejection fraction. The ejection fraction of LV increased from 53.7 percent to 66.2 percent for Normal case, 51.6 percent to 67.4 percent for HFpEF-I case, and 56.3 percent to 72.1 percent for HFpEF-II case. In addition, higher peak LV longitudinal (E_{ll}) and circumferential (E_{cc}) strains in both HFpEF cases were found which also indicates the improvement of LV function. In Normal case, the absolute peak E_{ll} increased from 16.1 percent to 21.8 percent and absolute peak E_{cc} increased from 16.1 percent to 24.3 percent, in HFpEF-I case, the absolute peak E_{ll} increased from 13.1 percent to 21.4 percent and absolute peak E_{cc} increased from 14.8 percent to 21.6 percent, and in HFpEF-II case, the absolute peak E_{ll} increased from 10.9 percent to 23.4 percent and absolute peak E_{cc} increased from 12.6 percent to 23.6 percent.
- In case of increased LA stiffness, similar results have been found for both HFpEF cases where LV ejection fraction and peak longitudinal and circumferential strains have gradually increased. The ejection fraction has been increased from 52.6 percent to 70.2 percent for HFpEF cases. The corresponding absolute peak E_{ll} has been increased from 9.6 percent to 24.9 percent, and the absolute peak E_{cc} has been increased from 13.6 percent to 24.5 percent for HFpEF cases.
- Finally, for both HFpEF instances, combinations of LA contractility and stiffness were utilized, which revealed a steady improvement in LV function as measured by the ejection fraction and peak longitudinal and circumferential strains with increased LA pressure.

- The study's findings show that enlarging the LA and increasing LA pressure improves overall LV function. Because expansion of the LA with increased LA pressure is frequently found in HFpEF, the findings imply that this mechanism might help the LV to preserve its ejection fraction. Moreover, the ejection fraction of LV has been increased from 59.3 percent to 78.3 percent for HFpEF cases. In addition, the absolute peak EII increased from 15.9 percent to 25.6 percent and the absolute peak Ecc increased from 17.6 percent to 27.9 percent for both the HFpEF cases. By decreasing the overall LV contractility or by changing the myofiber helix angle, the peak strains values can be reduced to match reduction of peak strain values found in some recent clinical studies in HFpEF patients keeping the ejection fraction preserved or in the normal range (>55%) which can be explored in future studies.

5.2 Limitations of the Work

Though it was shown that the model adequately reproduces the results found in the literature, however this model has some limitations. These are discussed below:

- LV was modeled using idealized half-prolate ellipsoid for simplicity although in reality, the human LV is asymmetric. However, numerous studies have modeled the LV as idealized ellipsoid in the past.
- Only Finite element model of Left ventricle was used in this study. The LA was modeled with a simple time-varying elastance model. Finite element model of left atrium could be incorporated to produce more accurate result.
- In this research, one parameter was changed while the others remained constant. There may be a linked impact among the parameters that cannot be assessed until more than one parameter is changed at the same time.
- The model ignores any regional activation patterns and assumes that the LV contracts uniformly.
- In this model, the myofiber helix angle changed linearly in the transmural direction from endocardium to epicardium, according to a rule-based myofiber orientation. In reality, myofiber orientation might be more complicated.
- The mechanical effects of the right ventricle (RV) and pulmonary circulation were not taken into account. Despite the fact that cavity pressure in the RV is far lower than in the LV, its presence may alter LV mechanics through the septum.

- Finally, because the pathophysiology of HFpEF is still a poorly understood topic, the proper connection between physiological alterations and HFpEF development is ambiguous. The correct HFpEF progression mechanism will require additional clinical research.

5.3 Recommendation for Future Works

As discussed, the present model has some limitations. The present model can be improved by incorporating the following suggestions:

- More realistic model acquired from MRI (Magnetic Resonance Imaging) scans of human heart and modeling with measured clinical data.
- Finite elements model of left atrium can be coupled with current left ventricle model which might help to achieve better insight.
- The model need to be updated time to time to incorporate new findings as, mechanism of HFpEF is still an active research area.

REFERENCES

- [1] Burkhoff, D., “Mechanical Properties of the Heart and Its Mechanical Properties of the Heart and Its Interaction with the Vascular System.” *Card. Physiol.*, 84, 1–23 (2002).
- [2] Virani, S. S., Alonso, A., Benjamin, E. J., Bittencourt, M. S., “Heart Disease and Stroke Statistics—2020 Update: A Report from the American Heart Association.” *Circul.*, vol. 141(9), pp. e139-e596, 2020. doi:10.1161/CIR.0000000000000757.
- [3] Zakeri, R. et al., “Left Atrial Remodeling and Atrioventricular Coupling in a Canine Model of Early Heart Failure with Preserved Ejection Fraction.” *Circ. Hear. Fail.*, 9, 1–11 (2016).
- [4] Bytyçi, I. & Bajraktari, G., “Left atrial changes in early stages of heart failure with preserved ejection fraction.” *Echocardiography* 33, 1479–1487 (2016).
- [5] Jean-Louis, G., Zizi, F., Clark, L. T., Brown, C. D. & McFarlane, S. I., “Obstructive sleep apnea and cardiovascular disease: Role of the metabolic syndrome and its components.” *J. Clin. Sleep Med.*, 4, 261–272 (2008).
- [6] Park, J. J., Park, J. B., Park, J. H. & Cho, G. Y., “Global Longitudinal Strain to Predict Mortality in Patients With Acute Heart Failure.” *J. Am. Coll. Cardiol.*, 71, 1947–1957 (2018).
- [7] Lekavich, C. L., Barksdale, D. J., Neelon, V. & Wu, J. R., “Heart failure preserved ejection fraction (HFpEF): an integrated and strategic review.” *Heart Fail. Rev.*, 20, 643–653 (2015).
- [8] Maas, S. A., Ellis, B. J., Rawlins, D. S. & Weiss, J. A., “Finite element simulation of articular contact mechanics with quadratic tetrahedral elements.” *J. Biomech.*, 49, 659–667 (2016).
- [9] Alnæs, M., Blechta, J., Hake, J., Johansson, A., Kehlet, B., Logg, A., Richardson, C., Ring, J., Rognes, M. E., Wells, G. N., “The FEniCS Project Version 1.5.” *Arch. Numer. Softw.*, 3, 9–23 (2015).
- [10] Ortale, J. R., Meciano Filho, J., Paccola, A. M. F., Leal, J. G. P. G. & Scaranari, C. A., “Anatomy of the lateral, diagonal and anterosuperior arterial branches of the left ventricle of the human heart.” *Brazilian J. Cardiovasc. Surg.*, 20, 149–158 (2005).
- [11] Zinchenko, Y.P. & Khoroshikh, Pavel & Alexandr, Sergievich & Smirnov, A.S. & Tumyalis, Alex & Kovalev, Artem & Gutnikov, S.A. & Golokhvast, Kirill., “Virtual

- reality is more efficient in learning human heart anatomy especially for subjects with low baseline knowledge.” *New Ideas Psychol.*, 59, 100786 (2020).
- [12] Sanchez-Quintana, D., Garcia-Martinez, V., Climent, V. & Hurler, J. M., “Morphological changes in the normal pattern of ventricular myoarchitecture in the developing human heart.” *Anat. Rec.*, 243, 483–495 (1995).
- [13] Guyton, A. C., Hall, J. E., “Textbook of medical physiology.” 9th ed. Philadelphia: W.B. Saunders (1996).
- [14] Tanné, D., Bertrand, E., Kadem, L., Pibarot, P. & Rieu, R., “Assessment of left heart and pulmonary circulation flow dynamics by a new pulsed mock circulatory system.” *Exp. Fluids*, 48, 837–850 (2010).
- [15] Hauck, A., Porta, N., Lestrud, S. & Berger, S., “The pulmonary circulation in the single ventricle patient.” *Children*, 4, 1–12 (2017).
- [16] Vonk Noordegraaf A, Chin KM, Haddad F, Hassoun PM, Hennes AR, Hopkins SR, Kawut SM, Langleben D, Lumens J, Naeije R., “Pathophysiology of the right ventricle and of the pulmonary circulation in pulmonary hypertension: An update.” *Eur. Respir. J.* 53, (2019).
- [17] Namani R, Lee L. C., Lanir Y., Kaimovitz B., Shavik S. M., Kassab G. S., “Effects of myocardial function and systemic circulation on regional coronary perfusion.” *J. Appl. Physiol.*, 128, 1106–1122 (2020).
- [18] Navaratnarajah, A. & Jackson, S. H. D., “The physiology of ageing.” *Med.*, (United Kingdom) 45, 6–10 (2017).
- [19] Thomas, L., Marwick, T. H., Popescu, B. A., Donal, E. & Badano, L. P., “Left Atrial Structure and Function, and Left Ventricular Diastolic Dysfunction: JACC State-of-the-Art Review.” *J. Am. Coll. Cardiol.*, 73, 1961–1977 (2019).
- [20] Stokke T. M., Hasselberg N. E., Smedsrud M. K., Sarvari S. I., Haugaa K. H., Smiseth O. A., Edvardsen T., Remme E. W., “Geometry as a Confounder When Assessing Ventricular Systolic Function: Comparison Between Ejection Fraction and Strain.” *J. Am. Coll. Cardiol.*, 70, 942–954 (2017).
- [21] Luis, S. A., Chan, J. & Pellikka, P. A., “Echocardiographic Assessment of Left Ventricular Systolic Function: An Overview of Contemporary Techniques, Including Speckle-Tracking Echocardiography.” *Mayo Clin. Proc.*, 94, 125–138 (2019).

- [22] Potter, L. R., Yoder, A. R., Flora, D. R., Antos, L. K. & Dickey, D. M., “Natriuretic peptides: Their structures, receptors, physiologic functions and therapeutic applications.” *Handb. Exp. Pharmacol.*, 191, 341–366 (2009).
- [23] Ota, T., Schwartzman, D., Francischelli, D., Hettrick, D. A. & Zenati, M. A. “Impact of beating heart left atrial ablation on left-sided heart mechanics.” *J. Thorac. Cardiovasc. Surg.*, 134, 982–988 (2007).
- [24] Appleton, C. P., Hatle, L. K. & Popp, R. L., “Relation of transmitral flow velocity patterns to left ventricular diastolic function: New insights from a combined hemodynamic and Doppler echocardiographic study.” *J. Am. Coll. Cardiol.*, 12, 426–440 (1988).
- [25] Stefanadis, C., Dernellis, J., Tsiamis, E. & Toutouzas, P., “Effects of pacing-induced and balloon coronary occlusion ischemia on left atrial function in patients with coronary artery disease.” *J. Am. Coll. Cardiol.*, 33, 687–696 (1999).
- [26] Toutouzas K., Trikas A., Pitsavos C., Barbetseas J., Androulakis A., Stefanadis C., Toutouzas P., “Echocardiographic features of left atrium in elite male athletes.” *Am. J. Cardiol.*, 78, 1314–1317 (1996).
- [27] Rossi A., Gheorghiade M., Triposkiadis F., Solomon S. D., Pieske B., Butler J., “Left atrium in heart failure with preserved ejection fraction structure, function, and significance.” *Circ. Hear. Fail.*, 7, 1042–1049 (2014).
- [28] Sisakian, H., “Cardiomyopathies: Evolution of pathogenesis concepts and potential for new therapies.” *World J. Cardiol.*, 6, 478 (2014).
- [29] NHFA CSANZ Heart Failure Guidelines Working Group, Atherton J. J., Sindone A., De Pasquale C. G., Driscoll A., MacDonald P. S., Hopper I., Kistler P. M., Briffa T., Wong J., Abhayaratna W., Thomas L., Audehm R., Newton P., O’Loughlin J., Branagan M., Connell C., “National Heart Foundation of Australia and Cardiac Society of Australia and New Zealand: Guidelines for the Prevention, Detection, and Management of Heart Failure in Australia 2018.” *Hear. Lung Circ.*, 27, 1123–1208 (2018).
- [30] Nagueh S. F., Smiseth O. A., Appleton C. P., Byrd B. F. 3rd, Dokainish H., Edvardsen T., Flachskampf F. A., Gillebert T. C., Klein A. L., Lancellotti P., Marino P., Oh J. K., Popescu B. A., Waggoner A. D., “Recommendations for the Evaluation of Left Ventricular Diastolic Function by Echocardiography: An Update from the American

- Society of Echocardiography and the European Association of Cardiovascular Imaging.” *J. Am. Soc. Echocardiogr.*, 29, 277–314 (2016).
- [31] Chen, Y. T., Wong, L. L., Liew, O. W. & Richards, A. M., “Heart Failure with Reduced Ejection Fraction (HFrEF) and Preserved Ejection Fraction (HFpEF): The Diagnostic Value of Circulating MicroRNAs.” *Cells*, 8, 1–13 (2019).
- [32] Borlaug, B. A. & Kass, D. A., “Ventricular-Vascular Interaction in Heart Failure.” *Heart Fail. Clin.*, 4, 23–36 (2008).
- [33] Louridas, G. E. & Lourida, K. G., “Heart failure in patients with preserved ejection fraction: Questions concerning clinical progression.” *J. Cardiovasc. Dev. Dis.*, 3, (2016).
- [34] Butler J., Hamo C. E., Udelson J. E., Pitt B., Yancy C., Shah S. J., Desvigne-Nickens P., Bernstein H. S., Clark R. L., Depre C., Dinh W., Hamer A., Kay-Mugford P., Kramer F., Lefkowitz M., Lewis K., Maya J., Maybaum S., Patel M. J., Pollack P. S., Roessig L., Rotman S., Salsali A., Sims J. J., Senni M., Rosano G., Dunnmon P., Stockbridge N., Anker S. D., Zile M. R., Gheorghiade M., “Exploring New Endpoints for Patients with Heart Failure with Preserved Ejection Fraction.” *Circ. Hear. Fail.*, 9, 1–8 (2016).
- [35] Trayanova, N. A. & Rice, J. J., “Cardiac electromechanical models: From cell to organ.” *Front. Physiol.*, 2 AUG, 1–19 (2011).
- [36] Capelli C., Sauvage E., Giusti G., Bosi G. M., Ntsinjana H., Carminati M., Derrick G., Marek J., Khambadkone S., Taylor A. M. and Schievano S., “Patient-specific simulations for planning treatment in congenital heart disease.” *Interface Focus*, 8, (2018).
- [37] Shavik, S. M., Wall, S. T., Sundnes, J., Burkhoff, D. & Lee, L. C., “Organ-level validation of a cross-bridge cycling descriptor in a left ventricular finite element model: Effects of ventricular loading on myocardial strains.” *Physiol. Rep.*, 5, 1–14 (2017).
- [38] Pfeffer, M. A., Shah, A. M. & Borlaug, B. A., “Heart Failure with Preserved Ejection Fraction in Perspective.” *Circ. Res.*, 124, 1598–1617 (2019).
- [39] Tan Y. T., Wenzelburger F., Lee E., Nightingale P., Heatlie G., Leyva F., Sanderson J. E., “Reduced left atrial function on exercise in patients with heart failure and normal ejection fraction.” *Heart*, 96, 1017–1023 (2010).
- [40] Melenovsky V., Hwang S. J., Redfield M. M., Zakeri R., Lin G., Borlaug B. A., “Left atrial remodeling and function in advanced heart failure with preserved or reduced ejection fraction.” *Circ. Hear. Fail.*, 8, 295–303 (2015).

- [41] Hoit, B. D., “Left atrial size and function: Role in prognosis.” *J. Am. Coll. Cardiol.*, 63, 493–505 (2014).
- [42] Shavik S. M., Wall S., Sundnes J., Guccione J. M., Sengupta P., Solomon S. D., Burkhoff D., Lee L. C., “Computational Modeling Studies of the Roles of Left Ventricular Geometry, Afterload, and Muscle Contractility on Myocardial Strains in Heart Failure with Preserved Ejection Fraction.” *J. Cardiovasc. Transl. Res.*, (2021) doi:10.1007/s12265-021-10130-y.
- [43] Lee, L. C., Sundnes, J., Genet, M., Wenk, J. F. & Wall, S. T., “An integrated electromechanical-growth heart model for simulating cardiac therapies.” *Biomech. Model. Mechanobiol.*, 15, 791–803 (2016).
- [44] Kerckhoffs, R. C. P., Narayan, S. M., Omens, J. H., Mulligan, L. J. & McCulloch, A. D., “Computational Modeling for Bedside Application.” *Heart Fail. Clin.*, 4, 371–378 (2008).
- [45] Guccione, J. M., McCulloch, A. D., “Mechanics of active contraction in cardiac muscle: Part I--Constitutive relations for fiber stress that describe deactivation.” *J. Biomech. Eng.*, 115, 72–81 (1993).
- [46] Solomon S. D., Zile M., Pieske B., Voors A., Shah A., Kraigher-Krainer E., Shi V., Bransford T., Takeuchi M., Gong J., Lefkowitz M., Packer M., McMurray J. J., “The angiotensin receptor neprilysin inhibitor LCZ696 in heart failure with preserved ejection fraction: A phase 2 double-blind randomised controlled trial.” *Lancet*, 380, 1387–1395 (2012).
- [47] Shoucri, R. M., “Clinical applications of the areas under ESPVR.” *Cardiovasc. Diagn. Ther.*, 3, 60–603 (2013).
- [48] Donal E., Raud-Raynier P., De Place C., Gervais R., Rosier A., Roulaud M., Ingels A., Carre F., Daubert J. C., Denjean A., “Resting Echocardiographic Assessments of Left Atrial Function and Filling Pressure Interest in the Understanding of Exercise Capacity in Patients with Chronic Congestive Heart Failure.” *J. Am. Soc. Echocardiogr.*, 21, 703–710 (2008).
- [49] Tamargo M., Obokata M., Reddy Y. N. V., Pislaru S. V., Lin G., Egbe A. C., Nishimura R. A., Borlaug B. A., “Functional mitral regurgitation and left atrial myopathy in heart failure with preserved ejection fraction.” *Eur. J. Heart Fail.*, 22, 489–498 (2020).

- [50] Santos AB, Kraigher-Krainer E, Gupta DK, Claggett B, Zile MR, Pieske B, Voors AA, Lefkowitz M, Bransford T, Shi V, Packer M, McMurray JJ, Shah AM, Solomon SD; PARAMOUNT Investigators., “Impaired left atrial function in heart failure with preserved ejection fraction.” *Eur. J. Heart Fail.*, 16, 1096–1103 (2014).
- [51] Vedula, V., George, R., Younes, L. & Mittal, R., “Hemodynamics in the left atrium and its effect on ventricular flow patterns.” *J. Biomech. Eng.*, 137, 1–8 (2015).
- [52] Pironet A., Dauby P. C., Paeme, Sabine, Kosta S., Chase J. G., Desaive T., “Simulation of Left Atrial Function Using a Multi-Scale Model of the Cardiovascular System.” *PLoS One*, 8, (2013).
- [53] Zingaro, A., Dede, L., Menghini, F. & Quarteroni, A., “Hemodynamics of the heart’s left atrium based on a Variational Multiscale-LES numerical method.” *Eur. J. Mech. B/Fluids*, 89, 380–400 (2021).
- [54] Land, S. & Niederer, S. A., “Influence of atrial contraction dynamics on cardiac function.” *Int. j. numer. method. biomed. eng.*, 34, 1–17 (2018).
- [55] He K.L., Burkhoff D., Leng WX, Liang ZR, Fan L, Wang J, Maurer MS., “Comparison of Ventricular Structure and Function in Chinese Patients With Heart Failure and Ejection Fractions >55% Versus 40% to 55% Versus <40%.” *Am. J. Cardiol.*, 103, 845–851 (2009).
- [56] Shavik, S. M., Zhong, L., Zhao, X. & Lee, L. C. “In-silico assessment of the effects of right ventricular assist device on pulmonary arterial hypertension using an image based biventricular modeling framework.” *Mech. Res. Commun.*, 97, 101–111 (2019).
- [57] Shavik, S. M., Jiang, Z., Baek, S. & Lee, L. C., “High spatial resolution multi-organ finite element modeling of ventricular-arterial coupling.” *Front. Physiol.*, 9, (2018).
- [58] S. Pezzuto and D. Ambrosi., “Active contraction of the cardiac ventricle and distortion of the microstructural architecture.” *Int. j. numer. method. biomed. eng.*, 30, 1578–1596 (2014).
- [59] Guccione, J. M., McCulloch, A. D. & Waldman, L. K., “Passive material properties of intact ventricular myocardium determined from a cylindrical model.” *J. Biomech. Eng.*, 113, 42–55 (1991).
- [60] Campos, R. S., Amorim, R. M., Oliveira, B. L., Rocha, B. M., Sundnes J., Barra, L. P., Lobosco, M., Santos, R. W., “3D heart modeling with cellular automata, mass-spring

- system and CUDA.” *Lect. Notes Comput. Sci.*, (including Subser. Lect. Notes Artif. Intell. Lect. Notes Bioinformatics) 7979 LNCS, 296–309 (2013).
- [61] Maurer, M. S., King, D. L., El-Khoury Rumbarger, L., Packer, M. & Burkhoff, D. “Left heart failure with a normal ejection fraction: Identification of different pathophysiologic mechanisms.” *J. Card. Fail.* 11, 177–187 (2005).
- [62] Shah, A. M., “Ventricular remodeling in heart failure with preserved ejection fraction.” *Curr. Heart Fail. Rep.*, 10, 341–349 (2013).
- [63] Streeter, D. D., Spotnitz, H. M., Patel, D. P., Ross, J. & Sonnenblick, E. H., “Fiber orientation in the canine left ventricle during diastole and systole.” *Circ. Res.*, 24, 339–347 (1969).
- [64] Gorcsan, J. & Tanaka, H., “Echocardiographic assessment of myocardial strain.” *J. Am. Coll. Cardiol.*, 58, 1401–1413 (2011).
- [65] Hoit, B. D., “Strain and strain rate echocardiography and coronary artery disease.” *Circ. Cardiovasc. Imaging*, 4, 179–190 (2011).
- [66] Smiseth, O. A., Torp, H., Opdahl, A., Haugaa, K. H. & Urheim, S., “Myocardial strain imaging: How useful is it in clinical decision making?” *Eur. Heart J.* 37, 1196-1207b (2016).
- [67] Adhyapak, S. M., Parachuri, V. R., “Architecture of the left ventricle: insights for optimal surgical ventricular restoration.” *Heart Fail. Rev.*, 15, 73–83 (2010).
- [68] Maurer, M. S., King, D. L., El-Khoury Rumbarger, L., Packer, M. & Burkhoff, D. “Left heart failure with a normal ejection fraction: Identification of different pathophysiologic mechanisms” *J. Card. Fail.* 11, 177–187 (2005).
- [69] Dabiri, Y., Sack, K. L., Shaul, S., Sengupta, P. P. & Guccione, J. M., “Relationship of transmural variations in myofiber contractility to left ventricular ejection fraction: Implications for modeling heart failure phenotype with preserved ejection fraction.” *Front. Physiol.*, 9, 1–11 (2018).
- [70] Adeniran, I., MacIver, D. H., Hancox, J. C. & Zhang, H., “Abnormal calcium homeostasis in heart failure with preserved ejection fraction is related to both reduced contractile function and incomplete relaxation: An electromechanically detailed biophysical modeling study.” *Front. Physiol.*, 6, 1–14 (2015).

- [71] Adapted from “Fowler NO: Cardiac Diagnosis and Treatment,” ed 3. *Philadelphia, JB Lippincott*, 1980, p. 11.
- [72] Kasner, M., Sinning, D., Burkhoff, D. & Tschöpe, C., “Diastolic pressure–volume quotient (DPVQ) as a novel echocardiographic index for estimation of LV stiffness in HFpEF.” *Clin. Res. Cardiol.*, 104, 955–963 (2015).
- [73] Von Roeder M, Rommel K. P., Kowallick J. T., Blazek S., Besler C., Fengler K., Lotz J., Hasenfuß G., Lücke C., Gutberlet M., Schuler G., Schuster A., Lurz P., “Influence of Left Atrial Function on Exercise Capacity and Left Ventricular Function in Patients with Heart Failure and Preserved Ejection Fraction.” *Circ. Cardiovasc. Imaging*, 10, 1–9 (2017).
- [74] Kraigher-Krainer E., Shah A. M., Gupta D. K., Santos A., Claggett B., Pieske B., Zile M. R., Voors A. A., Lefkowitz M. P., Packer M., McMurray J. J., Solomon S. D.; PARAMOUNT Investigators., “Impaired systolic function by strain imaging in heart failure with preserved ejection fraction.” *J. Am. Coll. Cardiol.*, 63, 447–456 (2014).
- [75] Shoucri, R. M., “Clinical applications of the areas under ESPVR.” *Cardiovasc. Diagn. Ther.*, 3, 60–603 (2013).
- [76] Hiebert, J. B., Vacek, J., Shah, Z., Rahman, F. & Pierce, J. D. “Use of speckle tracking to assess heart failure with preserved ejection fraction.” *J. Cardiol.*, 74, 397–402 (2019).
- [77] Mentz, R. J., Khouri, M. G., “Longitudinal strain in heart failure with preserved ejection fraction: Is there a role for prognostication?” *Circulation*, 132, 368–370 (2015).
- [78] Gazewood, J. D., Turner, P. L., “Heart Failure with Preserved Ejection Fraction: Diagnosis and Management.” *Am. Fam. Physician*, 96, 582–588 (2017).

NOMENCLATURE

HF	: Heart Failure
EF	: Ejection Fraction
HFrEF	: Heart Failure with reduced Ejection Fraction
HFpEF	: Heart Failure with preserved Ejection Fraction
ED	: End Diastole
ES	: End Systole
LV	: Left Ventricle
LA	: Left Atrium
RV	: Right Ventricle
RA	: Right Atrium
SL	: Semilunar Valve
HTN	: Hypertension
DD	: Diastolic Dysfunction
AV	: Atrioventricular Valve
SV	: Stroke Volume
MR	: Magnetic Resonance
ECG	: Electrocardiography
DBP	: Diastolic Blood Pressure
SBP	: Systolic Blood Pressure
ESPVR	: End-Systolic Pressure-Volume Relationship
EDPVR	: End-Diastolic Pressure-Volume Relationship
TPR	: Total Peripheral Resistance
Ees	: End Systolic Elastance